Charles University

Faculty of Science

Ph.D. study program: Biochemistry

Jiří Zahradník, M.Sc.

Targeted modifications of the protein-protein interactions: Ternary complex of interferon-γ as a model system

Cílené modifikace interakcí mezi proteiny: Ternární komplex interferonu-γ jako model

Doctoral thesis in Biochemistry

Supervisor: doc. Ing. Bohdan Schneider, CSc.

Institute of Biotechnology CAS, v.v.i.

Prague, 2018

Declaration

I hereby declare that this thesis is based on my own research carried out in the Laboratory of Biomolecular Recognition, Institute of Biotechnology, Academy of Sciences of the Czech Republic, v.v.i. and all used sources of information have been properly cited. This thesis has not been submitted previously in order to obtain the same or any other academic degree.

In Prague, 6th June, 2018 Jiří Zahradník

Acknowledgements

I would like to thank my supervisor doc. Ing. Bohdan Schneider, CSc. for his essential support, scientific advice and leadership. I would also like to thank all of my colleagues from the Laboratory of Biomolecular Recognition (Institute of Biotechnology, Academy of Sciences of the Czech Republic) and my family for their patience and support.

Dedicated to my father, who inspired me to study science

Declaration of co-authors

The thesis contains three original publications co-authored by Mgr. Jiří Zahradník and all the work presented here was performed under my supervision. Hence I am authorized to confirm that Mgr. Jiří Zahradník contributed substantially to all four papers that form the basis of the dissertation thesis. In more detail, he:

1. Cloned, expressed and purified most of the IFN-γR1 cavity and joint interface-cavity mutants and significantly participated in the biophysical measurements. Published in: Redesigning Protein Cavities as a Strategy for Increasing Affinity in Protein-Protein Interaction: Interferon-γ Receptor 1 as a Model. Černý, J., Biedermannová, L., Mikulecký, P., Zahradník, J., Charnavets, T., Šebo, P., Schneider, B. (2015) Biomed Res Int. 2015: 716945.

2. Cloned, expressed and purified IFN-γR2 protein. In production phase he analyzed our original crystal structure together with the other available type II receptors and wrote the manuscript. Published in: Crystal structure of human interferon-γ receptor 2 reveals the structural basis for receptor specificity. Mikulecký, P., Zahradník, J., Kolenko, P., Černý, J., Charnavets, T., Kolářová, L., Nečasová, I., Pham, P.N., Schneider, B. (2016) Acta Crystallogr D Struct Biol. Sep; 72(9):1017-25.

3. Cloned fish interferon-γ proteins and their receptors 1 and 2 and measured their biophysical properties. He designed the main features of the study, significantly participated in its bioinformatics part, and in the crystal related analyses. Published in: Interferons type II and their receptors R1 and R2 in fish species: Structure, function & evolution. Zahradník, J., Kolářová, L., Pařízková, H., Kolenko, P., Schneider, B. (2018) Fish and shellfish immunology, 79, 140-152.

Abstract

A key prerequisite for a deeper understanding of biological processes at molecular level is a detailed description of the three-dimensional structure of interaction partners and their complexes. We adopted the IFN-γ complex as our model system. Even though IFN-γ is one of the key modulators of the immunity response, which has been studied intensively for more than 60 years, the structure of the accessory receptor chain and the understanding of the IFN-γ complex is still lacking. In this work we firstly discussed the binary system between IFN-γ and its high affinity receptor R1 which is structurally known. Using a new innovative methodology we focused on the modulation of the affinity between IFN-γ and its receptor R1. Our approach was based on the modulation of protein – protein stability by mutating cavities in the proteins´ structure and increasing the affinity about seven-fold. Secondly, we crystallized and solved the structure of the IFN-γ receptor 2, the accessory receptor molecule. Our analysis of variable residues on the surface of the structures of type II family receptors, to which receptor 2 belongs, revealed the putative binding site for IFN-γ. In the third part of our work, we crystallized IFN-γ from olive flounder *Paralichthys olivaceus* and solved its structure at 2.3 Å resolution (PDB code 6f1e). This structure differs from the other IFN-γ structures and indicates how the fish IFN-γ diverged while preserving the overall fold. We resolved a co-evolutionary aspect between IFN-γ and its high affinity receptor by using bioinformatics and biophysical experiments. Finally, we integrated our results obtained by different techniques and postulated the topology of the IFN-γ ternary complex based on our structure of IFN-γR2, SAXS data, and mutational scanning.

Abstrakt (In Czech)

Klíčovým požadavkem pro detailní porozumění biologických procesů, až na molekulární úroveň, je znalost struktury interagujících molekul a jejich komplexů. Jako modelový systém, pro naši studii, jsme si zvolili IFN-γ. Ačkoliv je tato molekula jedním ze zásadních modulátorů imunitní odpovědi, a je studována již více než 60 let, tak struktura přídavného receptoru (IFN-γR2) a porozumění celému komplexu je nedostačující. V této práci jsme se nejprve zabývali binárním systémem IFN-γ s jeho receptorem, který vykazuje vysokou afinitu k IFN-γ a prostorová struktura obou dvou molekul je známa. Zaměřili jsme se tedy na modulaci afinity mezi IFN-γ a tímto receptorem. Náš přístup spočíval v inovativní metodě založené na modulaci stability protein-proteinových interakcí pomocí mutagenizace aminokyselinových zbytků umístěných uvnitř struktury proteinu. Podařilo se nám zvýšit afinitu testované interakce sedmkrát. Druhá část projektu byla zaměřena na krystalizaci, vyřešení a popis struktury druhého – přídavného receptoru pro IFN-γ. Naše analýza variabilních aminokyselinových zbytků na povrchu tohoto proteinu a strukturně příbuzných receptorů z rodiny typu II odhalila možné vazebné místo pro IFN-γ. Ve třetí části naší práce jsme se zaměřili na krystalizaci IFN-γ z platýze druhu *Paralichthys olivaceus* a tuto strukturu jsme vyřešili s rozlišením 2.3 Å (identifikační číslo proteinové databáze PDB: 6f1e). Získaná struktura se liší od ostatních známých struktur IFN-γ a indikuje divergenci rybích proteinů, i když celkové uspořádání a topologie molekuly (z angl.: fold) jsou stejné. Biofyzikální a bioinformatické pokusy navržené na základě této struktury nám umožnili vyřešit aspekty koevoluce mezi IFN-γ a jeho receptorem 1. Všechny získané poznatky, doplněné o data z mutagenizačních experimentů, SAXS techniky a analýz krystalových struktur, nám na závěr práce umožnili postulovat topologii ternárního komplexu IFN-γ .

List of Abbreviations

FIL10	Interleukin-10 family
GAS	Gamma activator sequence
IFN	Interferon
IRF	Interferon response factor
JAK	Janus Kinase
NK	Natural killer cells
PPI	Protein – protein interactions
RCSB PDB	Research Collaboratory for Structural Bioinformatics Protein Data Bank
SAXS	Small Angle X-ray diffraction
SOCS	Suppressor of cytokine signaling
SPR	Surface plasmon resonance
STAT	Signal Transducer and Activator of Transcription
TGF	Transforming growth factor
TIRF	Total internal reflection fluorescence

List of Contents

1. Introduction

Structural biology is an exciting interdisciplinary field of life sciences branching molecular biology, biochemistry, biophysics, and bioinformatics. It focuses on detailed description of three-dimensional structures of biological macromolecules – a key component of all known life forms. The main objects of structural biology studies are proteins and nucleic acids. Structural biology is not just studying their spatial arrangement, but also functional aspect on a molecular level with the effort to understand them [1].

Proteins and their interactions are the dominant carriers of functions in the living cell. A cell is an open system which needs an information input from the environment, its transfer and analysis to accommodate necessary reactions. These functions are mediated by receptor proteins and subsequent signalization cascades. In the population of multicellular organisms, the need for communication between cells arises. This communication between cells is also mediated mainly, but not exclusively, by proteins and their cognate receptors. The present study focuses on the structural aspects of one of these communication channels involved in the human immune system – the interferon gamma system. Although there are more than four thousand of scientific papers with the key word "interferon gamma" published every year, the structural aspects of ternary complex are not completely resolved. The complexity, novelty, and potential applications motivated us to analyze this difficult target. The following chapters introduce the results of my work on this project. The results were published in three publications:

1) Redesigning Protein Cavities as a Strategy for Increasing Affinity in Protein-Protein Interaction: Interferon-γ Receptor 1 as a Model

2) Crystal structure of human interferon-c receptor 2 reveals the structural basis for receptor specificity

3) Interferons type II and their receptors R1 and R2 in fish species: evolution, structure, and function

To extend my thesis and complete the scientific contribution of our work, I also included the major findings from the manuscript under preparation. Because of the manuscript incompleteness, it is not included in full as a supplement.

4) Topology of complexes between interferon-gamma and extracellular portions of its two receptors R1 and R2

1.1 Cytokines

The origin of the word cytokine well describes its meaning. It comes from Greek words - cyto and kytos that mean cell and movement. Cytokines can be described as molecules traveling between cells. In fact, cytokines represent a category of small secreted proteins that mediate signaling and immunomodulatory effects between cells in an autocrine, paracrine, and endocrine fashion. Cytokines may be further divided into smaller functional categories chemokines, interferons, interleukins, lymphokines, and tumor necrosis factors. Regardless the category, they all regulate a broad spectrum of cell processes by their activation or inhibition. The response is mediated by specific cytokine receptors on the cell surface [2].

1.2. Interferons

Interferon, the first discovered cytokine, is a small protein described more than 60 years ago by two phenomenal British researchers Alick Isaacs and Jean Lindenmann [3]. The name interferon has been inspired by its ability to interfere with a viral infection. Subsequently, other molecules with the same ability were described. Therefore, the need for classification of these molecules emerged. Interferons were divided into three independent type groups (I, II, III) according to their differences in sequences, cognate receptors, genome localization, and cellular traits. Even today, thanks to the systematic genomics research new interferons are being discovered. A good example is the human interferon λ4 discovered in 2013 [4] and fish interferons [5]. Interferons were described in extant cartilaginous fish and their presence in the earliest *gnatohostomes* is expected [6]. Thus, they represent ancient immunity elements.

The exact role of interferons in organisms emerged later and is still under investigative debates. They modulate myriads of cellular processes and play a crucial role in modulating innate and adaptive immune reactions against various stimuli, including viruses [7], intracellular bacteria [8,9], and also intrinsic signals from tumors and proliferating cells [10].

All three types of interferons are secreted proteins with their detection receptors on the cell surface. The primary high affinity receptors capture the interferon molecule; the second receptors, which are accessory factors, play modulatory roles. The affinities of the second receptors are usually lower and bind after the formation of the binary complexes. Following this ternary complex formation, a signal is transmitted into the cell cytoplasm and a signaling cascade via the Janus Kinase (JAK) and Signal Transducer and Activator of Transcription (STAT) pathway occurs. A combination of different JAKs and STATs results in the

regulation of transcription of various interferon-regulated genes [11] and also in the regulation of the stability of various mRNA and other epigenetic signals.

1.2.1 Type I interferons

The interferon type I family is the biggest one with five structurally dissimilar members and 17 proteins overall in humans: interferon α (IFN-α, 13 subtypes), IFN-β, IFN-ε, IFN-κ, and IFN-ω. This family is even broader in some other species. IFN-δ and IFN-τ were described in pigs and cattle, respectively, and many subtypes were described in fish species. Members of type I are co-localized with strong gene synteny on chromosome 9 in humans, which suggests their origin by gene duplication [12].

The type I interferons signal through only one ternary receptor complex, but with large differences in the response. Thus, they cannot be viewed as iso-molecules. All type I members bind to IFNα receptor 1 (IFN-αR1) and receptor 2 (IFN-αR2) subunits. Subsequent JAK/STAT pathways differ significantly. Usually IFN-α subtypes bind JAK1, STAT1, and STAT2 proteins. For other types and specific cells STATs3-6 can be activated [13,14,15] [15]. The descent outcomes in the cellular responses are modulated by differential expression, binding affinities [16], and JAKs/STATs [17,18,19].

1.2.2 Type II interferons

The type II interferon family is unique in its structure. It seems that all canonical members are dimers in contrast to monomers in the type I and III family*. The non-canonical members are fusion proteins with an IFN-γ domain (XP_006012494.1) and their protein products or biological role is unknown.

Type II interferon genes evolved early in the chordate evolution together with type I interferons. It is assumed that they have evolved from a class II helical cytokine ancestor. Unfortunately, there are no data of when and how the dimerization occurred. Representatives of the type II family are IFN-γ, which is the exclusive member in all tetrapods, and IFN-γ is accompanied by IFN-γrel in fish species. The gene for IFN-γ is located on chromosome 12 in humans together with genes from the interleukin 10 family (FIL10). This genomic organization can be found in all tetrapods. The gene for IFN-γrel is not located on the same chromosome and its origin has been proposed by duplication of the whole genome.

The IFN-γ molecule signals through the formation of the ternary complex comprising of IFN-γ, IFN-γ receptor 1 (IFN-γR1), and IFN-γ receptor 2 (IFN-γR2). The dimeric behavior of IFN-γ implies the formation of a ternary complex with more complex stoichiometries than in the case of other interferons. It is expected that the IFN-γ binds to two molecules of IFN-γR1 and to two IFN-γR2 [20], but other possibilities are not excluded. The mutation of one interface with the IFN-γR1 resulted in the formation of a 1:1 complex in vitro and addition of this mutant variant of IFN-γ to the cells led to an antiviral effect.

Unlike the widely expressed receptors, the IFN-γ molecule itself is produced only by immune system cells, including the natural killer (NK) cells, CD4 T helper 1 (Th1) cells, and CD8 cytotoxic suppressor cells [21,22]. Although the cellular sources of IFNγ are limited, almost all cell types can respond to it. This regulation scheme is also characteristic for type II interferons [23].

(* - Members of the type III family might form dimers by intermolecular disulfide bridges. The biological role of this phenomenon is not known and the possibility of experimental artifact cannot be excluded.)

1.2.2.1 Interferon gamma

The functions of IFN-γ are pleiotropic. On one hand IFN-γ is able to modulate the innate and adaptive immune response against pathogens and tumors and on the other hand its presence is required to maintain immune homeostasis [24]. Moreover, an altered, disturbed, or aberrant IFN-γ expression and protein is associated with a number of auto-inflammatory and autoimmune diseases [25,26,27].

The IFN-γ molecule is a glycoprotein borne from a single 6 kb gene located on the human chromosome 12 (I2q24. 1) in the vicinity of IFN-γ antisense RNA 1 on one side (IFNG-AS1, Gencode Gene: ENSG00000255733.5) and genes for IL-26 and IL-22 on the other side (Gencode Gene: ENSG00000111536.4). The IFN-γ gene shares a pattern of interleukins from the family of interleukin 10 with 4 exons and 5 introns [28].

The processing of the IFN-γ protein includes two major steps: Secretion with the N-terminal cleavage of the signal peptide and cleavage of C-terminal propeptide. The naïve single polypeptide chain with 143 amino acids has 16.7 kDa, but the two glycosylation sites (Asn48, Asn120) that are variably N-glycosylated increase the molecular mass up to 25 kDa [29]. The

C-terminal propeptide proteolytic cleavage is responsible for IFN-γ alternative endings at predominant G157, minor G150, and minor G161 [30]. Therefore, the mature protein molecular weight may vary between 34 kDa and 50 kDa in its native homodimer state [28]. Variations in the term of single nucleotide polymorphism, which result in amino-acid changes, are defined at positions 29 and 160 (UniProtKB - P01579).

Three-dimensional structures of the IFN-γ protein have been solved by X-ray diffraction. There are multiple different IFN-γ structures solved from four different organisms: human, 1hig [31], 1fg9 [32], 3bes [33]), rabbit *Oryctolagus cuniculus* 2rig [34], bovine, 1d9c [35], 1RFB [36], and fish *Paralichthys olivaceus* 6f1e [37]. The entire structures showed a unique similar interferon gamma fold, which is composed of two identical subunits, each with 6 alpha helices (A – F) parallel to the dimer twofold axis (**Figure 1.2A**). An exception was found in the *P. olivaceus* IFN-γ structure that has a similar fold, but one additional helix G at the C terminus in one monomer [37] (**Figure 3.3A)**. The first four helices from one subunit form a four-helix bundle with a cleft that allows intertwining of the C-terminal helix from the second subunit. By contrast to the IL-10 dimer there are multiple hydrophobic contacts among all of the helices, but most are between the C and D helices. The C helices are the most hydrophobic in the structure and are buried in the core of the dimer [31].

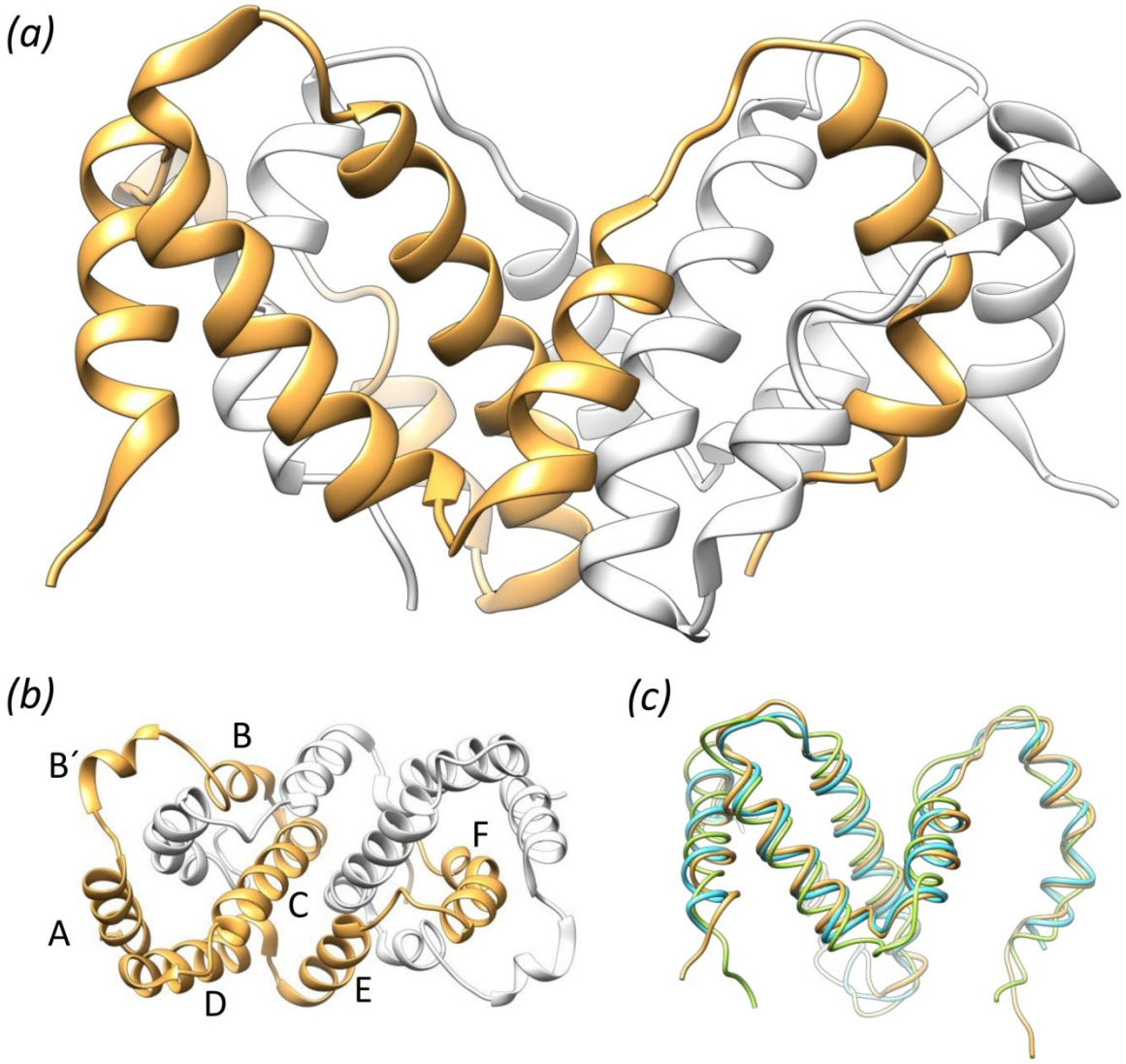

Figure 1.2A – Three dimensional structures of mammalians IFN-γ. a) The side view of the structure of human IFN-γ (pdb 1fg9, [32]). The two monomers in the homodimer are depicted in yellow and white. b) The top view representation of human IFN-γ represented in *(a)*. The helices A-F are marked in one monomer. c) Comparison of IFN-γ monomer from different mammals: human 1fg9 (yellow, [32]), rabbit 2rig (green, [34]), and bovine, 1d9c (blue, [35]).

Effective signalization of IFN-γ in cells requires the formation of a ternary complex between IFN-γ, its high affinity cell receptor IFN-γ receptor 1 (IFN-γR1) and accessory factor IFN-γ receptor 2 (IFN-γR2). Initial experiment-based assumptions describing the receptors distribution were with free receptors on the cell membrane [38], but later the pre-assembly of receptors has been proposed [39]. The re-examination of previous findings by new microscopic super-resolution techniques, e.g. FTIR microscopy, finally denies the existence of the preassembly complex as an artifact of receptor over-expression (Jacob Piehler, University of Osnabrück, Molecular and cellular determinants of cytokine receptor activation,

Molecular Perspectives on Protein-Protein Interactions conference, December 3-7, 2017, paper will be published). IFN-γ interacts with IFN-γR1 and forms a binary complex, which is targeted subsequently by IFN-γR2 to form the final ternary complex. The signaling complex creation results in the reorientation of receptor intracellular domains and thereby initiates the JAK/STAT pathway, which is used by more than 50 cytokines, growth factors, and hormones for gene regulation [40]. Recently it has been shown that the JAK/STAT pathway works under cooperative crosstalk with other ubiquitous pathways, including MAP kinase, PI3 kinase, CaM kinase II, and NFκB to regulate specific IFN-γ effects [41,42]. There are also hypotheses that a certain level of signal specificity is mediated by endocytosis and localization [43,44].

The first subsequent events after ternary complex formation are the binding of JAK2 on the IFN-γR2 cytoplasmic domain and JAK1 on the IFN-γR1, respectively. In contrast, some reports assume the constitutive presence of JAK1 and JAK2 kinases associated with the intracellular domain of IFNgR1 and IFNgR2, respectively [21,45]. After the signalization complex assembly, the kinases are activated by binding to their cognate receptor partner. These activations lead to a cascade of phosphorylation reactions between kinases and the proteins themselves commonly referred as auto-transphosphorylation. At the last stage, activated JAK1 phosphorylates Y457 of IFNgR1. This residue is the critical one for forming a docking site for STAT1 that is further activated by phosphorylation, probably by JAK2 [46]. The above-mentioned phosphorylation cascade takes less than one minute [47].

After STAT1 undergoes specific phosphorylation, dimerization, two scenarios are possible. The STAT1 homodimer enters the nucleus and directly induces changes in the expression of hundreds of primary regulated genes by the interaction with the so-called GAS site (for gamma activator sequence, [48]). Moreover, one of the primary activated genes is known as interferon response factor 1 (IRF1) which subsequently activates dozens of secondary response genes with mainly immunomodulatory functions. The negative regulators of this pathway are SOCS (suppressors of cytokine signaling) proteins. They inhibit the phosphorylation of JAKs and STAT1 and drive them out of the nucleus [49]. This pathway is known as the canonical or classical pathway (**Figure 1.2B**). Although the classical model describes only the STAT1 homodimer other complexes such as STAT1 / STAT2 and STAT1/STAT1/IRF-9 or STAT1/STAT2/IRF-9 may form [50,51].

The second scenario is called a non-canonical IFN-γ signaling pathway (**Figure 1.2B**). It involves creation of the IFN-γ /R1/STAT1α/JAK1/JAK2 complex and its subsequent

endocytosis [43]. The nuclear localization signal (NLS) and polycationic C-terminus present in the IFN-γ molecule are responsible for targeting the whole complex to the cell nucleus and thus for the non-canonical IFN-γ signaling [52,53]. This pathway is however not completely described. Other signaling scenarios include the association of receptors with lipid micro-domains and their clathrin-dependent internalization or clustering of receptors with other proteins and triggering clathrin-independent endocytosis [44].

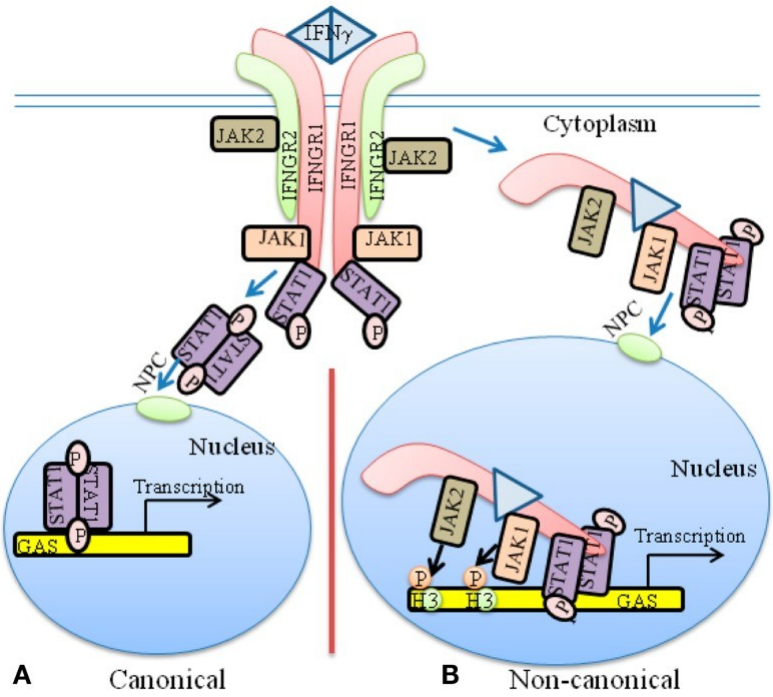

Figure 1.2B – Schematic representation of canonical and non-canonical pathways in IFN-γ signaling. A) The classical pathway of IFN-γ signaling consists of a ternary complex assembly, a phosphorylation cascade and the translocation of STAT1 homodimer into the nucleus. B) The non-classical pathway is driven by endocytosis and nuclear transport of the whole complex. Details of both pathways are described in chapter 1.2.2.1. (The Figure was adopted from Johnson et. al. 2013 [54]).

The major sources of IFN-γ in the body are T cells, natural killer cells, and natural killer T cells [55]. The expression has been identified also in macrophages, dendritic cells, and B cells [56]. The mechanisms which regulate IFN-γ expression of immune cells include various extracellular signals [57] and also internal signals like DNA epigenetic control [58]. The most proficient extracellular signals are associated with infections by viruses [59,60], bacteria [61] [62], or intracellular protozoans including *Toxoplasma gondii* [63] and *Leishmania donovani* [64]. Almost all cell types can respond at least to some extent to an IFN-γ stimulus (The Human protein atlas accession: IFNGR1, IFNGR2) [65,51].

Biological functions of IFN-γ (**Figure 1.2C**) were historically considered to be pro-inflammatory. This attribute was concluded by its ability to strongly activate macrophages which are crucial for host defense against intracellular pathogens and inflammatory tissue changes. This activation is further exacerbated by a positive autocrine feedback loop [66,67] [38]. Furthermore, this picture was strengthened with the paradigm of an IFN-γ driven Th1 immune response [68]. The current picture is a more complex one that is based on pleiotropic IFN-γ functions and balanced pro- and anti-inflammatory responses to IFN-γ signaling [69] [24]. The major functions in modulation of pro- and anti-inflammatory responses are summarized in **Figure 1.2C**.

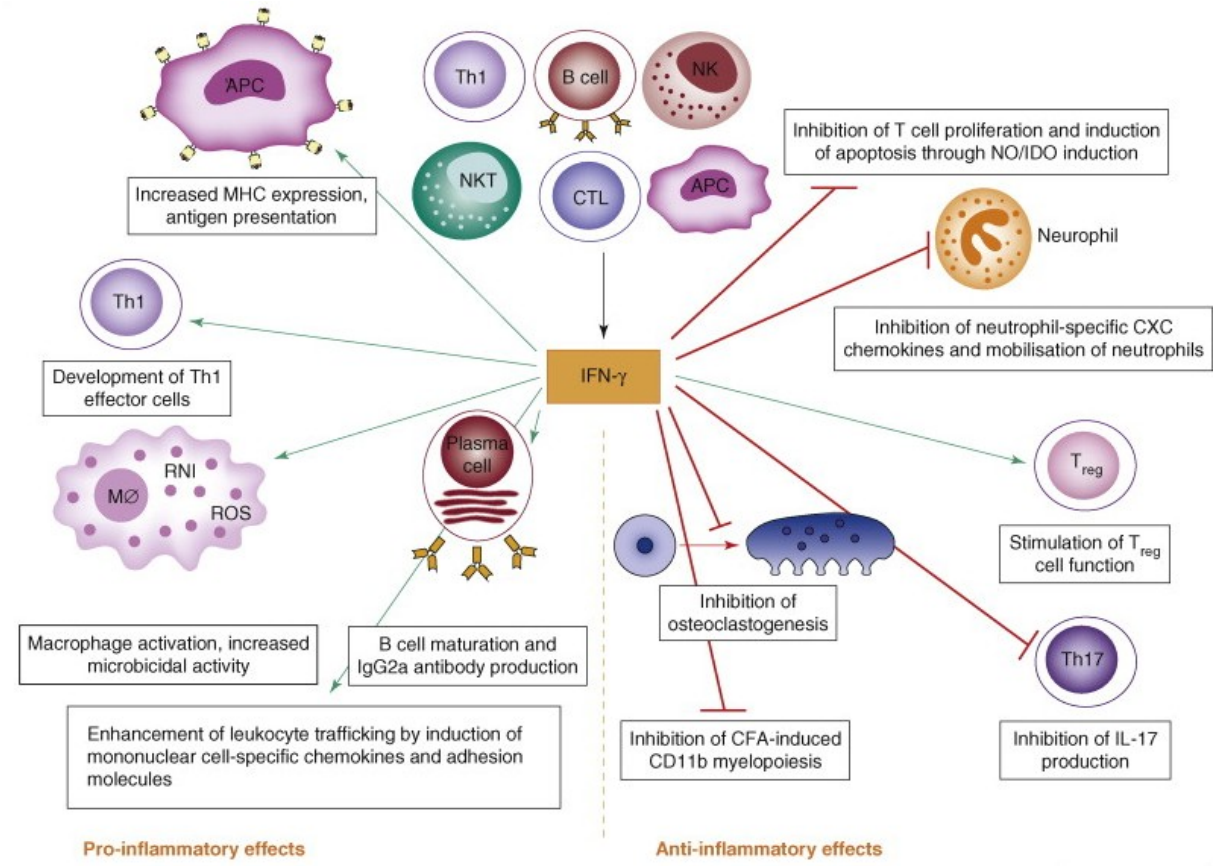

Figure 1.2C – The overview of the most general functions of interferon gamma. The left part of the picture highlights the pro-inflammatory functions and the right shows the anti-inflammatory effects. Green arrow lines correspond to stimulatory effects whereas the red lines depict inhibitory effects. (Original picture was published by Kelchterman et al. [69]).

The delicate signaling by IFN-γ is very sensitive to any changes. Therefore, it is not surprising that IFN-γ is associated with numerous auto-inflammatory and autoimmune diseases. Specific alleles are associated with higher susceptibility to multiple sclerosis [70], tuberculosis [71] [72,73], aplastic anaemia [74], kidney angiomyolipomas [75] or they can even protect against

tuberculosis [76] or be important for hepatitis C virus clearance [77]. The altered protein expression is connected with systemic lupus erythematosus [78,79] and chronic inflammatory arthritis [80]. Aberrations of interferon gamma are also associated with some tumor types [81,82,83]. All these findings have led to efforts of researchers to develop IFN-γ based agonistic or antagonistic immunomodulatory therapies. Recombinant protein (Actimmune) is an approved drug [84]. Antagonistic effects are available by approved antibody (HuZAF) used for treatment of psoriasis [85], rheumatoid arthritis, and multiple sclerosis [86].

1.2.3 Type III interferons

Type III interferons belong with their genomic organization [87], sequence, and structure to the Interleukin-10 family of cytokines but their antiviral properties rank them into the interferon group. This group of interferons is the most recent one [88] and has four different subtype members known as interferons lambda (IFN-λ1 – 4). Their categorization in FIL10 yielded alternative synonymous names: IFN-λ1 = IL-29, IFN-λ2 = IL-28A, IFN-λ3 = IL-28B. All type III interferons are located on the human chromosome 19 and share a high degree of similarity, which suggests the existence of their common ancestor. The IFN-λ2 and IFN-λ3 share 96 % of similarity which corresponds to 8 mutations. IFN-λ1 is not as similar (74 % identity and 82 % positivity with IFN-λ2) and IFN-λ4 is not similar (40.8 % similarity to λ3). IFN- λ4's differences arise as a consequence of a large frame-shift mutation generating a new sequence, interestingly with all the disulfide bridges preserved [89].

The type III interferon signaling complex is formed by IFN-λ1 – 4, IFN-λ receptor 1 (IFN-λR1, IL-28R1 alternatively) and interleukin 10 receptor 2 (IL-10R2). Unlike other interferons the receptor complex is not specific only for interferons lambda but IL-10R2 is shared also with other members of the FIL10 family such as IL-10, IL-22, and IL-26. This phenomenon is known as receptor sharing or receptor promiscuity and is common for FIL-10 and some other interleukin families. Although the interferons type I and III signaling is mediated through completely different receptors (IFN-αR1 vs. IL-28R1, etc.), the subsequent signalization cascade utilizes the same JAK1, tyrosine kinase 2 (TYK2), and common JAK/STAT pathway to stimulate their activities [90,91].

Lambda interferons are responsible for modulating the host response to pathogens. Despite a high degree of homology, they have markedly different antiviral activities. Interestingly, almost every cell type expresses IFN-λ1 – 3 as a consequence of a viral infection, but the primary producers are myeloid and plasmacytoid dendritic cells. The major role for interferons lambda seems to be in airway epithelial cells after respiratory virus infections. Because of the receptors for interferons lambda are restricted to this and other barrier tissue cells. Only a small subset of immune cells expresses receptors. This pattern gives a great potential for lambda interferons in immune therapy, because less severe side effects are expected than observed in other interferon therapies [92].

1.3. Cytokine receptors

Cytokine receptors are cell surface proteins which are able to transmit the incoming signal provided by cytokine through the cell membrane. Therefore, they represent the bridge between extracellular and the intracellular signals. A large proportion of cytokine related illnesses are connected with these receptors [93,94]. Receptors are usually variable by multiple possible isoforms and single nucleotide polymorphisms displaying thus a wide range of potential functional changes.

A classification of cytokine receptors has been proposed on the basis of their three-dimensional structures and recognizes six independent receptor families (**Figure 1.3A)**: Type I and II cytokine receptors, Immunoglobulin family receptors, Tumor necrosis factor family, Chemokine receptors, and Transforming growth factor beta receptors.

The first two groups type I cytokine receptors and type II cytokine receptors are composed of an assembly of usually 2 fibronectin III domains. They significantly differ in the S-S bond pattern and in the presence of specific motifs. Type I cytokine receptors have four conserved cysteine residues in the N-terminal region and WSXWS motif located in close proximity to the transition between extracellular and transmembrane parts of receptors [95]. The recognition of type II cytokine receptors can be performed by an analysis of a sequentially discontinuous motif (X)WRWR(X), where X is K, R, or H. This feature together with detailed characterization of type II receptors is described bellow in the manuscript entitled: "Crystal structure of human interferon-c receptor 2 reveals the structural basis for receptor specificity "[96].

Immunoglobulin receptor superfamily members are composed of several types of Ig-like domains [97]. The name of this family has been proposed due to their homology with immunoglobulin, cell adhesion molecules, and some cytokines. The tumor necrosis factor receptor family is a cytokine receptor family with the ability to bind tumor necrosis factors (TNFs) by an extracellular cysteine-rich domain [98]. Many members of this family have non-cytokine ligands like extracellular parts of other receptors. Chemokine receptors are receptors with the ability to bind cytokines that are able to induce chemotaxis. The name was derived from the term chemotactic cytokines. Chemokine receptors are structurally G protein-coupled receptors containing 7 transmembrane domains [99]. The last family of cytokine receptors is the Transforming growth factor receptors (TGF). They are homo- or heterodimers and transduce the signal by adopting serine or threonine kinase activity [100].

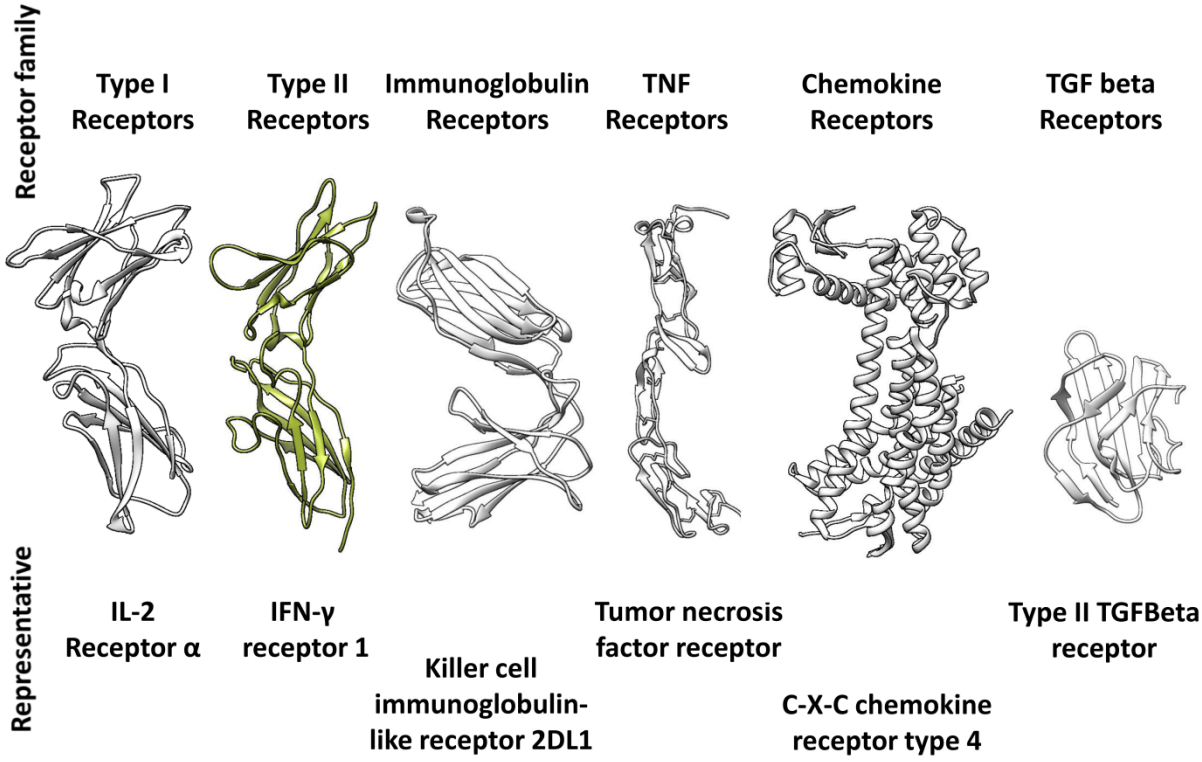

Figure 1.3A – Structural comparison of representatives from six receptor families within cytokine receptors. Type II cytokine receptors (in color) are described in detail in this thesis (chapter 1.3.1). The following structures were depicted: IL-2Rα, 2b5i [101]; IFN-γR1, 1fg9 [32]; Killer cell immunoglobulin-like receptor, 2dl1 [102], Tumor necrosis factor receptor, 1ext [103]; C-X-C chemokine receptor type 4, 4rws [104]; type II Transforming Growth Factor Beta receptor, 4p7u [105].

1.3.1. Type II cytokine receptors

As mentioned, type II cytokine receptors are structurally formed mostly by two Fibronectine type III domains. The family can be divided by function into high affinity receptors and low affinity receptors. The high affinity receptors are IFN-γR1 (Uniprot P15260), IL-10R1 (Q13651), IL-20R1 (Q9UHF4), IL-22R1 (Q8N6P7), IL22BP, and IL-28R1 (Q8IU57)). Their corresponding low affinity receptors or so-called accessory chains are IFN-γR2 (P38484), IL-10R2 (Q08334), IL-20R2 (Q6UXL0). The term accessory chain is more appropriate because the affinity of IL-20R1 to IL-20 is lower than IL-20R2 [106]. The signaling ternary complexes are heterodimers or multimers with high and low affinity components. By comparing the number of receptors in both group, the need for receptor sharing, which is characteristic trait for FIL10 is evident. In contrast to FIL10, both receptors of IFN-γ are unique and specific only for IFN-γ signaling.

1.3.1. 1. Interferon gamma receptor 1

The human IFN-γR1 (Uniprot P15260, CD119) is a transmembrane glycoprotein with a single transmembrane α-helix. The protein is encoded by a 30-kb gene located on chromosome 6 [107,108]. The gene consists of five exons encoding the extracellular domain and two exons encoding the intracellular part of the protein [21]; the corresponding mRNA is 2.3 kb long [109]. The nascent polypeptide undergoes an endoplasmic reticulum secretory pathway together with an S-S bond formation, glycosylation, and cleavage of signal peptide (AA 1-17) [110,111]. The mature receptor has 472 amino acids with a predicted mass of 52.5 kDa. The extracellular, transmembrane, and intracellular parts correspond to the amino acids 18 – 245, 246 – 266, and 267 – 489, respectively (**Figure 1.3B**).

There are known natural variants of the receptor with altered signaling. Immunodeficiency 27A is known as the disease caused by mutations in IFN-γR1 [112]. The mutations C87Y [113], V61E [114], and the multiple deletion variants [115] are very severe because they completely abrogate IFN-γ signaling which increases susceptibility to mycobacterial infections and immune disbalance.

The first structure of IFN-γR1 has been solved as a part of the binary complex between IFN-γR1 and IFN-γ in the year 1995 [20]. Later the D1 domain was crystallized [116] and other binary complexes have been solved [32,117]. The only available structure of free IFN-γR1 is the chicken structure [118]. Extracellular domain is composed of two fibronectin type III domains [119] connected by a short linker with six residues. The D1 domain is composed of residues 14–102 and forms a β-sandwich with three β-strands stacked on a layer of four β-strands. The D2 domain is composed of amino acid residues 114–221 and forms a similar β-sandwich with four strands stacked on four β-strands. The linker between both domains is common for other members of the type II receptor family and allows variations of the hinge angle [32].

The extracellular domain of IFN-γR1 contains four confirmed glycosylation sites at residues 17, 62, 69, and 162 [32], one variable at residue 240 [120,121] and four S-S bond clearly visible in the electron density maps [32]. The disulfide bonds are formed between residues Cys77-Cys85, Cys122-Cys167, Cys195-Cys200, and Cys214-Cys235, and are crucial for activity [122]. The oligosaccharide moieties contribute to the molecular weight of the receptor by approximately 25 kDa [123].

The IFN-γR1 extracellular part is responsible for mediating high-affinity binding of IFN-γ. The affinity of this interaction was measured by SPR with Kd 30.8 nM [124] and has a very high specificity [109]. The interaction between IFN-γR1 and IFN-γ is mediated by extensive contacts. The D1 and D2 domains form an angle complementary to the V-shaped IFN-γ molecule. Receptor loops bind to helix A, the AB loop, and helix B on the one monomer of IFN-γ [20].

The intracellular domain structure is unknown. Mutation studies demonstrate the presence of so called Box 1 and Box 2 motifs on the intracellular domain which collaborate in the association and activation of Jak1 [125]. Some guidance can be extracted from the structure of interferon lambda receptor 1 (IL-28R1) with human kinase Jak1 (PDB: 5l04) [126]. The receptor chain creates a long stretch intercalated into the Jak1 structure with only a very limited amount of a secondary structure. The same situation can be observed in the structure of the human TYK2 FERM and SH2 domains with an IFNAR1 intracellular peptide (PDB: 4po6) [127]. Both structures showed that box1 and box2 regions bind simultaneously to the FERM and SH2-like domains of JAK1. The further intracellular parts of receptors were studied only by mutations and residues Tyr457, Asp458, and His461 were found to be functionally important [128].

1.3.1. 2. Interferon gamma receptor 2

The second IFN-γR2 receptor (UniProt P38484) is similar to IFN-γR1 in many ways (**Figure 1.3B**). It is borne by a 33-kb gene on chromosome 21 [129,130] and consists of 7 exons [131]. The IFN-γR2 protein comprises of 310 amino acids with a predicted molecular mass of 35 kDa. Contrary to IFN-γR1, the intracellular part is very short (residues 269 – 337). The transmembrane part (248 – 268) and the extracellular parts (28 – 247) are similar to IFN-γR1.

The IFN-γR2 gene variability is rather high and connected to the manifestation of a severe disease known as immunodeficiency 28 [132,133,134]. Interestingly, one of the mutations leading to IFN-γR2 associated immunodeficiency is due to a gain of N-glycosylation [133].

The extracellular domain of IFN-γR2 is structured into two Fibronectin type III domains with 5 cysteine residues and 6 potential N-linked glycosylation sites (Asn56, Asn85, Asn110, Asn137, Asn219, and Asn231). Glycosylation contributes to the significant size heterogeneity, even in the same cell type, with Mr values that range from 61 to 67 kDa [135]. The analysis of the IFN-γR2 structure is the subject of one paper included in the thesis and will be described further in detail [96]. In the last 6 years, our knowledge of ternary

complexes increased due to solving the IL-20 ternary complex (PDB: 4doh) [106] and the interferon lambda ternary complex (PDB: 5t5w) [136]. Based on the analogy with these complexes, we assume that for the IFN-γ binding the interactions with both IFN-γR1 and IFN-γR2 are important. This has been suggested by Pestka et al. using cross-linking experiments [137]. IFN-γR2 plays a minor role in IFN-γ binding but it is crucial for signaling [45].

The transcription of IFN-γR2 is highly regulated [138] although it appears in many cells together with IFN-γR1. As expected, Th1 cells are producers of IFN-γ but they down-regulate the expression of IFN-γR2 becoming IFN-γ unresponsive. In contrast to Th1 cells, Th2 cells are responsive to IFN-γ but they cannot produce IFN-γ itself [135,139].

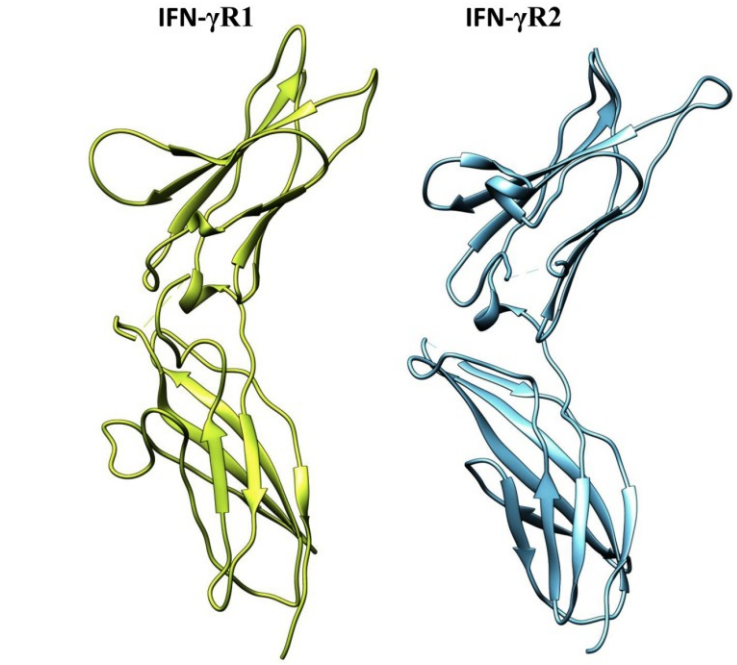

Figure 1.3B – Comparison of human receptors for IFN-γ. Although different localization, the receptors' extracellular parts are similar in size and overall shape. They significantly differ in the number of cysteines, intracellular domains, and their biochemical and biophysical characteristics.

1.3.1. 3. Interferon gamma receptor complex

Although the multiple cytokine ternary complexes were solved (Table 1.3A), the structure of the IFN-γ ternary complex remains undiscovered. The homodimeric nature of IFN-γ increases the complexity of the ternary complex, the feature that can be possibly used to tune the cytokine receptor signaling [140]. Deeper knowledge of the ternary complex will enable us to uncover this issue.

Table 1.3A – Known structures of ternary signaling complexes

Cytokine / receptor ternary complex composition	PDB ID	Reference
Growth hormone/ GHbp/ GHbp	3hhr	[141]
Erythropoietin/ sEPOR/ sEPOR	1eer	[142]
Placental lactogen/ prolactin receptor/ prolactin receptor	1f6f	[143]
Interleukin-6/ IL-6Rα/ IL-6Rβ	1p9m	[144]
Interleukin-2/ IL-2Rα/ IL-2Rβ/ γ-chain	2b5i	[101]
Interleukin-13/ IL-13Rα/ IL-4Rα	3bpo, 2erj	[145,146]
Interleukin-20/ IL-20R1/ IL-20R2	4doh	[106]
IFN-λ3/ IL-28R1/ IL-10R2	5t5e	[136]

2. Aims

The ultimate aims of this study are the development of novel approaches in the field of modulation of protein – protein interactions (PPIs). A model system used for the study is IFN-γ and its receptors IFN-γR1 and IFN-γR2 and description of their ternary complex. We concentrated on the insufficiently studied IFN-γR2, mechanisms of formation of the ternary complex IFN-γ/R1/R2, and the complex evolution.

I. Modulation of PPIs by changing the stability of a protein – protein complex. The process is aimed at changing amino-acid residue in the receptor cavities and the development of a novel technique for such stability modifications. This novel approach might complement the current methodological portfolio and enable to preserve the interaction interface intact.

II. Production, biophysical, and structural characterization of IFN-γR2. Characterization of specific features for this receptor and other members of the type II family. The structural biology analysis of IFN-γR2 was important to extend the present knowledge of protein structure and enable the study of its interaction with IFN-γ

III. Phylogeny of type II interferons in fish species and analysis of their co-evolution. Production, biophysical, and structural characterization of some fish IFN-γ signaling molecules. Analysis of possible interaction pairs by biophysics and bioinformatics approaches. The results can shed a light on the fish type II interferon system that is more diverse than the mammalian one.

IV. The study of topology and structure of complexes between IFN-γ and extracellular portions of its two receptors IFN-γR1 and IFN-γR2.

3 Results and discussion

We applied different strategies to modulate the affinity of the extracellular part of human IFN-γR1 to IFN-γ. The first set of mutations was on the interface between both partners [124] and is not included in this thesis. The study was followed by a study of "cavity" mutants (chapter 3.1). In the second paper described in the thesis, we focused on the unknown structure of IFN-γR2 and solved it. This enabled us to characterize the structure in detail and propose some features important for the IFN-γ ternary complex (chapter 3.2). The acquired knowledge has allowed us to study the evolutionary aspects of the IFN-γ ternary complex and to describe putative changes that shaped the interfaces between receptors. The evolutionary aspect of all parts of the ternary complex are analyzed in the third publication which describes the evolutionary aspect together with the structure of IFN-γ from the Japanese halibut *Paralichthys olivaceus* (chapter 3.3). Finally, we focused on the ternary complex topology and composition (chapter 3.4).

3.1 IFN-γR1 cavities

> Černý, J., Biedermannová, L., Mikulecký, P., **Zahradník, J.**, Charnavets, T., Šebo, P., Schneider, B. (2015): Redesigning Protein Cavities as a Strategy for Increasing Affinity in Protein-Protein Interaction: Interferon-γ Receptor 1 as a Model. *Biomed Res Int* 2015: 716945.

The approach to influence the affinity between IFN-γR1 and IFN-γ was developed in our laboratory. The idea of the study is built on the premise that the majority of PPI studies are based on structural properties of the interface [147] but significant contribution to the binding affinity is given by conformational dynamics and thus by entropic forces. The entropic penalty of binding can be reduced by lowering complex flexibility. The contribution of flexibility to the entropic penalty in protein-protein complexes has been shown previously by molecular dynamics simulations [148].

We analyzed in detail two available binary complexes with four slightly different IFN-γ and IFN-γR1 interactions in the available crystal structures of 1fyh [117] and 1fg9 [32]. We did not include the uncomplexed IFN-γR1 chains because their structure is significantly different from the structure of the receptor bound to IFN-γ. The cavity mutant methodology was described in a publication (Supplement 1) and is described in detail in chapters 3.1.1 – 3.1.2.

This study is a follow-up study to Mikulecky et al paper Increasing affinity of interferon-γ receptor 1 to interferon-γ by computer-aided design [124] and is briefly discussed to keep the topic in context.

3.1.1 IFN-γR1 cavities study design

Crystal structures of complexes were analyzed by the 3V program [149] to identify the cavities useful for our study. This analysis revealed a different number and size of cavities for each binary interaction system used (**Table 3.1A**). The structure of cavities is highlighted in **Figure 3.1A**. We subsequently analyzed 52 amino acids forming the cavities in the *in silico* mutation analysis by empirical force field implemented in the FoldX software [150]. We searched for mutants that would increase the stability of IFN-γR1 and/or the affinity to IFN-γ. We focused on the selection of 12 promising positions, out of 200 analyzed that were predicted in similar manner in at least three crystal structures. The positions were analyzed by comparison of changes of free energies ($\Delta\Delta G$) calculated using the FoldX program supported by averaged 500 snapshots of 10 ns molecular dynamics relaxation. Three different changes of free energy were calculated – $\Delta\Delta G$ of folding of IFN-γR1 in complex, $\Delta\Delta G$ of folding of free IFN-γR1, and $\Delta\Delta G$ of binding. The results of these computations for the 12 promising positions in the IFN-γR1 chain C (PDB 1fg9) are shown in **Figure 3.1B**. Analogical matrices were calculated for the 3 remaining IFN-γ and IFN-γR1 complexes. All selected IFN-γR1 variants were cloned, expressed, and purified to homogeneity. All mutants were also combined with the previously identified N96W mutant located on interaction interface [124]. The purified proteins were characterized in detail by biophysical techniques and the change of binding affinity was accessed by Surface Plasmon resonance (SPR) measurements.

Table 3.1A – Cavities in the four binary complexes between IFN-γR1 and IFN-γ (PDB: 1fg9, 1fyh). The receptor chains are labeled according to PDB file.

	Surface [Å^2]*	Number of residues lining the cavity†	Residues selected for mutation	Cavity observed in IFNγR1 chain of 1fg9	1fyh
1	134	7	V35, A114	C D	-
2	133	5	-	-	B E
3	470	14	D124	C D	-
4	262	9	H222	C D	B E
5	120	6	-	C D	E
6	165	7	-	C D	E
7	177	7	-	D	B E
8	138	5	-	C	B

*Surface calculated with a probe radius of 0.25 ˚A for cavities combined from all relevant receptor chains.
†Some residues are shared by neighboring cavities.

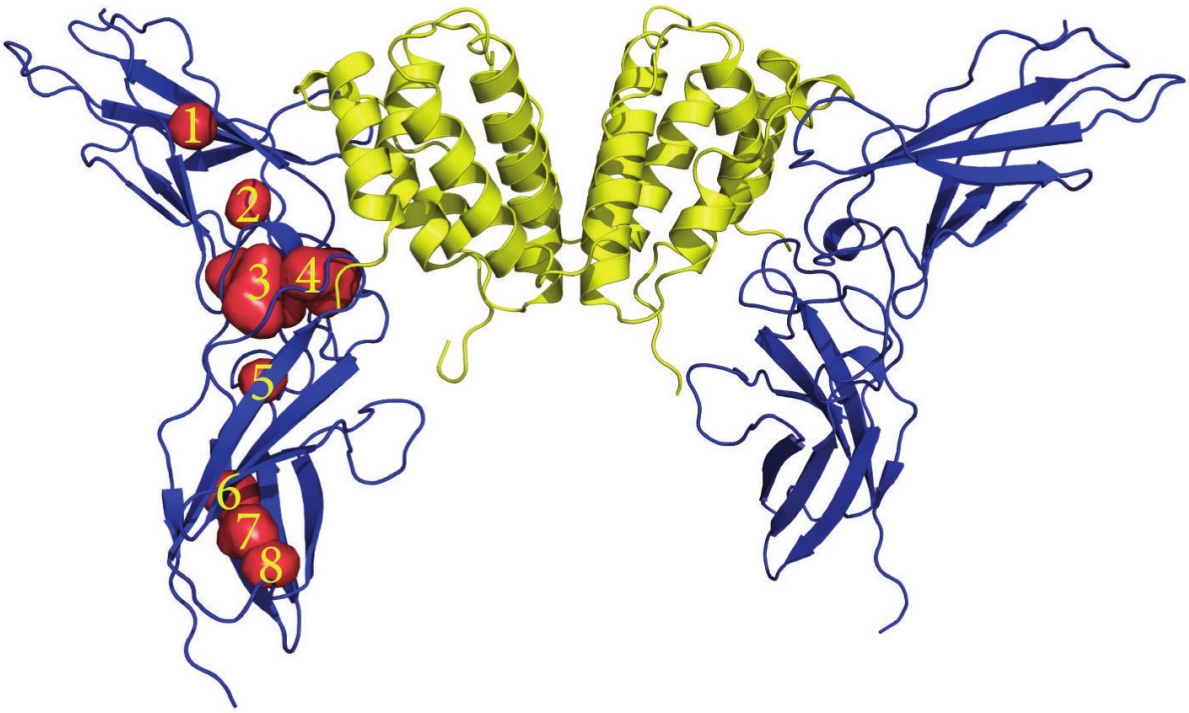

Figure 3.1A – The binary complex between IFN-γ and IFN-γR1 from the crystal structure of PDB code 1fg9 [32]. The molecules of IFN-γR1 are drawn in blue and the IFN-γ homodimer is in yellow. The protein cavities analyzed in this study are drawn as red surface and numbered from the top (N-terminus) to the bottom (C-terminus). Analyzed mutants are located in the cavities 1 (V35, A114), 3 (D124), and 4 (H222)

[1]		GLY	ALA	VAL	LEU	ILE	SER	THR	CYS	MET	ASN	GLN	LYS	ARG	HIS	PRO	ASP	GLU	PHE	TYR	TRP
VAL	35	2.8	2.0	0.0	−0.9	−0.4	2.9	1.6	1.3	0.1	2.0	2.5	3.5	5.1	4.7	1.2	3.4	3.5	4.3	7.3	10.6
VAL	46	3.8	2.2	0.0	−0.1	−0.3	3.1	1.8	1.8	0.6	2.4	3.0	4.1	6.4	6.4	2.0	3.6	3.7	4.0	6.6	9.1
VAL	100	5.6	3.7	0.0	0.3	−0.3	4.2	2.4	2.7	0.8	3.6	3.9	5.4	7.6	6.2	5.0	5.5	5.1	4.0	6.8	9.8
VAL	102	5.2	3.3	0.0	1.2	−0.4	4.0	2.2	2.5	1.8	3.6	4.1	7.1	11.9	9.4	4.8	4.9	4.9	7.5	11.2	15.6
ALA	114	1.0	0.0	−0.2	0.1	0.1	0.3	0.2	0.1	0.3	0.6	0.2	0.2	0.7	3.3	2.3	1.1	0.3	0.7	1.0	1.9
ASP	124	3.0	2.2	2.5	1.4	2.5	2.3	2.7	2.0	1.7	0.7	1.4	1.8	2.1	2.3	5.7	0.0	1.5	1.4	1.6	2.5
GLY	125	0.0	2.0	6.0	6.4	7.7	2.9	5.6	3.0	4.7	5.7	6.8	8.1	10.1	31.3	6.2	7.1	7.1	12.0	14.1	21.8
ILE	169	5.1	3.7	1.1	0.1	0.0	4.7	3.2	2.9	0.3	3.0	3.2	4.1	5.5	3.9	1.8	4.2	3.6	1.9	4.7	7.0
HIS	222	0.7	0.1	0.8	−0.3	1.1	−0.3	0.6	0.4	−0.3	−0.6	0.5	−0.1	0.3	0.0	2.9	−0.1	0.5	−1.1	−0.7	1.1
VAL	223	2.5	2.0	0.0	0.7	0.3	3.7	1.4	2.3	0.9	3.0	3.2	3.8	6.3	14.2	7.3	4.6	4.9	7.6	11.5	15.6
TRP	224	5.5	4.7	3.5	2.8	3.1	5.5	4.9	4.5	2.4	4.8	4.2	4.2	4.0	3.3	4.6	5.9	5.2	1.1	1.5	0.0
GLY	225	0.0	1.5	3.3	2.0	3.4	2.0	3.3	1.8	1.6	2.1	2.5	2.6	2.9	4.7	4.3	2.9	3.0	2.4	2.6	2.9

[2]		GLY	ALA	VAL	LEU	ILE	SER	THR	CYS	MET	ASN	GLN	LYS	ARG	HIS	PRO	ASP	GLU	PHE	TYR	TRP
VAL	35	2.8	2.0	0.0	−0.9	−0.4	2.9	1.6	1.3	0.1	2.0	2.5	3.6	5.3	4.5	1.2	3.4	3.5	4.3	7.3	10.7
VAL	46	5.0	3.0	0.0	−0.2	−0.5	4.1	2.4	2.4	0.5	3.2	3.8	5.1	8.1	7.6	2.9	4.8	4.8	4.4	7.9	11.5
VAL	100	5.7	3.8	0.0	0.3	−0.3	4.2	2.4	2.7	0.8	3.7	4.0	5.5	7.7	5.9	5.0	5.5	5.1	4.1	6.8	9.7
VAL	102	5.2	3.3	0.0	1.2	−0.4	4.0	2.2	2.5	1.8	3.6	4.1	7.1	11.9	9.5	4.8	4.9	4.9	7.5	11.2	15.7
ALA	114	1.0	0.0	−0.2	0.2	0.2	0.3	0.2	0.1	0.4	0.7	0.3	0.3	0.7	3.4	2.3	1.2	0.5	0.8	1.1	2.0
ASP	124	2.4	1.6	2.0	0.7	1.7	1.8	2.1	1.6	0.9	0.9	1.3	1.0	1.4	1.5	4.8	0.0	1.4	1.0	1.2	1.8
GLY	125	0.0	2.0	6.0	6.4	7.8	2.9	5.6	3.0	4.8	5.8	6.8	8.2	10.2	32.2	6.2	7.1	7.2	12.1	14.2	21.9
ILE	169	5.1	3.7	1.1	0.1	0.0	4.7	3.2	2.9	0.3	3.0	3.2	4.2	5.6	3.8	1.8	4.2	3.7	1.9	4.7	7.0
HIS	222	−0.1	−0.6	0.5	−0.4	0.6	−1.0	0.2	−0.1	−0.4	−0.7	0.2	−0.5	0.0	0.0	2.3	−0.3	−0.2	−0.9	−0.7	0.6
VAL	223	0.9	0.6	0.0	0.2	−0.2	1.7	0.4	1.2	0.1	1.2	1.1	0.5	0.9	1.0	5.6	1.6	1.2	0.1	0.3	0.6
TRP	224	2.7	2.1	1.3	1.2	1.1	2.5	2.1	1.9	0.9	2.2	1.9	1.6	2.0	2.0	2.2	2.4	2.0	0.3	0.6	0.0
GLY	225	0.0	1.2	1.9	0.8	1.7	1.2	1.7	1.1	0.6	0.9	0.9	0.8	1.0	1.0	2.8	1.0	1.0	0.4	0.5	0.3

[3]		GLY	ALA	VAL	LEU	ILE	SER	THR	CYS	MET	ASN	GLN	LYS	ARG	HIS	PRO	ASP	GLU	PHE	TYR	TRP
VAL	35	0.0	0.0	0.0	0.0	0.0	0.0	0.0	0.0	0.0	0.0	0.0	−0.1	−0.2	0.0	0.0	0.0	0.0	0.0	0.0	−0.1
VAL	46	0.0	0.0	0.0	0.0	0.0	0.0	0.0	0.0	0.0	0.0	0.0	0.0	0.0	0.0	0.0	0.0	0.0	0.0	0.0	0.0
VAL	100	0.0	0.0	0.0	0.0	0.0	0.0	0.0	0.0	0.0	0.0	0.0	0.0	0.0	0.0	0.0	0.0	0.0	0.0	0.0	0.0
VAL	102	0.0	0.0	0.0	0.0	0.0	0.0	0.0	0.0	0.0	0.0	0.0	0.0	0.0	0.0	0.0	0.0	0.0	0.0	0.0	0.0
ALA	114	0.0	0.0	0.0	−0.1	−0.1	0.0	0.0	0.0	−0.1	−0.1	−0.1	−0.1	0.0	−0.1	0.0	−0.1	−0.2	−0.1	−0.1	−0.1
ASP	124	0.2	0.1	0.0	−0.1	0.1	0.1	0.0	−0.1	−0.1	−0.2	−0.2	−0.1	−0.1	0.1	0.2	0.0	−0.1	−0.1	−0.1	0.1
GLY	125	0.0	0.0	0.0	0.0	−0.1	0.0	0.0	0.0	0.0	0.0	0.0	−0.1	−0.1	−0.1	−0.1	0.0	0.0	−0.1	−0.1	−0.1
ILE	169	0.0	0.0	0.0	0.0	0.0	0.0	0.0	0.0	0.0	0.0	0.0	0.0	0.0	0.0	0.0	0.0	0.0	0.0	0.0	0.0
HIS	222	1.3	1.2	0.9	0.7	0.8	1.1	0.9	0.7	0.4	0.3	0.5	0.4	0.2	0.0	1.2	0.5	0.6	0.1	0.2	0.8
VAL	223	1.7	1.4	0.0	0.1	0.4	2.0	0.8	1.2	0.3	1.5	1.6	2.0	3.2	6.1	2.2	2.7	2.9	5.7	8.2	10.4
TRP	224	3.3	3.1	2.6	1.8	2.2	3.3	3.0	3.0	1.4	2.9	2.3	2.4	2.0	1.3	2.8	3.6	3.1	0.9	0.8	0.0
GLY	225	0.0	0.3	1.1	0.6	1.2	0.6	1.2	0.4	0.3	0.8	0.9	0.9	0.9	2.9	1.3	1.4	1.3	1.1	1.1	1.4

Figure 3.1B – Changes of free energies (ΔΔG values, average value from 500 10 ns molecular dynamic relaxation snapshots) calculated using the FoldX program for 12 promising residues located in the IFN-γR1 chain C protein cavities (PDB 1fg9 [32]). Conditional formatting is used to highlight the differences. Red color indicates stabilization (negative ΔΔG values), blue color is for positive ΔΔG values (destabilization). 1) ΔΔG of folding of IFN-γR1 in complex; 2) ΔΔG of folding of free IFN-γR1; 3) ΔΔG of binding;

3.1.2 Binding kinetics determination

Only four consensus candidates were chosen from the 12 promising positions for the verification. Interestingly, two mutations (V35L and H222Y) were predicted to increase ΔΔG for both the complexed and free IFN-γR1 and the second pair (A114E and D124N) was predicted to slightly improve ΔΔG of binding (complex) while their ΔΔG of folding were destabilizing. Affinities relative to wt measured by SPR for all cavity mutants are shown in **Figure 3.1C** together with the analysis of N96W and cavity double mutants. The dissociation constants (Kd values) for the four selected "cavity" single amino acid mutants showed almost no change in affinity. Conservative changes were acquired for H222Y (decrease) and V35L (increase). The combination of cavity mutants with previously identified N96W showed more

interesting results and additive effects. Except the N96W + D124N mutant the measured affinities were significantly higher than wt and N96W alone. Moreover, the stability measurement showed a correlation of our results with computed stability differences analyzed in the term of ΔΔG changes. These results proved the suitability of this method for modulation of protein-protein interactions.

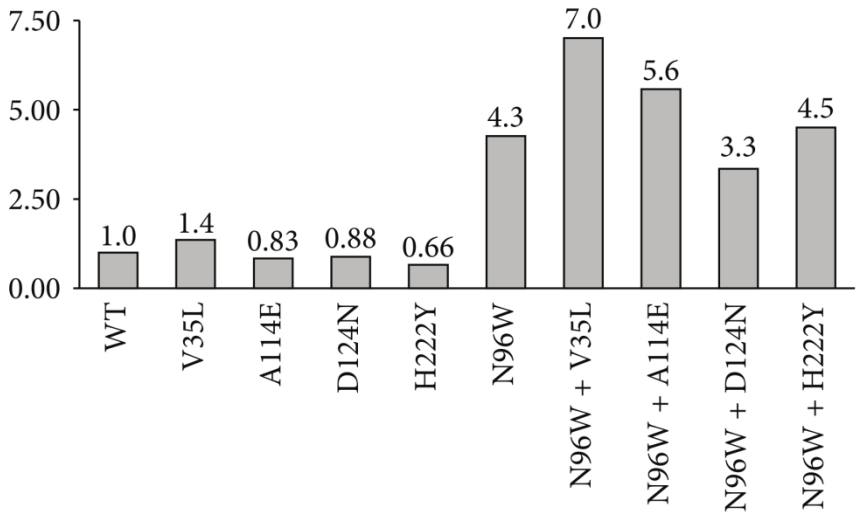

Figure 3.1C – SPR measured affinities between the IFN-γ single chain variant [117] and IFN-γR1"cavity mutants". Values are normalized to wt IFN-γR1 (labeled WT). The mutation N96W is the best mutant located on interaction interface identified in our previous study [124].

3.2 Structural biology analysis of IFN-γR2

Mikulecký, P., **Zahradník, J.**, Kolenko, P., Černý, J., Charnavets, T., Kolářová, L., Nečasová, I., Pham, P.N., Schneider, B. (2016) Crystal structure of human interferon-γ receptor 2 reveals the structural basis for receptor specificity. *Acta Crystallogr D Struct Biol* 72(9):1017-25.

The molecular structure of the extracellular portion of human IFN-γR2 was investigated. This study uncovered the structure of the so far missing part of the IFN-γ complex and also the last unknown structure of the class II receptor family. It was also the critical prerequisite for the study of the whole ternary complex composition. The structure has been solved by molecular replacement phasing at 1.8 Å crystallographic resolution. A structure-based bioinformatics analysis and comparison with other members of class II family receptors revealed independent structural and evolutionary aspects of IFN-γR2. We also identified the putative binding site for interferon gamma by an analysis of variable regions and by the analogy with other receptors. Obtained results were described in a structural biology oriented journal publication (Supplement 2) and the structure was deposited into PDB under the code: 5eh1.

3.2.1 Crystallization of IFN-γR2, data collection and structure refinement

After the initial trials' failure to produce IFN-γR2 in bacterial expression systems we adopted *Drosophila melanogaster* Schneider´s S2 cells. The cell line was derived by Dr. Imogene Schneider from the late stages of *Drosophila* embryos [151]. We cloned the extracellular part of IFN-γR2 (residues 28–247; UniProt P38484) into the pMT/BiP/V5-His A vector by *Bgl*II and *Age*I restriction enzymes to create an expression construct with N-terminal insect BiP signal peptide and C-terminal His tag. We transfected the S2 cells with constructed plasmid and established a stable cell line in a HyClone SFX-Insect medium supplemented by Blasticidine S. This procedure led to good production with the overall yield of approximately 50 mg/L. The purified protein was deglycosylated by Endoglycosidase H and crystals were grown by using the sitting-drop vapor-diffusion method. The diffraction quality crystals were mounted, cryoprotected and the data were collected at 100 K on beamline MX 14.1 of the BESSY II synchrotron-radiation source at the Helmholtz-Zentrum Berlin (HZB). Diffraction data were processed, scaled (XDS program package, [152], and solved by a molecular replacement pipeline (BALBES, [153]). Subsequent refinement was carried out with REFMAC5 [154]. The structure was validated and deposited into the PDB database.

3.2.2 IFN-γR2 and its characteristics

The IFN-γR2 protein produced in S2 cells has a classical type II receptor structure. The receptor is composed of two Fibronectine type III domains connected by a short linker. The extracellular part of the receptor has five potential glycosylation sites (Asn56, Asn110, Asn137, Asn231, Asn85) occupied and only one glycosylation site was not used (Asn219). Interestingly, glycosylation at positions Asn110 and Asn137 shields the hydrophobic surface of Trp131 by formation of a sandwich-like structure (**Figure 3.2A**). We confirmed the indispensability of these two glycosylations by a mutation study. The disulfide bond analysis identified bonds linking Cys86 to Cys94, Cys209 to Cys234, and the fifth residue Cys174 forms an unusual S-S bond to free amino acid cysteine probably due to its occurrence in the culture media. Our analysis of the structure revealed a distinct structural motif of six stacked residues interacting by π-cation interaction: Lys68, Trp74, Arg114, Trp126, Arg116, and His123 (**Figure 3.2A**). An analogous stacking motif is known from the type I receptor family as the motif with the consensus sequence WSXWS [119].

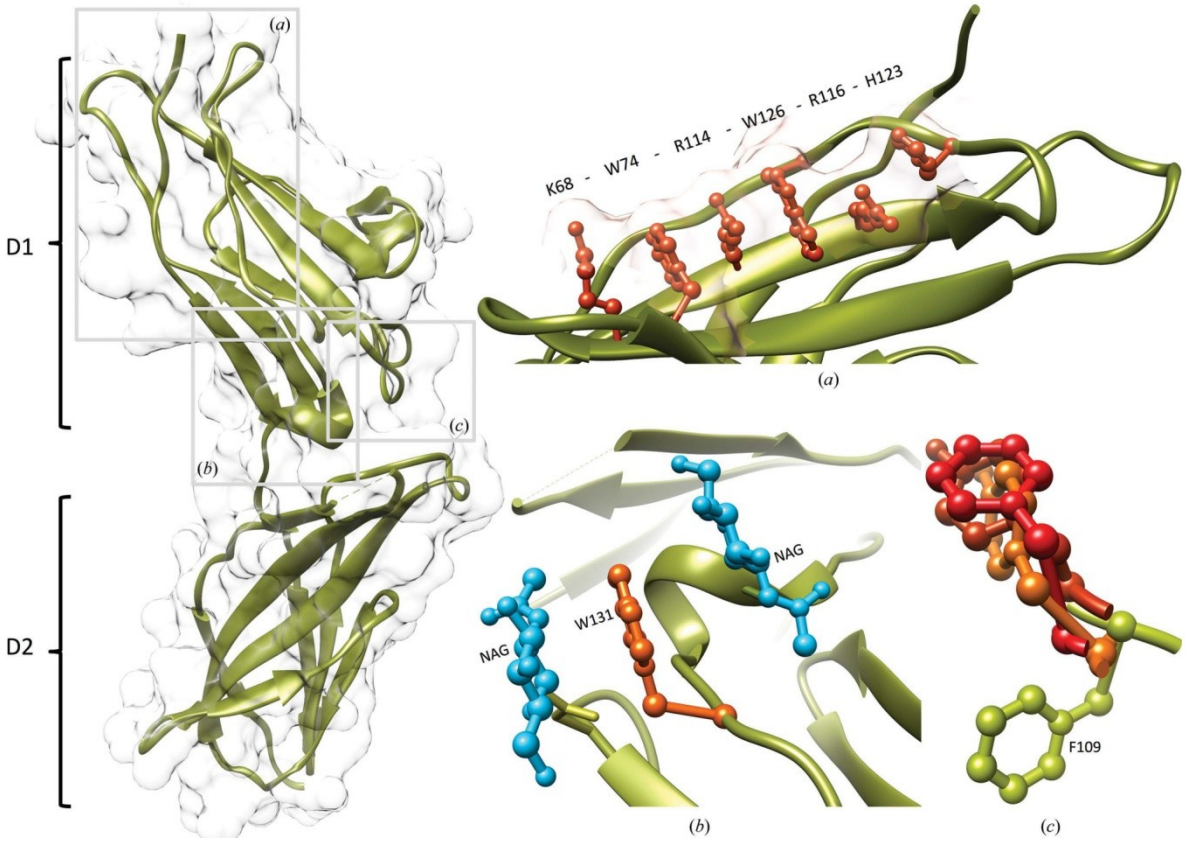

Figure 3.2A – Structure of IFN-γR2 in ribbon and surface representations. Insets: (a) Stacking motif of residues Lys68, Trp74, Arg114, Trp126, Arg116, and His123 in the D1 domain. (b) N-Acetyl-d-glucosamine attached to Asn110 and Asn137 (NAGs; blue) forms a sandwich with Trp131 (orange) and thus shields its hydrophobic character. (c) The superposition of matching central residues of binding epitopes among IFN-γR2 (Phe109 in green), IL-10R2 (Tyr82) [155], gp130 (Phe169) [156], and γc (Tyr103) [157].

In an attempt to find the interface on the IFN-γR2 surface that binds to its ligand IFN-γ, we computed an alignment of IFN-γR2 sequences from 90 different species and used the ConSurf server [158] to indicate sequence (dis)similarities as they project on the surface of the only known structure of IFN-γR2 (**Figure 3.2B**). The residues that are subject to the fastest evolution form one patch on the IFN-γR2 surface. This patch is situated between D1 and D2 domains and centered on the F109. This residue is in the virtually identical position (Figure 3.2A) in all known receptor structures IL10R2 (PDB entry 3lqm; [155]), Phe169 of gp130 [PDB entry 1bqu; [156]), and Tyr103 of γc receptor (PDB entry 4gs7; [157]). We therefore hypothesize that the surface patch putatively interacting with IFN-γ is situated among these highly variable residues.

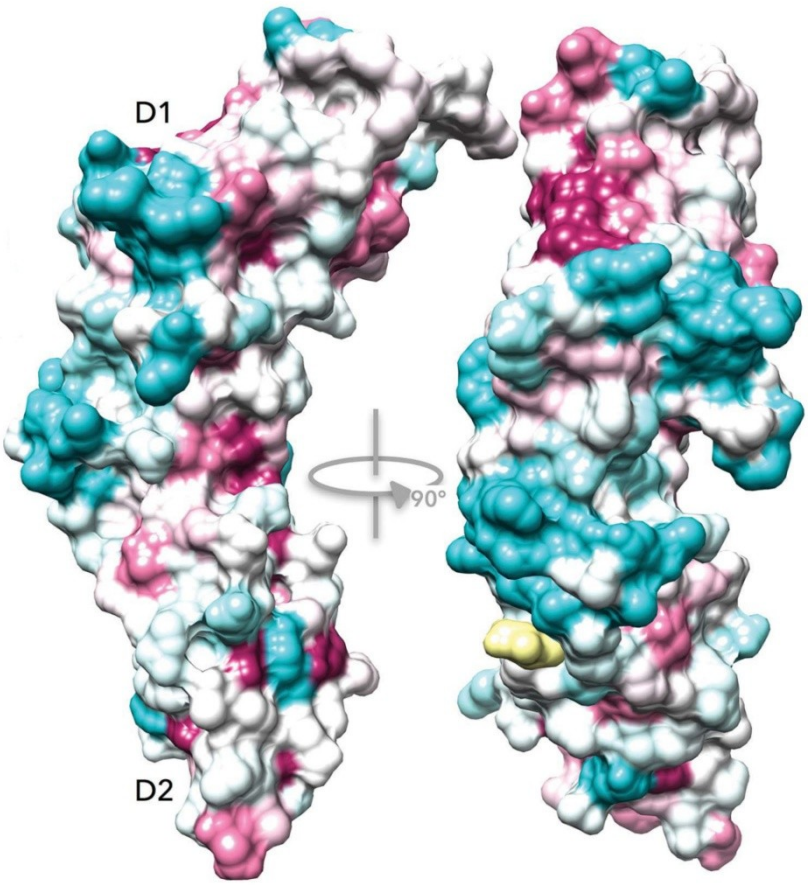

Figure 3.2B – Structurally variable regions in the IFN-γR2 structure and the proposed interaction interface with IFN-γ. Color coded sequence variability was produced by using an alignment of IFN-γR2 from 90 different species and the ConSurf server [158]. The most variable regions are colored cyan and conserved regions are drawn in purple. The free cysteine attached on odd Cys174 is highlighted in yellow. The putative interface creates a circle of highly variable residues in the middle of the IFN-γR2 structure.

3.2.3 Comparison of class II receptors

We performed a structural alignment of all structures of class II receptors by overlapping all possible receptor pairs (in total 144 pairs). Domains D1 and D2 were aligned independently and the mutual angle between D1 and D2 domains varied among receptors and was discarded for a better alignment. The numerical representation of the alignment results is shown in Figure 3.2C. Interestingly, the D1 domains are mutually more similar than the D2 domains.

Our analysis of class II receptors also showed a similar motif, but sequentially non-continuous with the sequence (X)WRWR(X), where X is K, R, or H. An analysis of interaction energies for this motif suggests that it contributes significantly to the overall stability. Besides the motif (X)WRWR(X) we found a continuous chain of residues R-L/VR-A (residues Arg114-Leu115-Arg116-Ala117 in IFN-γR2). The comparison of D2 revealed a considerable variability, two conserved proline residues, Pro142 and Pro143, a structurally well conserved motif 175-YNVAXW-180, and a disulfide bridge between Cys209 and Cys234 (IFN-γR2 numbering).

PDB code	1fg9	5eh1	1j7v	3lqm	4doh	4doh	3dlq	3g9v	3og6	3se4	3se4	2puq
Chain ID	*C*	*A*	*R*	*A*	*E*	*B*	*R*	*A*	*B*	*A*	*C*	*T*
Receptor	IFNγR1	IFNγR2	IL10R1	IL10R2	IL20R1	IL20R2	IL22R	IL22BP	IL28R	IFNαR1	IFNαR2	TF
IFNγR1	*0.82*	0.87	0.73	0.73	0.80	0.78	0.90	0.71	0.82	1.35	1.12	0.85
IFNγR2	1.27	*0.79*	0.93	0.97	0.79	0.79	0.96	0.80	0.85	1.45	1.25	1.04
IL10R1	1.22	1.12	*1.07*	0.74	0.97	0.88	0.94	1.43	1.13	0.81	0.67	0.66
IL20R2	1.00	1.14	1.05	*0.89*	0.95	1.05	0.65	0.87	0.68	0.80	1.11	0.93
IL20R1	0.93	1.32	0.89	1.33	*1.59*	0.93	0.97	0.63	0.75	0.59	1.36	1.15
IL20R2	1.32	1.51	1.23	0.99	1.33	*0.91*	0.93	0.66	0.82	1.48	1.25	1.21
IL22R	1.20	1.49	1.09	0.86	1.04	1.16	*4.19*	1.20	1.19	0.87	0.98	1.03
IL22BP	1.32	1.48	0.94	1.20	1.18	1.30	1.17	*0.93*	1.02	1.16	1.11	0.96
IL28R	1.21	1.16	1.34	1.29	1.30	1.32	1.18	1.45	*0.91*	1.09	0.77	0.86
IFNαR1	1.16	0.96	1.31	1.33	1.33	0.98	1.75	1.26	1.59	*1.77*	0.94	1.20
IFNαR2	1.35	1.80	1.40	1.29	1.19	1.81	1.58	1.14	1.46	1.22	*1.43*	1.02
TF	1.38	1.16	1.23	1.26	1.44	1.04	1.16	1.40	1.43	1.16	1.81	*0.86*

Figure 3.2C – The global comparison of all 12 members of the class II cytokine receptor family. The structural differences between the N-terminal (D1, above diagonal) and C-terminal (D2, below diagonal) domains are gauged by the root mean square deviations (r.m.s.d.) for backbone atoms of their 34 residues. The diagonal (in grey) shows the lowest r.m.s.d. values for 34 residues from D1 and D2 of each receptor. The differences among r.m.s.d are highlighted by color: lower values of r.m.s.d. are in blue, i.e. more similar structures, red indicates less similar structures. References to the analyzed structures are as follows: IFN-γR1 [32]; IL-10R1 [159]; IL-10R2 [155]; IL-20R1 and IL-20R2 [106]; IL-22R [160]; IL22BP [161]; IL28R [162]; IFN-αR1 and IFN-αR2 [163]; TF (human tissue factor) [164]

3.3 Interferons type II and their receptors in fish species

> **Zahradník, J.**, Kolářová, L., Pařízková, H., Kolenko, P., Schneider, B. (2018) Interferons type II and their receptors R1 and R2 in fish species: Structure, function & evolution. *Fish Shellfish Immunol* 79, 140-152

Type II interferons evolved early in the evolution of chordates and are therefore present in extant cartilaginous fish, bony fish, as well as in tetrapods [165]. Fish and tetrapods split about 225 - 333 million years ago and they show a specific evolutionary adaptation [166]. Therefore, the teleost fish are an attractive target for studying evolution. Their attractiveness is strengthened by their vast genomic variability [167]. In contrast to the mammalian type II interferon, the fish type II family is broader in majority of species, consisting of two independent members, IFN-γ and fish-specific IFN-γ related (IFN-γrel) proteins. Moreover, in some fish species the interferon genes are additionally duplicated resulting in more copies. This huge variability of type II interferons in fish species motivated us for a deeper analysis. We did a thorough phylogeny study of IFN-γ and its receptors in fish species. Based on this phylogeny, we studied their-whose co-evolution in fish species and supported our computations by biophysical interaction measurements. To shed a light on the differences of fish type II we determined the crystal structure of IFN-γ from olive flounder *Paralichthys olivaceus* (PDB code 6f1e) and the low-resolution topologies of four other fish interferons by Small Angle X-ray diffraction (SAXS). Our results were published in the official journal of the International Society of Fish and Shellfish Immunology.

3.3.1 Structure of IFN-γ from *Paralichthys olivaceus*

After an extensive screening for multiple fish interferons we established a *Paralichthys olivaceus* IFN-γ production from E. coli Rosetta (DE3) without any tags. The easy purification was enabled by the extreme pI of the protein (10.5). Diffraction quality crystals were obtained only after elimination of 11 amino-acids at the C terminus. The structure was solved at 2.3 Å resolution only after experimental phasing using selenourea labeling [168]. Our data were deposited into the PDB database under the ID 6f1e. It shows the expected homodimer with an IFN-γ fold, but with some unpredicted features (**Figure 3.3A**). One monomer depicted in **Figure 3.3A** by blue color is not composed of six α-helices as in all other known IFN-γ structures, but of seven with the additional helix G close to the C-terminus. The second interesting feature distinguishing the IFN-γ from *Paralichthys olivaceus* from its mammalian counterparts is the mutual orientation of helices D and E, which resulted in the extension of the whole structure.

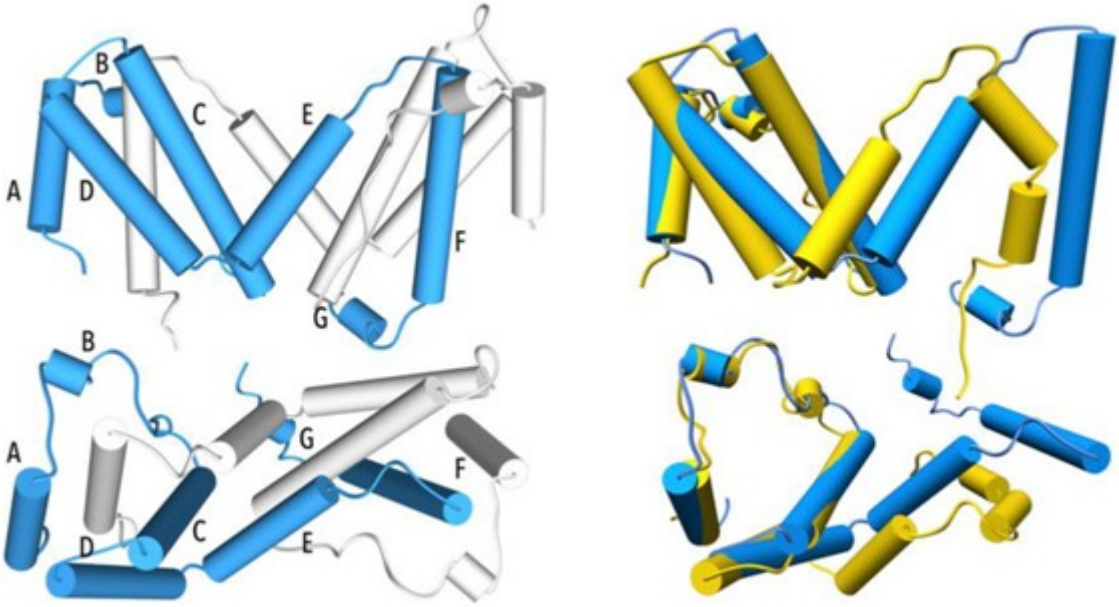

Figure 3.3A – Three-dimensional structure of the IFN-γ from *Paralichthys olivaceus* (PDB 6f1e, in left). Monomers are drawn in blue and white. Helices are displayed in cylinders representation and labeled A – G. The right part shows the superposition of the IFN-γ from *Paralichthys olivaceus* with the human IFN-γ (PDB 1fg9, [32]). The top and bottom images are related by an approximately 90° rotation.

3.3.2 Phylogeny of fish IFN-γ and its receptors

We performed an extensive search for all available IFN-γ complex members in available databases (NCBI Protein, UniProt and Ensembl). Only a small proportion of sequences were correctly annotated. Other hits were carefully considered if they belonged to IFN-γ complex members. The majority of proteins were identified by using gene synteny with human genome. We identified or newly annotated 28 IFN-γ and IFN-γrel, 60 IFN-γR1, and 40 IFN-γR2. The changes of annotations for all IFN-γ, IFN-γR1, and IFN-γR2 were recorded, reflected in ZFIN (Zebrafish Information Network; zfin.org), and submitted to the NCBI database. After curating our data, the ZFIN database created a new consistent nomenclature of IFN-γ, IFN-γrel, IFN-γR1, IFN-γR1-like, and IFN-γR2 proteins identified in fish species.

All successfully gained sequences were subjected to the phylogenetic analysis by the Bayesian inference and maximum likelihood methods. Our results are summarized in **Figure 3.3B.** The phylogeny of IFN-γ protein genes confirmed the existence of two closely related type II members in fish species – IFN-γ and the IFN-γ related protein IFN-γrel. Surprisingly, we observed that there are likely two independent groups of IFN-γrel proteins: IFN-γ relC occurring in *Cypriniformes*, *Characiformes* and *Siluriformes,* and IFN-γrelA occurring in

Acanthomorpha. Our data for IFN-γR1 proteins indicate the presence of two distinct genes (*IFN-γR1* and *IFN-γR1-like*) in all fish orders except the evolutionarily oldest one, *Holostei.* This situation was expected due to the presence of two type II interferons. In contrast to IFN-γR1 proteins the phylogeny of the extracellular domains of fish IFN-γR2 almost exactly reflects the evolution of fish species and no fission occurs. Therefore, there is no evidence for the two groups of IFN-γR2 corresponding to two completely different ternary complexes. We hypothesized the receptor sharing of IFN-γR2 which is common for the accessory chains belonging to class II cytokine receptors [155].

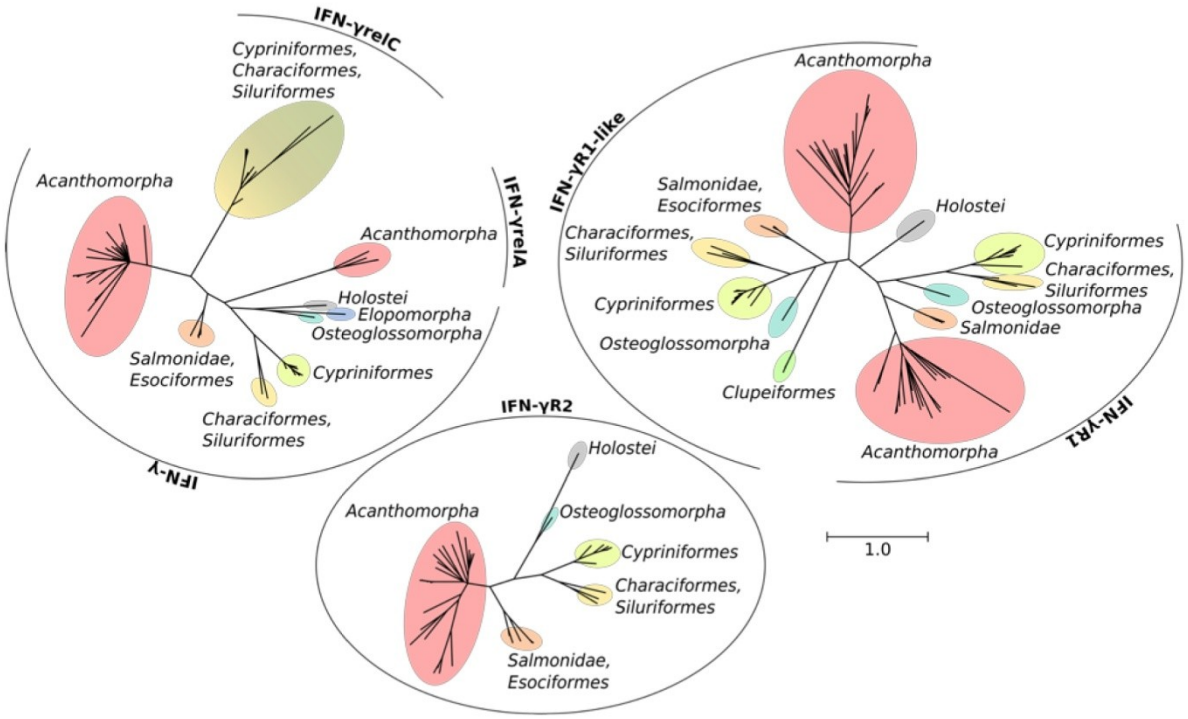

Figure 3.3B – Phylogeny of fish IFN-γ (top left), IFN-γ receptor 1 (top right), and IFN-γ receptor 2 (bottom) inferred by Bayesian inference. Branches with posterior probability lower than 0.5 were collapsed. Color scheme reflects fish classification.

3.3.3 Coevolution of fish IFN-γ with its receptors

The detailed phylogeny inference enabled us to study the molecular co-evolution between two identified receptors R1, IFN-γ and IFN-γrel proteins. We tested the interactions both programmatically by searching for the coevolution of the receptor-ligand pairs and experimentally by determination of interaction Kd. The computations were performed on the level of phylogeny by using the Parafit software [169]. For the receptor-ligand co-evolution at the amino acids level we used the i-COMS web-server [170]. Unfortunately, our Parafit

computations were not significant due to the low p-values. Despite this it can be concluded that IFN-γ more likely to co-evolve with IFN-γ R1 and not with IFN-γR1-like. Results of i-COMS on aminoacid co-evolution level were also not demonstrable. Analysis revealed core associated coevolving pairs rather than intermolecular contacts, a previously reported ‚common problem of covariance-based methods [171]. In contrast to the bioinformatics, biophysical measurements showed consistent results of interaction between IFN-γ and IFN-γR1 with approximately 100 nM Kd for three different fish species. The interaction pair IFN-γ and IFN-γR1-like also exhibits measurable affinity which is almost three times higher (~300 nM). Our results are thus in good agreement with the previous results in Zebrafish [172] and can be generalized.

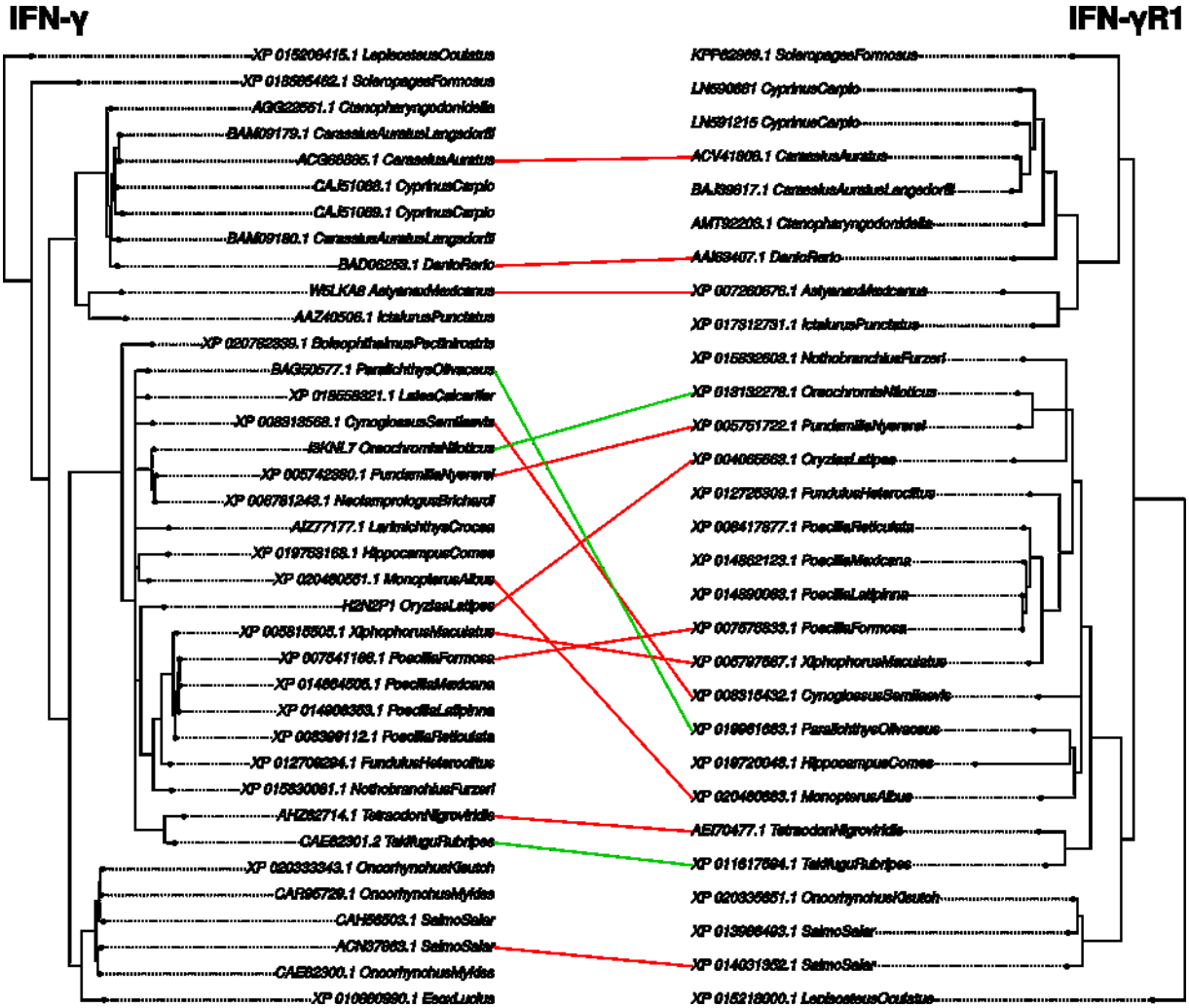

Figure 3.3C – Graphical representation of co-evolution between IFN-γ and IFN-γR1 in fish species. Phylograms were computed by Bayesian inference and correspond to Fig. 3.3B. Red links between the receptor and the ligand correspond to significant evolutionary links (p-value lower than 0.1). Green links correspond to the interactions we confirmed biophysically.

3.4 The topology of the ternary complex

> Manuscript in preparation: Zahradník, J., Mikulecký, P., Biedermannová, L., Černý, J., Klumpler, T., Kolářová, L., Kukačka, Z., Pham, P.N., Schneider, B.: **Topology of complexes between interferon-gamma and extracellular portions of its two receptors R1 and R2.**

All knowledge gained during the study of IFN-γ enabled us to investigate the topology of the ternary complex, which is currently unknown. Most of the current models of the ternary complex suggest that it comprises of two R1 receptor chains [20,173] and two R2 chains [174,175] forming thus a symmetrical complex. However, various experimental data including ours suggest that the situation is more complex. The crystal structure of IFN-γ in complex with R1 shows an unexpected stoichiometry of 1:3 (one IFN-γ dimer interacting with three IFN-γR1 chains) [32]. Moreover, signaling activity was observed in a modified IFN-γ with only one binding site for IFN-γR1 but two for IFN-γR2 [117]. The formation of the assumed symmetrical complex is therefore not a necessary prerequisite for signaling. The hypothesis behind our study is that the variability in ternary complex topology is an important biologically relevant trait with a consequence on signaling.

Our investigation is still ongoing and the manuscript is being prepared. Nevertheless, I would like to briefly introduce the most important parts of our results on ternary complex to complete the story about IFN-γ covered in my thesis. The results will be published in an impacted scientific journal with a biophysical and biochemical scope.

3.4.1 Determination of the binding site of IFN-γR2

The crucial missing part of our knowledge about the ternary complex is the location of the binding interface for the IFN-γ. Unfortunately, the direct measurement of binding affinity and the alanine scanning or other common technique are restricted due to the affinity between IFN-γ and IFN-γR2 (below detection limit). A similar observation was described for the IL-10R2 in the ternary complex with IFN-λ [136]. Therefore, we developed a new competitive assay based on the dual luciferase reporter system. The principle of the assay was simple. The native ternary complex assembly on the cell surface competed with the artificial ternary complex added to the cell media. The artificial complex consists of the extracellular portion of IFN-γR1 and the extracellular portion of different mutants of FN-γR2. The competition was recorded by a measurement of different luciferase activation under the control of GAS

element. To increase the signal to noise ratio in our assay we did not use alanine scanning but the more dramatic changes of amino acid. We analyzed these mutations: K12Q, K48Q, M55Y, S75Y, S77Y, D83K, E122R, D142R, F147G, D175R, K195Q, F199A, and H203A. The results are shown in **Figure 3.4A**. Our results showed that residues at positions 48, 77, 83, 142, and 195 are at the interface or in its close proximity. This result is in good agreement with our previous bioinformatics study [96].

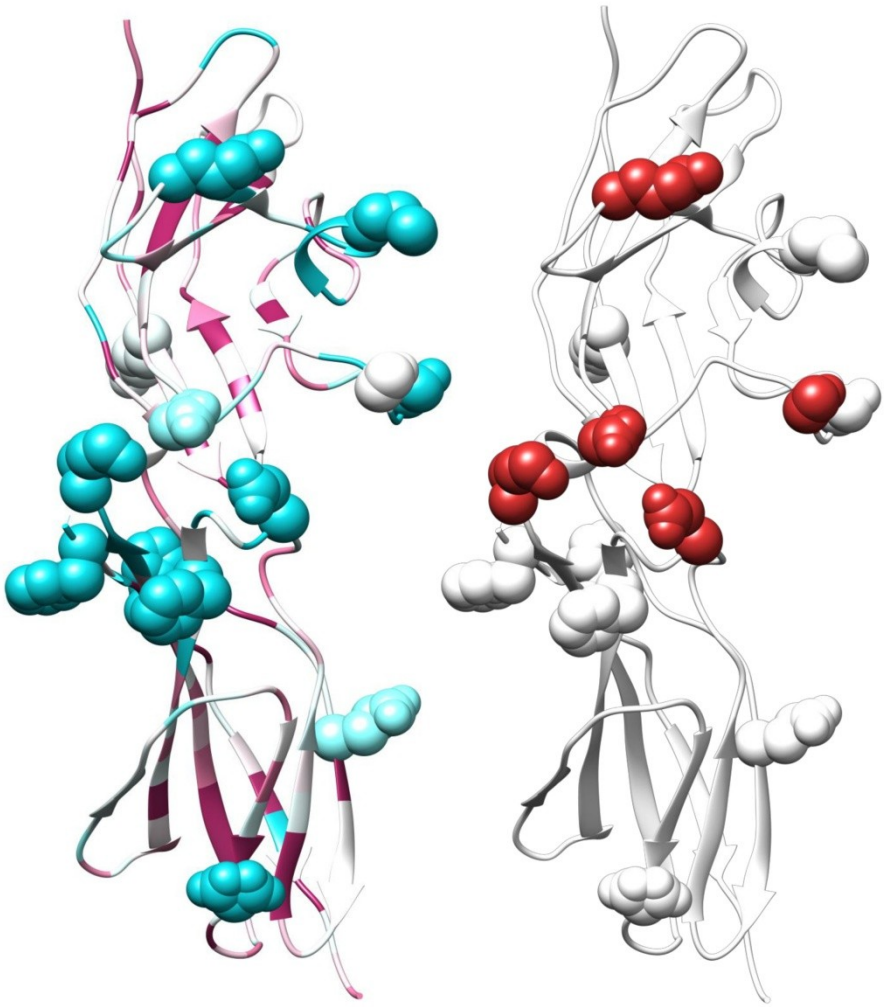

Figure 3.4A – Determination of IFN-γR2 binding site. The left schema represents a Consurf server [158] analysis of variable regions in the IFN-γR2 structure with sphere representation of mutated residues. The most variable regions are colored cyan and conserved regions are drawn in purple. Only high (cyan) to medium (white) residues were considered for the study. The right structure highlights in red the mutations with significant impact on IFN-γR2 activity in the competition assay.

3.4.2 Low resolution topology

To simplify this section all the data and methodology are only briefly introduced and I focus on the results and their discussion. To elucidate the topology of the complexes of IFN-γ with its receptors, we performed multiple Small Angle X-ray Scattering (SAXS) experiments. Our data showed high concentration dependency and therefore we decided to use the combination of size exclusion chromatography with SAXS (SEC-SAXS technique) [176]. Only this approach gave us relevant data which were analyzed mainly by rigid body modeling. We generated tens of models with different settings. The models were grouped according to their similarity and those biologically not relevant were discarded. The surface representation of the best model group is shown in Figure 3.4B. The position of IFN-γR2 in the ternary complex can be supported by analogy with IL-20 [106] and IFN-λ3 [136]. The position of the second receptor can be inferred by structural superposition of R1 chains. The result for this superposition is shown in Figure 3.4B, panel c.

Interestingly, both molecular weight calculations and models showed only one IFN-γR2 molecule bound in the complex. Similar results were obtained with different concentrations of IFN-γR2. Our preliminary data suggest the presence of 1:2:1 complex in the solution, which is a different model of IFN-γ complex than is generally assumed. Our results show high asymmetry. We do not exclude the possibility of the existence of 2:2:2 complexes which are generally expected but this stoichiometry is probably not the major one. Therefore, we propose that complex 2:2:1 is fully able to activate the Jak kinases and induce the cell response. The delicate balance between complexes may be used as a regulatory mechanism.

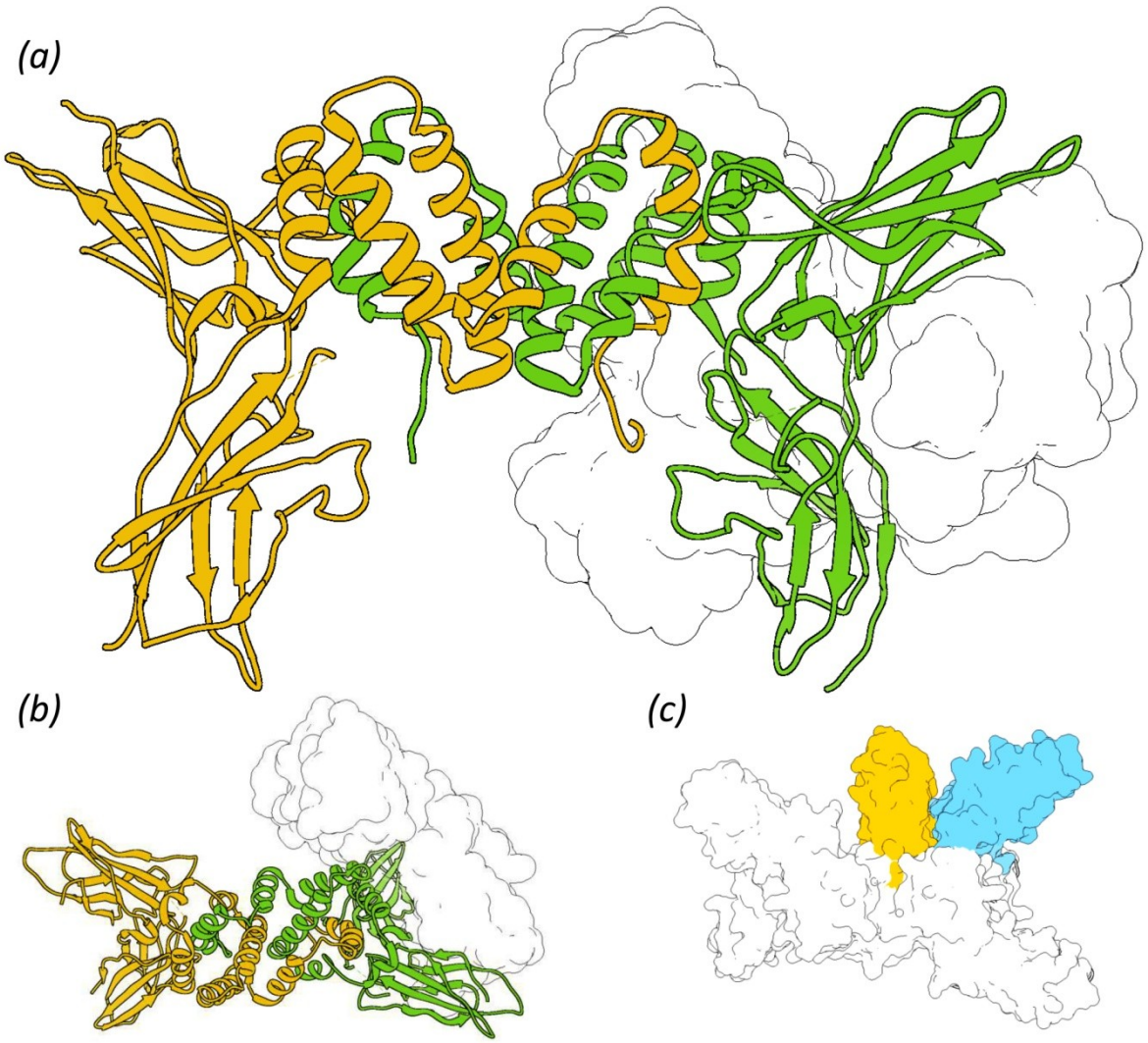

Figure 3.4B – Determination of IFN-γ ternary complex topology by SAXS technique and the analogy with known ternary complexes of FIL10 members. a) The putative position of the IFN-γR2 chain obtained from the SEC-SAXS analysis. The yellow and green represents individual halves of the symmetrical IFN-γ binary complex observed in pdb 1fg9 [32]. The position is indicated by ambient surface based on superposition of individual SEC-SAXS solutions (rigid body modelling). Side view representation. b) Top view representation of *(a)*. c) Determination of the putative position of IFN-γR2 by analogy with known ternary complexes. The IFN-γ binary complex os represented in ambien surface representation. The top view is similar to *(b)*. The R1 chains were superimposed and the position of accessory chains of IL-20 [106] and IFN-λ3 [136] is shown in blue and yellow, respectively. The corresponding R1 chains and ligands are not displayed.

4. Conclusions

This thesis describes a complex study of protein-protein interactions and their modulation in the IFN-γ ternary complex. It summarizes the content of three published manuscripts and one manuscript in preparation. These are the most important results:

I. The novel methodology which can be used for modulation of protein-protein interactions was successfully described. The method is based on the stabilization of interaction partners therefore lowering their flexibility. Lower flexibility decreases the entropic penalty which acts against binding.

II. The human IFN-γR2 was produced, purified, and crystallized. The structure was solved at 1.8 Å and deposited into PDB under the accession 5eh1. The structure was precisely described and compared with other class II cytokine receptor family members.

III. Fish members of the IFN-γ signaling complex were identified, annotated, and inferred by bioinformatic analysis. The comparison of fish evolution and the phylogeny of signaling complex members showed interesting information about the type II cytokine in fish. There are at least two type II interferon members IFN-γ and IFN-γrel. We identified also two specific receptors IFN-γR1 and IFN-γR1-like but only one IFN-γR2. Interaction affinities of three pairs of IFN-γ/ IFN-γR1 and IFN-γ/ IFN-γR1-like were biophysically determined and the crystal structure of IFN-γ from olive flounder *Paralichthys olivaceus* was solved at 2.3 Å (PDB code 6f1e). The unique features were identified and described. The structure enabled us to describe molecular co-evolution between IFN-γ and its high affinity receptor.

IV. The SEC-SAXS technique and mutations scanning was successfully used to analyze the IFN-γ ternary complex topology. By combined bioinformatic, biophysical, and biochemical methods we characterized the putative binding interface between IFN-γ and IFN-γR2.

5. References

1. Rupp, B. *Biomolecular Crystallography: Principles, Practice, and Application to Structural Biology*, Garland Science 2010.
2. Lackie, J., O'Callaghan, C.A. A *Dictionary of Biomedicine*, OUP Oxford 2010.
3. Isaacs, A., Lindenmann, J. Virus interference. I. (1957) The interferon, *Proc R Soc Lond, B, Biol Sci* 147(927) 258-67.
4. Prokunina-Olsson, L.; Muchmore, B.; Tang, W.; Pfeiffer, R. M.; Park, H.; Dickensheets, H.; Hergott, D.; Porter-Gill, P.; Mumy, A.; Kohaar, I.; Chen, S.; Brand, N.; Tarway, M.; Liu, L.; Sheikh, F.; Astemborski, J.; Bonkovsky, H. L.; Edlin, B. R.; Howell, C. D.; Morgan, T. R.; Thomas, D. L.; Rehermann, B.; Donnelly, R. P.; O'Brien, T. R. (2013) A variant upstream of IFNL3 (IL28B) creating a new interferon gene IFNL4 is associated with impaired clearance of hepatitis C virus. *Nat Genet 45* (2), 164-71.
5. Milne, D. J.; Campoverde, C.; Andree, K. B.; Chen, X.; Zou, J.; Secombes, C. J. (2018) The discovery and comparative expression analysis of three distinct type I interferons in the perciform fish, meagre (Argyrosomus regius). *Dev Compar Immunol 84*, 123-132.
6. Secombes, C. J.; Zou, J. (2017) Evolution of Interferons and Interferon Receptors. *Front Immunol 8* (209).
7. Karupiah, G.; Xie, Q. W.; Buller, R. M.; Nathan, C.; Duarte, C.; MacMicking, J. D. (1993) Inhibition of viral replication by interferon-gamma-induced nitric oxide synthase. *Science 261* (5127), 1445-1448.
8. Weiss, G.; Schaible, U. E. (2015) Macrophage defense mechanisms against intracellular bacteria. *Immunol Rev 264* (1), 182-203.
9. McNab, F.; Mayer-Barber, K.; Sher, A.; Wack, A.; O'Garra, A. (2015) Type I interferons in infectious disease. *Nat Rev Immunol 15* (2), 87-103.
10. Corrales, L.; Gajewski, T. F. (2015) Molecular Pathways: Targeting the Stimulator of Interferon Genes (STING) in the Immunotherapy of Cancer. *Clin Cancer Res 21* (21), 4774-9.
11. Stark, George R.; Darnell, James E. (2012) The JAK-STAT Pathway at Twenty. *Immunity 36* (4), 503-514.
12. Pestka, S.; Langer, J. A.; Zoon, K. C.; Samuel, C. E. (1987) Interferons and their actions. *Annu Rev Biochem 56*, 727-77.

13. Fasler-Kan, E.; Pansky, A.; Wiederkehr, M.; Battegay, M.; Heim, M. H. (1998) Interferon-alpha activates signal transducers and activators of transcription 5 and 6 in Daudi cells. *Eur J Biochem 254* (3), 514-9.
14. Matikainen, S.; Sareneva, T.; Ronni, T.; Lehtonen, A.; Koskinen, P. J.; Julkunen, I. (1999) Interferon-alpha activates multiple STAT proteins and upregulates proliferation-associated IL-2Ralpha, c-myc, and pim-1 genes in human T cells. *Blood 93* (6), 1980-91.
15. Sadler, A. J.; Williams, B. R. (2008) Interferon-inducible antiviral effectors. *Nat Rev Immunol 8* (7), 559-68.
16. Pestka, S. (2007) The interferons: 50 years after their discovery, there is much more to learn. *J Biol Chem 282* (28), 20047-51.
17. Jaitin, D. A.; Roisman, L. C.; Jaks, E.; Gavutis, M.; Piehler, J.; Van der Heyden, J.; Uze, G.; Schreiber, G. (2006) Inquiring into the differential action of interferons (IFNs): an IFN-alpha2 mutant with enhanced affinity to IFNAR1 is functionally similar to IFN-beta. *Mol Cell Biol 26* (5), 1888-97.
18. Kalie, E.; Jaitin, D. A.; Podoplelova, Y.; Piehler, J.; Schreiber, G. (2008) The stability of the ternary interferon-receptor complex rather than the affinity to the individual subunits dictates differential biological activities. *J Biol Chem 283* (47), 32925-36.
19. Moraga, I.; Harari, D.; Schreiber, G.; Uze, G.; Pellegrini, S. (2009) Receptor density is key to the alpha2/beta interferon differential activities. *Mol Cell Biol 29* (17), 4778-87.
20. Walter, M. R.; Windsor, W. T.; Nagabhushan, T. L.; Lundell, D. J.; Lunn, C. A.; Zauodny, P. J.; Narula, S. K. (1995) Crystal structure of a complex between interferon-gamma and its soluble high-affinity receptor. *Nature 376* (6537), 230-5.
21. Bach, E. A.; Aguet, M.; Schreiber, R. D. (1997) The IFN gamma receptor: a paradigm for cytokine receptor signaling. *Annu Rev Immunol 15*, 563-91.
22. Young, H. A. (1996) Regulation of interferon-gamma gene expression. *J Interferon Cytokine Res 16* (8), 563-8.
23. Valente, G.; Ozmen, L.; Novelli, F.; Geuna, M.; Palestro, G.; Forni, G.; Garotta, G. (1992) Distribution of interferon-gamma receptor in human tissues. *Eur J Immunol 22* (9), 2403-12.
24. Lin, F.-C.; Young, H. A. (2013) The talented interferon-gamma. *Adv Biosci Biotechnol.* 4 (7) 8.

25. Reinhardt, R. L.; Liang, H.-E.; Bao, K.; Price, A. E.; Mohrs, M.; Kelly, B. L.; Locksley, R. M. (2015) A Novel Model for IFN-γ–Mediated Autoinflammatory Syndromes. *J Immunol 194* (5), 2358-2368.
26. Lees, J. R. (2015) Interferon gamma in autoimmunity: A complicated player on a complex stage. *Cytokine 74* (1), 18-26.
27. Hartung, H. P.; Schäfer, B.; Meide, P. H. V. D.; Fierz, W.; Heininger, K.; Toyka, K. V. (1990) The role of interferon-gamma in the pathogenesis of experimental autoimmune disease of the peripheral nervous system. *Ann Neurol 27* (3), 247-257.
28. Gray, P. W.; Goeddel, D. V. (1982) Structure of the human immune interferon gene. *Nature 298* (5877), 859-63.
29. Kelker, H. C.; Le, J.; Rubin, B. Y.; Yip, Y. K.; Nagler, C.; Vilcek, J. (1984) Three molecular weight forms of natural human interferon-gamma revealed by immunoprecipitation with monoclonal antibody. *J Biol Chem 259* (7), 4301-4.
30. Pan, Y. C.; Stern, A. S.; Familletti, P. C.; Khan, F. R.; Chizzonite, R. (1987) Structural characterization of human interferon gamma. Heterogeneity of the carboxyl terminus. *Eur J Biochem 166* (1), 145-9.
31. Ealick, S. E.; Cook, W. J.; Vijay-Kumar, S.; Carson, M.; Nagabhushan, T. L.; Trotta, P. P.; Bugg, C. E. (1991) Three-dimensional structure of recombinant human interferon-gamma. *Science 252* (5006), 698-702.
32. Thiel, D. J.; le Du, M. H.; Walter, R. L.; D'Arcy, A.; Chène, C.; Fountoulakis, M.; Garotta, G.; Winkler, F. K.; Ealick, S. E. (2000) Observation of an unexpected third receptor molecule in the crystal structure of human interferon-gamma receptor complex. *Structure 8* (9), 927-936.
33. Nuara, A. A.; Walter, L. J.; Logsdon, N. J.; Yoon, S. I.; Jones, B. C.; Schriewer, J. M.; Buller, R. M.; Walter, M. R. (2008) Structure and mechanism of IFN-gamma antagonism by an orthopoxvirus IFN-gamma-binding protein. *Proc Natl Acad Sci U S A 105* (6), 1861-6.
34. Samudzi, C. T.; Burton, L. E.; Rubin, J. R. (1991) Crystal structure of recombinant rabbit interferon-gamma at 2.7-A resolution. *J Biol Chem 266* (32), 21791-7.
35. Randal, M.; Kossiakoff, A. A. (2000) The 2.0 A structure of bovine interferon-gamma; assessment of the structural differences between species. *Acta Crystallogr D Biol Crystallogr 56* (1), 14-24.
36. Samudzi, C. T.; Rubin, J. R. (1993) Structure of recombinant bovine interferon-gamma at 3.0 A resolution. *Acta Crystallogr D Biol Crystallogr 49* (6), 513-21.

37. Zahradník, J.; Kolářová, L.; Pařízková, H.; Kolenko, P.; Schneider, B. (2018) Interferons type II and their receptors R1 and R2 in fish species: Evolution, structure, and function. *Fish Shellfish Immunol 79*, 140-152.
38. Gessani, S.; Belardelli, F. (1998) IFN-gamma expression in macrophages and its possible biological significance. *Cytokine Growth Factor Rev 9* (2), 117-23.
39. Krause, C. D.; Mei, E.; Xie, J.; Jia, Y.; Bopp, M. A.; Hochstrasser, R. M.; Pestka, S. (2002) Seeing the light: preassembly and ligand-induced changes of the interferon gamma receptor complex in cells. *Mol Cell Proteomics 1* (10), 805-15.
40. Subramaniam, P. S.; Torres, B. A.; Johnson, H. M. (2001) So many ligands, so few transcription factors: a new paradigm for signaling through the STAT transcription factors. *Cytokine 15* (4), 175-87.
41. Gough, D. J.; Levy, D. E.; Johnstone, R. W.; Clarke, C. J. (2008) IFNgamma signaling-does it mean JAK-STAT? *Cytokine Growth Factor Rev 19* (5-6), 383-94.
42. Liu, X.; Ye, L.; Bai, Y.; Mojidi, H.; Simister, N. E.; Zhu, X. (2008) Activation of the JAK/STAT-1 signaling pathway by IFN-gamma can down-regulate functional expression of the MHC class I-related neonatal Fc receptor for IgG. *J Immunol 181* (1), 449-63.
43. Ahmed, C. M.; Johnson, H. M. (2013) The role of a non-canonical JAK-STAT pathway in IFN therapy of poxvirus infection and multiple sclerosis: An example of Occam's Broom? *Jak-stat 2* (4), e26227.
44. Blouin, C. M.; Lamaze, C. (2013) Interferon Gamma Receptor: The Beginning of the Journey. *Front Immunol 4*, 267.
45. Schroder, K.; Hertzog, P. J.; Ravasi, T.; Hume, D. A. (2004) Interferon-gamma: an overview of signals, mechanisms and functions. *J Leukocyte Biol 75* (2), 163-89.
46. Briscoe, J.; Rogers, N. C.; Witthuhn, B. A.; Watling, D.; Harpur, A. G.; Wilks, A. F.; Stark, G. R.; Ihle, J. N.; Kerr, I. M. (1996) Kinase-negative mutants of JAK1 can sustain interferon-gamma-inducible gene expression but not an antiviral state. *EMBO J 15* (4), 799-809.
47. Greenlund, A. C.; Farrar, M. A.; Viviano, B. L.; Schreiber, R. D. (1994) Ligand-induced IFN gamma receptor tyrosine phosphorylation couples the receptor to its signal transduction system (p91). *EMBO J 13* (7), 1591-1600.
48. Hertzog, P.; Forster, S.; Samarajiwa, S. (2011) Systems biology of interferon responses. *J Interferon Cytokine Res 31* (1), 5-11.

49. Zaidi, M. R.; Merlino, G. (2011) The Two Faces of Interferon-γ in Cancer. *Clin Canc Res 17* (19), 6118-6124.

50. Matsumoto, M.; Tanaka, N.; Harada, H.; Kimura, T.; Yokochi, T.; Kitagawa, M.; Schindler, C.; Taniguchi, T. (1999) Activation of the transcription factor ISGF3 by interferon-gamma. *Biol Chem 380* (6), 699-703.

51. Stark, G. R.; Kerr, I. M.; Williams, B. R.; Silverman, R. H.; Schreiber, R. D. (1998) How cells respond to interferons. *Annu Rev Biochem 67*, 227-64.

52. Subramaniam, P. S.; Green, M. M.; Larkin, J., 3rd; Torres, B. A.; Johnson, H. M. (2001) Nuclear translocation of IFN-gamma is an intrinsic requirement for its biologic activity and can be driven by a heterologous nuclear localization sequence. *J Interferon Cytokine Res 21* (11), 951-9.

53. Michalski, W. P.; Shiell, B. J.; O'Neil, T. E.; Beddome, G.; Lowenthal, J. W. (1999) Recombinant chicken IFN-gamma expressed in Escherichia coli: analysis of C-terminal truncation and effect on biologic activity. *J Interferon Cytokine Res 19* (4), 383-92.

54. Johnson, H. M.; Noon-Song, E. N.; Dabelic, R.; Ahmed, C. M. (2013) IFN signaling: how a non-canonical model led to the development of IFN mimetics. *Front Immunol 4*, 202.

55. Schoenborn, J. R.; Wilson, C. B. (2007) Regulation of Interferon-γ During Innate and Adaptive Immune Responses. *Adv Immunol* 96, pp 41-101.

56. Meyer, O. (2009) Interferons and autoimmune disorders. *Joint Bone Spine. 76* (5), 464-73.

57. Young, H. A. (1996) Regulation of Interferon-γ Gene Expression. *J Interferon Cytokine Res 16* (8), 563-568.

58. de Araujo-Souza, P. S.; Hanschke, S. C.; Viola, J. P. (2015) Epigenetic control of interferon-gamma expression in CD8 T cells. *J Immunol Res 2015*, 849573.

59. Abboud, G.; Tahiliani, V.; Desai, P.; Varkoly, K.; Driver, J.; Hutchinson, T. E.; Salek-Ardakani, S. (2016) Natural Killer Cells and Innate Interferon Gamma Participate in the Host Defense against Respiratory Vaccinia Virus Infection. *J Virol 90* (1), 129-141.

60. Fuchs, D.; Hausen, A.; Reibnegger, G.; Werner, E. R.; Werner-Felmayer, G.; Dierich, M. P.; Wachter, H. (1989) Interferon-gamma concentrations are increased in sera from individuals infected with human immunodeficiency virus type 1. *J Acquir Immune Defic Syndr 2* (2), 158-162.

61. Aachoui, Y.; Kajiwara, Y.; Leaf, Irina A.; Mao, D.; Ting, Jenny P. Y.; Coers, J.; Aderem, A.; Buxbaum, Joseph D.; Miao, Edward A. (2015) Canonical Inflammasomes Drive IFN-γ to Prime Caspase-11 in Defense against a Cytosol-Invasive Bacterium. *Cell Host Microbe. 18* (3), 320-332.

62. Naglak, E. K.; Morrison, S. G.; Morrison, R. P. (2016) Gamma Interferon Is Required for Optimal Antibody-Mediated Immunity against Genital Chlamydia Infection. *Infect Immun 84* (11), 3232-3242.
63. Mammari, N.; Vignoles, P.; Halabi, M. A.; Dardé, M.-L.; Courtioux, B. (2015) Interferon gamma effect on immune mediator production in human nerve cells infected by two strains of Toxoplasma gondii. *Parasite 22*, 39.
64. Murray, H. W.; Luster, A. D.; Zheng, H.; Ma, X. (2017) Gamma Interferon-Regulated Chemokines in Leishmania donovani Infection in the Liver. *Infect Immun 85* (1).
65. Hu, X.; Ivashkiv, L. B. (2009) Cross-regulation of signaling pathways by interferon-gamma: implications for immune responses and autoimmune diseases. *Immunity 31* (4), 539-50.
66. Darwich, L.; Coma, G.; Peña, R.; Bellido, R.; Blanco, E. J. J.; Este, J. A.; Borras, F. E.; Clotet, B.; Ruiz, L.; Rosell, A.; Andreo, F.; Parkhouse, R. M. E.; Bofill, M. (2009) Secretion of interferon-γ by human macrophages demonstrated at the single-cell level after costimulation with interleukin (IL)-12 plus IL-18. *Immunology 126* (3), 386-393.
67. Held, T. K.; Weihua, X.; Yuan, L.; Kalvakolanu, D. V.; Cross, A. S. (1999) Gamma Interferon Augments Macrophage Activation by Lipopolysaccharide by Two Distinct Mechanisms, at the Signal Transduction Level and via an Autocrine Mechanism Involving Tumor Necrosis Factor Alpha and Interleukin-1. *Infect Immun 67* (1), 206-212.
68. Bradley, L. M.; Dalton, D. K.; Croft, M. (1996) A direct role for IFN-gamma in regulation of Th1 cell development. *J Immunol 157* (4), 1350-8.
69. Kelchtermans, H.; Billiau, A.; Matthys, P. (2008) How interferon-γ keeps autoimmune diseases in check. *Trends Immunol 29* (10), 479-486.
70. Kantarci, O. H.; Hebrink, D. D.; Schaefer-Klein, J.; Sun, Y.; Achenbach, S.; Atkinson, E. J.; Heggarty, S.; Cotleur, A. C.; de Andrade, M.; Vandenbroeck, K.; Pelfrey, C. M.; Weinshenker, B. G., (2008) Interferon gamma allelic variants: sex-biased multiple sclerosis susceptibility and gene expression. *Arch Neurol 65* (3), 349-57.
71. Rossouw, M.; Nel, H. J.; Cooke, G. S.; van Helden, P. D.; Hoal, E. G. (2003) Association between tuberculosis and a polymorphic NFkappaB binding site in the interferon gamma gene. *Lancet 361* (9372), 1871-2.
72. Bulat-Kardum, L.; Etokebe, G. E.; Knezevic, J.; Balen, S.; Matakovic-Mileusnic, N.; Zaputovic, L.; Pavelic, J.; Beg-Zec, Z.; Dembic, Z. (2006) Interferon-gamma receptor-1

gene promoter polymorphisms (G-611A; T-56C) and susceptibility to tuberculosis. *Scand J Immunol 63* (2), 142-50.

73. Ansari, A.; Hasan, Z.; Dawood, G.; Hussain, R. (2011) Differential combination of cytokine and interferon- gamma +874 T/A polymorphisms determines disease severity in pulmonary tuberculosis. *PloS one 6* (11), e27848.
74. Dufour, C.; Capasso, M.; Svahn, J.; Marrone, A.; Haupt, R.; Bacigalupo, A.; Giordani, L.; Longoni, D.; Pillon, M.; Pistorio, A.; Di Michele, P.; Iori, A. P.; Pongiglione, C.; Lanciotti, M.; Iolascon, A. (2004) Homozygosis for (12) CA repeats in the first intron of the human IFN-gamma gene is significantly associated with the risk of aplastic anaemia in Caucasian population. *Br J Haematol 126* (5), 682-5.
75. Dabora, S. L.; Roberts, P.; Nieto, A.; Perez, R.; Jozwiak, S.; Franz, D.; Bissler, J.; Thiele, E. A.; Sims, K.; Kwiatkowski, D. J. (2002) Association between a high-expressing interferon-gamma allele and a lower frequency of kidney angiomyolipomas in TSC2 patients. *Am J Hum Genet 71* (4), 750-8.
76. Flynn, J. L.; Chan, J.; Triebold, K. J.; Dalton, D. K.; Stewart, T. A.; Bloom, B. R. (1993) An essential role for interferon gamma in resistance to Mycobacterium tuberculosis infection. *J Exp Med 178* (6), 2249-2254.
77. Huang, Y.; Yang, H.; Borg, B. B.; Su, X.; Rhodes, S. L.; Yang, K.; Tong, X.; Tang, G.; Howell, C. D.; Rosen, H. R.; Thio, C. L.; Thomas, D. L.; Alter, H. J.; Sapp, R. K.; Liang, T. J. (2007) A functional SNP of interferon-gamma gene is important for interferon-alpha-induced and spontaneous recovery from hepatitis C virus infection. *Proc Natl Acad Sci U S A 104* (3), 985-90.
78. Graninger, W. B.; Hassfeld, W.; Pesau, B. B.; Machold, K. P.; Zielinski, C. C.; Smolen, J. S. (1991) Induction of systemic lupus erythematosus by interferon-gamma in a patient with rheumatoid arthritis. *J Rheumatol 18* (10), 1621-1622.
79. Machold, K. P.; Smolen, J. S. (1990) Interferon-gamma induced exacerbation of systemic lupus erythematosus. *J Rheumatol 17* (6), 831-832.
80. Alvaro-Gracia, J. M.; Zvaifler, N. J.; Firestein, G. S. (1990) Cytokines in chronic inflammatory arthritis. V. Mutual antagonism between interferon-gamma and tumor necrosis factor-alpha on HLA-DR expression, proliferation, collagenase production, and granulocyte macrophage colony-stimulating factor production by rheumatoid arthritis synoviocytes. *J Clin Invest 86* (6), 1790-1798.
81. Budczies, J.; Bockmayr, M.; Klauschen, F.; Endris, V.; Frohling, S.; Schirmacher, P.; Denkert, C.; Stenzinger, A (2017) Mutation patterns in genes encoding interferon

signaling and antigen presentation: A pan-cancer survey with implications for the use of immune checkpoint inhibitors. *Genes Chromosomes Cancer 56* (8), 651-659.

82. Clarke, B.; Chetty, R. (2001) Cell Cycle Aberrations in the Pathogenesis of Squamous Cell Carcinoma of the Uterine Cervix. *Gynecol Oncol 82* (2), 238-246.
83. Tartour, E.; Gey, A.; Fridman, W. H.; Sastre-Garau, X.; Lombard Surin, I.; Mosseri, V. (1998) Prognostic Value of Intratumoral Interferon Gamma Messenger RNA Expression in Invasive Cervical Carcinomas. *J Natl Cancer Inst 90* (4), 287-294.
84. Azhar, A.; Ahmad, E.; Zia, Q.; Owais, M.; Md Ashraf, G. (2017) Recent Updates on Molecular Genetic Engineering Approaches and Applications of Human Therapeutic Proteins. *Curr Protein Pept Sci 18* (3), 217-232.
85. Harden, J. L.; Johnson-Huang, L. M.; Chamian, M. F.; Lee, E.; Pearce, T.; Leonardi, C. L.; Haider, A.; Lowes, M. A.; Krueger, J. G. (2013) Humanized anti-IFN-x3b3; (HuZAF) in the treatment of psoriasis. *J Allergy Clin Immunol 135* (2), 553-556.e3.
86. Miller, C. H. T.; Maher, S. G.; Young, H. A. (2009) Clinical Use of Interferon-γ. *Ann N Y Acad Sci 1182* (1), 69-79.
87. Kotenko, S. V.; Gallagher, G.; Baurin, V. V.; Lewis-Antes, A.; Shen, M.; Shah, N. K.; Langer, J. A.; Sheikh, F.; Dickensheets, H.; Donnelly, R. P. (2003) IFN-lambdas mediate antiviral protection through a distinct class II cytokine receptor complex. *Nat Immunol 4* (1), 69-77.
88. Pestka, S.; Krause, C. D.; Walter, M. R. (2004) Interferons, interferon-like cytokines, and their receptors. *Immunol Rev 202*, 8-32.
89. Egli, A.; Santer, D. M.; O'Shea, D.; Tyrrell, D. L.; Houghton, M. (2014) The impact of the interferon-lambda family on the innate and adaptive immune response to viral infections. *Emerg Microbes Infect 3* (7), e51.
90. Bolen, C. R.; Ding, S.; Robek, M. D.; Kleinstein, S. H. (2014) Dynamic expression profiling of type I and type III interferon-stimulated hepatocytes reveals a stable hierarchy of gene expression. *Hepatology 59* (4), 1262-72.
91. Marcello, T.; Grakoui, A.; Barba-Spaeth, G.; Machlin, E. S.; Kotenko, S. V.; MacDonald, M. R.; Rice, C. M. (2006) Interferons alpha and lambda inhibit hepatitis C virus replication with distinct signal transduction and gene regulation kinetics. *Gastroenterology 131* (6), 1887-98.
92. Lasfar, A.; Gogas, H.; Zloza, A.; Kaufman, H. L.; Kirkwood, J. M. (2016) IFN-λ cancer immunotherapy: new kid on the block. *Immunotherapy 8* (8), 877-888.

93. Heaney, M. L.; Golde, D. W. (1998) Soluble receptors in human disease. *J Leukocyte Biol 64* (2), 135-46.

94. Miyajima, A.; Kitamura, T.; Harada, N.; Yokota, T.; Arai, K.-i. (1992) Cytokine Receptors and Signal Transduction. *Annu Rev Immunol 10* (1), 295-331.

95. Cosman, D.; Lyman, S. D.; Idzerda, R. L.; Beckmann, M. P.; Park, L. S.; Goodwin, R. G.; March, C. J. (1990) A new cytokine receptor superfamily. *Trends Bioch Sci 15* (7), 265-270.

96. Mikulecky, P.; Zahradnik, J.; Kolenko, P.; Cerny, J.; Charnavets, T.; Kolarova, L.; Necasova, I.; Pham, P. N.; Schneider, B. (2016) Crystal structure of human interferon-gamma receptor 2 reveals the structural basis for receptor specificity. *Acta Crystallogr D, Struct Biol 72* (Pt 9), 1017-25.

97. Maenaka, K.; Juji, T.; Stuart, D. I.; Jones, E. Y. (1999) Crystal structure of the human p58 killer cell inhibitory receptor (KIR2DL3) specific for HLA-Cw3-related MHC class I. *Structure 7* (4), 391-398.

98. Locksley, R. M.; Killeen, N.; Lenardo, M. J. (2001) The TNF and TNF Receptor Superfamilies. *Cell 104* (4), 487-501.

99. Arimont, M.; Sun, S. L.; Leurs, R.; Smit, M.; de Esch, I. J. P.; de Graaf, C. (2017) Structural Analysis of Chemokine Receptor-Ligand Interactions. *J Med Chem 60* (12), 4735-4779.

100. Dore, J. J., Jr.; Edens, M.; Garamszegi, N.; Leof, E. B. (1998) Heteromeric and homomeric transforming growth factor-beta receptors show distinct signaling and endocytic responses in epithelial cells. *J Biol Chem 273* (48), 31770-7.

101. Wang, X.; Rickert, M.; Garcia, K. C. (2005) Structure of the quaternary complex of interleukin-2 with its alpha, beta, and gammac receptors. *Science 310* (5751), 1159-63.

102. Fan, Q. R.; Mosyak, L.; Winter, C. C.; Wagtmann, N.; Long, E. O.; Wiley, D. C. (1997) Structure of the inhibitory receptor for human natural killer cells resembles haematopoietic receptors. *Nature 389* (6646), 96-100.

103. Naismith, J. H.; Devine, T. Q.; Kohno, T.; Sprang, S. R. (1996) Structures of the extracellular domain of the type I tumor necrosis factor receptor. *Structure 4* (11), 1251-1262.

104. Qin, L.; Kufareva, I.; Holden, L. G.; Wang, C.; Zheng, Y.; Zhao, C.; Fenalti, G.; Wu, H.; Han, G. W.; Cherezov, V.; Abagyan, R.; Stevens, R. C.; Handel, T. M. (2015) Structural biology. Crystal structure of the chemokine receptor CXCR4 in complex with a viral chemokine. *Science 347* (6226), 1117-1122.

105. Wangkanont, K.; Forest, K. T.; Kiessling, L. L. (2015) The non-detergent sulfobetaine-201 acts as a pharmacological chaperone to promote folding and crystallization of the type II TGF-β receptor extracellular domain. *Protein Expr Purif 115*, 19-25.

106. Logsdon, N. J.; Deshpande, A.; Harris, B. D.; Rajashankar, K. R.; Walter, M. R. (2012) Structural basis for receptor sharing and activation by interleukin-20 receptor-2 (IL-20R2) binding cytokines. *Proc Natl Acad Sci U S A 109* (31), 12704-12709.

107. Aguet, M.; Dembic, Z.; Merlin, G. (1988) Molecular cloning and expression of the human interferon-gamma receptor. *Cell 55* (2), 273-80.

108. Le Coniat, M.; Alcaide-Loridan, C.; Fellous, M.; Berger, R. (1989) Human interferon gamma receptor 1 (IFNGR1) gene maps to chromosome region 6q23-6q24. *Human Genet 84* (1), 92-4.

109. Farrar, M. A.; Schreiber, R. D. (1993) The molecular cell biology of interferon-gamma and its receptor. *Annu Rev Immunol 11*, 571-611.

110. Hershey, G. K.; Schreiber, R. D. (1989) Biosynthetic analysis of the human interferon-gamma receptor. Identification of N-linked glycosylation intermediates. *J Biol Chem 264* (20), 11981-8.

111. Mao, C.; Aguet, M.; Merlin, G. (1989) Molecular characterization of the human interferon-gamma receptor: analysis of polymorphism and glycosylation. *J Interferon Res 9* (6), 659-69.

112. Jouanguy, E.; Lamhamedi-Cherradi, S.; Altare, F.; Fondaneche, M. C.; Tuerlinckx, D.; Blanche, S.; Emile, J. F.; Gaillard, J. L.; Schreiber, R.; Levin, M.; Fischer, A.; Hivroz, C.; Casanova, J. L. (1997) Partial interferon-gamma receptor 1 deficiency in a child with tuberculoid bacillus Calmette-Guerin infection and a sibling with clinical tuberculosis. *J Clin Invest 100* (11), 2658-64.

113. Noordzij, J. G.; Hartwig, N. G.; Verreck, F. A.; De Bruin-Versteeg, S.; De Boer, T.; Van Dissel, J. T.; De Groot, R.; Ottenhoff, T. H.; Van Dongen, J. J. (2007) Two patients with complete defects in interferon gamma receptor-dependent signaling. *J Clinical Immunol 27* (5), 490-6.

114. Jouanguy, E.; Dupuis, S.; Pallier, A.; Doffinger, R.; Fondaneche, M. C.; Fieschi, C.; Lamhamedi-Cherradi, S.; Altare, F.; Emile, J. F.; Lutz, P.; Bordigoni, P.; Cokugras, H.; Akcakaya, N.; Landman-Parker, J.; Donnadieu, J.; Camcioglu, Y.; Casanova, J. L. (2000) In a novel form of IFN-gamma receptor 1 deficiency, cell surface receptors fail to bind IFN-gamma. *J Clin Invest 105* (10), 1429-36.

115. Prando, C.; Boisson-Dupuis, S.; Grant, A. V.; Kong, X. F.; Bustamante, J.; Feinberg, J.; Chapgier, A.; Rose, Y.; Janniere, L.; Rizzardi, E.; Zhang, Q.; Shanahan, C. M.; Viollet, L.; Lyonnet, S.; Abel, L.; Ruga, E. M.; Casanova, J. L. (2010) Paternal uniparental isodisomy of chromosome 6 causing a complex syndrome including complete IFN-gamma receptor 1 deficiency. *Am J Med Genet A 152a* (3), 622-9.

116. Sogabe, S.; Stuart, F.; Henke, C.; Bridges, A.; Williams, G.; Birch, A.; Winkler, F. K.; Robinson, J. A. (1997) Neutralizing epitopes on the extracellular interferon gamma receptor (IFNgammaR) alpha-chain characterized by homolog scanning mutagenesis and X-ray crystal structure of the A6 fab-IFNgammaR1-108 complex. *J Mol Biol 273* (4), 882-897.

117. Randal, M.; Kossiakoff, A. A. (2001) The structure and activity of a monomeric interferon-gamma:alpha-chain receptor signaling complex. *Structure 9* (2), 155-163.

118. Ping, Z.; Qi, J.; Sun, Y.; Lu, G.; Shi, Y.; Wang, X.; Gao, G. F.; Wang, M. (2014) Crystal structure of the interferon gamma receptor alpha chain from chicken reveals an undetected extra helix compared with the human counterparts. *J Interferon Cytokine Res 34* (1), 41-51.

119. Bazan, J. F. (1990) Structural design and molecular evolution of a cytokine receptor superfamily. *Proc Natl Acad Sci U S A 87* (18), 6934-6938.

120. Manneberg, M.; Friedlein, A.; Kurth, H.; Lahm, H. W.; Fountoulakis, M. (1994) Structural analysis and localization of the carbohydrate moieties of a soluble human interferon gamma receptor produced in baculovirus-infected insect cells. *Prot Scie 3* (1), 30-8.

121. Razaghi, A.; Owens, L.; Heimann, K. (2016) Review of the recombinant human interferon gamma as an immunotherapeutic: Impacts of production platforms and glycosylation. *J Biotechnol 240*, 48-60.

122. Stuber, D.; Friedlein, A.; Fountoulakis, M.; Lahm, H. W.; Garotta, G. (1993) Alignment of disulfide bonds of the extracellular domain of the interferon gamma receptor and investigation of their role in biological activity. *Biochemistry 32* (9), 2423-30.

123. Fischer, T.; Thoma, B.; Scheurich, P.; Pfizenmaier, K. (1990) Glycosylation of the human interferon-gamma receptor. N-linked carbohydrates contribute to structural heterogeneity and are required for ligand binding. *J Biol Chem 265* (3), 1710-7.

124. Mikulecký, P.; Černý, J.; Biedermannová, L.; Petroková, H.; Kuchař, M.; Vondrášek, J.; Malý, P.; Šebo, P.; Schneider, B. (2013) Increasing Affinity of Interferon-γ Receptor 1 to Interferon-γ by Computer-Aided Design. *Biomed Res Int 2013*, 752514.

125. Usacheva, A.; Sandoval, R.; Domanski, P.; Kotenko, S. V.; Nelms, K.; Goldsmith, M. A.; Colamonici, O. R. (2002) Contribution of the Box 1 and Box 2 motifs of cytokine receptors to Jak1 association and activation. *J Biol Chem 277* (50), 48220-6.

126. Zhang, D.; Wlodawer, A.; Lubkowski, J. (2016) Crystal Structure of a Complex of the Intracellular Domain of Interferon lambda Receptor 1 (IFNLR1) and the FERM/SH2 Domains of Human JAK1. *J Mol Biol 428* (23), 4651-4668.

127. Wallweber, H. J. A.; Tam, C.; Franke, Y.; Starovasnik, M. A.; Lupardus, P. J. (2014) Structural basis of IFNα receptor recognition by TYK2. *Nat Struct Mol Biol 21* (5), 443-448.

128. Greenlund, A. C.; Morales, M. O.; Viviano, B. L.; Yan, H.; Krolewski, J.; Schreiber, R. D. (1995) Stat recruitment by tyrosine-phosphorylated cytokine receptors: an ordered reversible affinity-driven process. *Immunity 2* (6), 677-87.

129. Cook, J. R.; Emanuel, S. L.; Donnelly, R. J.; Soh, J.; Mariano, T. M.; Schwartz, B.; Rhee, S.; Pestka, S. (1994) Sublocalization of the human interferon-gamma receptor accessory factor gene and characterization of accessory factor activity by yeast artificial chromosomal fragmentation. *The J Biol Chem 269* (9), 7013-8.

130. Soh, J.; Donnelly, R. J.; Kotenko, S.; Mariano, T. M.; Cook, J. R.; Wang, N.; Emanuel, S.; Schwartz, B.; Miki, T.; Pestka, S. (1994) Identification and sequence of an accessory factor required for activation of the human interferon gamma receptor. *Cell 76* (5), 793-802.

131. Rhee, S.; Ebensperger, C.; Dembic, Z.; Pestka, S. (1996) The structure of the gene for the second chain of the human interferon-gamma receptor. *J Biol Chem 271* (46), 28947-52.

132. Doffinger, R.; Jouanguy, E.; Dupuis, S.; Fondaneche, M. C.; Stephan, J. L.; Emile, J. F.; Lamhamedi-Cherradi, S.; Altare, F.; Pallier, A.; Barcenas-Morales, G.; Meinl, E.; Krause, C.; Pestka, S.; Schreiber, R. D.; Novelli, F.; Casanova, J. L. (2000) Partial interferon-gamma receptor signaling chain deficiency in a patient with bacille Calmette-Guerin and Mycobacterium abscessus infection. *J Infect Dis 181* (1), 379-84.

133. Vogt, G.; Chapgier, A.; Yang, K.; Chuzhanova, N.; Feinberg, J.; Fieschi, C.; Boisson-Dupuis, S.; Alcais, A.; Filipe-Santos, O.; Bustamante, J.; de Beaucoudrey, L.; Al-Mohsen, I.; Al-Hajjar, S.; Al-Ghonaium, A.; Adimi, P.; Mirsaeidi, M.; Khalilzadeh, S.; Rosenzweig, S.; de la Calle Martin, O.; Bauer, T. R.; Puck, J. M.; Ochs, H. D.; Furthner, D.; Engelhorn, C.; Belohradsky, B.; Mansouri, D.; Holland, S. M.; Schreiber, R. D.; Abel, L.; Cooper, D. N.; Soudais, C.; Casanova, J. L. (2005) Gains of

glycosylation comprise an unexpectedly large group of pathogenic mutations. *Nat Genet 37* (7), 692-700.

134. Kilic, S. S.; van Wengen, A.; de Paus, R. A.; Celebi, S.; Meziane, B.; Hafizoglu, D.; van Dissel, J. T.; van de Vosse, E. (2012) Severe disseminated mycobacterial infection in a boy with a novel mutation leading to IFN-gammaR2 deficiency. *J Infect 65* (6), 568-72.
135. Bach, E. A.; Szabo, S. J.; Dighe, A. S.; Ashkenazi, A.; Aguet, M.; Murphy, K. M.; Schreiber, R. D., (1995) Ligand-induced autoregulation of IFN-gamma receptor beta chain expression in T helper cell subsets. *Science 270* (5239), 1215-8.
136. Mendoza, J. L.; Schneider, W. M.; Hoffmann, H.-H.; Vercauteren, K.; Jude, K. M.; Xiong, A.; Moraga, I.; Horton, T. M.; Glenn, J. S.; de Jong, Y. P.; Rice, C. M.; Garcia, K. C. (2017) The IFN-λ-IFN-λR1-IL-10Rβ Complex Reveals Structural Features Underlying Type III IFN Functional Plasticity. *Immunity 46* (3), 379-392.
137. Pestka, S.; Kotenko, S. V.; Muthukumaran, G.; Izotova, L. S.; Cook, J. R.; Garotta, G. (1997) The interferon gamma (IFN-gamma) receptor: a paradigm for the multichain cytokine receptor. *Cytokine Growth Factor Rev 8* (3), 189-206.
138. Ebensperger, C.; Rhee, S.; Muthukumaran, G.; Lembo, D.; Donnelly, R.; Pestka, S.; Dembic, Z. (1996) Genomic organization and promoter analysis of the gene ifngr2 encoding the second chain of the mouse interferon-gamma receptor. *Scand J Immunol 44* (6), 599-606.
139. Sakatsume, M.; Finbloom, D. S. (1996) Modulation of the expression of the IFN-gamma receptor beta-chain controls responsiveness to IFN-gamma in human peripheral blood T cells. *J Immunol 156* (11), 4160-4166.
140. Moraga, I.; Wernig, G.; Wilmes, S.; Gryshkova, V.; Richter, C. P.; Hong, W.-J.; Sinha, R.; Guo, F.; Fabionar, H.; Wehrman, T. S.; Krutzik, P.; Demharter, S.; Plo, I.; Weissman, I. L.; Minary, P.; Majeti, R.; Constantinescu, S. N.; Piehler, J.; Garcia, K. C. (2015) Tuning cytokine receptor signaling by re-orienting dimer geometry with surrogate ligands. *Cell 160* (6), 1196-1208.
141. de Vos, A. M.; Ultsch, M.; Kossiakoff, A. A. (1992) Human growth hormone and extracellular domain of its receptor: crystal structure of the complex. *Science 255* (5042), 306-12.
142. Syed, R. S.; Reid, S. W.; Li, C.; Cheetham, J. C.; Aoki, K. H.; Liu, B.; Zhan, H.; Osslund, T. D.; Chirino, A. J.; Zhang, J.; Finer-Moore, J.; Elliott, S.; Sitney, K.; Katz, B. A.; Matthews, D. J.; Wendoloski, J. J.; Egrie, J.; Stroud, R. M., (1998) Efficiency of

signalling through cytokine receptors depends critically on receptor orientation. *Nature 395* (6701), 511-6.

143. Elkins, P. A.; Christinger, H. W.; Sandowski, Y.; Sakal, E.; Gertler, A.; de Vos, A. M.; Kossiakoff, A. A. (2000) Ternary complex between placental lactogen and the extracellular domain of the prolactin receptor. *Nat Struct Biol 7* (9), 808-15.
144. Boulanger, M. J.; Chow, D. C.; Brevnova, E. E.; Garcia, K. C. (2003) Hexameric structure and assembly of the interleukin-6/IL-6 alpha-receptor/gp130 complex. *Science 300* (5628), 2101-4.
145. LaPorte, S. L.; Juo, Z. S.; Vaclavikova, J.; Colf, L. A.; Qi, X.; Heller, N. M.; Keegan, A. D.; Garcia, K. C. (2008) Molecular and structural basis of cytokine receptor pleiotropy in the interleukin-4/13 system. *Cell 132* (2), 259-72.
146. Stauber, D. J.; Debler, E. W.; Horton, P. A.; Smith, K. A.; Wilson, I. A. (2006) Crystal structure of the IL-2 signaling complex: paradigm for a heterotrimeric cytokine receptor. *Proc Natl Acad Sci U S A 103* (8), 2788-93.
147. Kastritis, P. L.; Bonvin, A. M. (2013) Molecular origins of binding affinity: seeking the Archimedean point. *Curr Opin Struct Biol 23* (6), 868-77.
148. Grunberg, R.; Nilges, M.; Leckner, J. (2006) Flexibility and conformational entropy in protein-protein binding. *Structure 14* (4), 683-93.
149. Voss, N. R.; Gerstein, M. (2010) 3V: cavity, channel and cleft volume calculator and extractor. *Nucleic Acids Res 38*, W555-62.
150. Schymkowitz, J.; Borg, J.; Stricher, F.; Nys, R.; Rousseau, F.; Serrano, L. (2005) The FoldX web server: an online force field. *Nucleic acids Res 33*, W382-8.
151. Schneider, I. (1972) Cell lines derived from late embryonic stages of Drosophila melanogaster. *J Embryol Exper Morphol 27* (2), 353-65.
152. Kabsch, W. (2010) XDS. *Acta Crystallogr D Biol Crystallogr 66* (2), 125-132.
153. Long, F.; Vagin, A. A.; Young, P.; Murshudov, G. N. (2008) BALBES: a molecular-replacement pipeline. . *Acta Crystallogr D Biol Crystallogr 64* (1), 125-132.
154. Murshudov, G. N.; Skubák, P.; Lebedev, A. A.; Pannu, N. S.; Steiner, R. A.; Nicholls, R. A.; Winn, M. D.; Long, F.; Vagin, A. A. (2011) REFMAC5 for the refinement of macromolecular crystal structures. . *Acta Crystallogr D Biol Crystallogr 67* (4), 355-367.
155. Yoon, S. I.; Jones, B. C.; Logsdon, N. J.; Harris, B. D.; Deshpande, A.; Radaeva, S.; Halloran, B. A.; Gao, B.; Walter, M. R. (2010) Structure and mechanism of receptor sharing by the IL-10R2 common chain. *Structure 18* (5), 638-48.

156. Bravo, J.; Staunton, D.; Heath, J. K.; Jones, E. Y. (1998) Crystal structure of a cytokine-binding region of gp130. *EMBO J 17* (6), 1665-1674.

157. Ring, A. M.; Lin, J. X.; Feng, D.; Mitra, S.; Rickert, M.; Bowman, G. R.; Pande, V. S.; Li, P.; Moraga, I.; Spolski, R.; Ozkan, E.; Leonard, W. J.; Garcia, K. C. (2012) Mechanistic and structural insight into the functional dichotomy between IL-2 and IL-15. *Nat Immunol 13* (12), 1187-95.

158. Glaser, F.; Pupko, T.; Paz, I.; Bell, R. E.; Bechor-Shental, D.; Martz, E.; Ben-Tal, N. (2003) ConSurf: identification of functional regions in proteins by surface-mapping of phylogenetic information. *Bioinformatics 19* (1), 163-4.

159. Josephson, K.; Logsdon, N. J.; Walter, M. R. (2001) Crystal structure of the IL-10/IL-10R1 complex reveals a shared receptor binding site. *Immunity 15* (1), 35-46.

160. Bleicher, L.; de Moura, P. R.; Watanabe, L.; Colau, D.; Dumoutier, L.; Renauld, J. C.; Polikarpov, I. (2008) Crystal structure of the IL-22/IL-22R1 complex and its implications for the IL-22 signaling mechanism. *FEBS letters 582* (20), 2985-92.

161. de Moura, P. R.; Watanabe, L.; Bleicher, L.; Colau, D.; Dumoutier, L.; Lemaire, M. M.; Renauld, J. C.; Polikarpov, I. (2009) Crystal structure of a soluble decoy receptor IL-22BP bound to interleukin-22. *FEBS letters 583* (7), 1072-7.

162. Miknis, Z. J.; Magracheva, E.; Li, W.; Zdanov, A.; Kotenko, S. V.; Wlodawer, A. (2010) Crystal structure of human interferon-lambda1 in complex with its high-affinity receptor interferon-lambdaR1. *J Mol Biol 404* (4), 650-64.

163. Thomas, C.; Moraga, I.; Levin, D.; Krutzik, P. O.; Podoplelova, Y.; Trejo, A.; Lee, C.; Yarden, G.; Vleck, S. E.; Glenn, J. S.; Nolan, G. P.; Piehler, J.; Schreiber, G.; Garcia, K. C. (2011) Structural linkage between ligand discrimination and receptor activation by type I interferons. *Cell 146* (4), 621-32.

164. Larsen, K. S.; Ostergaard, H.; Bjelke, J. R.; Olsen, O. H.; Rasmussen, H. B.; Christensen, L.; Kragelund, B. B.; Stennicke, H. R. (2007) Engineering the substrate and inhibitor specificities of human coagulation Factor VIIa. *Biochem J 405* (3), 429-38.

165. Venkatesh, B.; Lee, A. P.; Ravi, V.; Maurya, A. K.; Lian, M. M.; Swann, J. B.; Ohta, Y.; Flajnik, M. F.; Sutoh, Y.; Kasahara, M.; Hoon, S.; Gangu, V.; Roy, S. W.; Irimia, M.; Korzh, V.; Kondrychyn, I.; Lim, Z. W.; Tay, B. H.; Tohari, S.; Kong, K. W.; Ho, S.; Lorente-Galdos, B.; Quilez, J.; Marques-Bonet, T.; Raney, B. J.; Ingham, P. W.; Tay, A.; Hillier, L. W.; Minx, P.; Boehm, T.; Wilson, R. K.; Brenner, S.; Warren, W. C.

(2014) Elephant shark genome provides unique insights into gnathostome evolution. *Nature 505* (7482), 174-9.

166. Savan, R.; Ravichandran, S.; Collins, J. R.; Sakai, M.; Young, H. A. (2009) Structural conservation of interferon gamma among vertebrates. *Cytokine Growth Factor Rev 20* (2), 115-24.
167. Volff, J. N. (2005) Genome evolution and biodiversity in teleost fish. *Heredity 94* (3), 280-94.
168. Luo, Z. (2016) Selenourea: a convenient phasing vehicle for macromolecular X-ray crystal structures. *Sci Rep 6*, 37123.
169. Legendre, P.; Desdevises, Y.; Bazin, E. (2002) A statistical test for host-parasite coevolution. *Syst Biol 51* (2), 217-34.
170. Iserte, J.; Simonetti, F. L.; Zea, D. J.; Teppa, E.; Marino-Buslje, C. (2015) I-COMS: Interprotein-COrrelated Mutations Server. *Nucleic Acids Res 43*, W320-W325.
171. Talavera, D.; Lovell, S. C.; Whelan, S. (2015) Covariation Is a Poor Measure of Molecular Coevolution. *Mol Biol Evol 32* (9), 2456-2468.
172. Aggad, D.; Stein, C.; Sieger, D.; Mazel, M.; Boudinot, P.; Herbomel, P.; Levraud, J. P.; Lutfalla, G.; Leptin, M. (2010) In vivo analysis of Ifn-gamma1 and Ifn-gamma2 signaling in zebrafish. *J Immunol 185* (11), 6774-82.
173. Fountoulakis, M.; Gentz, R. (1992) Effect of glycosylation on properties of soluble interferon gamma receptors produced in prokaryotic and eukaryotic expression systems. *Bio/technology 10* (10), 1143-7.
174. Kotenko, S. V.; Izotova, L. S.; Pollack, B. P.; Mariano, T. M.; Donnelly, R. J.; Muthukumaran, G.; Cook, J. R.; Garotta, G.; Silvennoinen, O.; Ihle, J. N. (1995) Interaction between the components of the interferon gamma receptor complex. *J Biol Chem 270* (36), 20915-21.
175. Marsters, S. A.; Pennica, D.; Bach, E.; Schreiber, R. D.; Ashkenazi, A. (1995) Interferon gamma signals via a high-affinity multisubunit receptor complex that contains two types of polypeptide chain. *Proc Natl Acad Sci U S A 92* (12), 5401-5.
176. Watanabe, Y.; Inoko, Y. (2009) Size-exclusion chromatography combined with small-angle X-ray scattering optics. *J Chromatogr A 1216* (44), 7461-7465.

6. Curriculum vitae

JIŘÍ ZAHRADNÍK
zahradj@ibt.cas.cz / Tylai@seznam.cz

Home adress:
Vančurova 5, Plzeň – Bílá Hora, Vančurova 5, 301 00 Plzeň, Czech Republic
IBT adress:
BIOCEV, Průmyslová 5, 252 42 Vestec, Czech Republic, http://www.biocev.eu/en/
Current adress:
Weizmann Institute of Science, Rehovot Israel 7610001

CURRENT POSITION

Weizmann Institute of Science
Laboratory Protein-protein Interactions
pre-Postdock

EDUCATION

2014 – present	**PhD. Degree in Biochemistry; Charles University, Prague**
2013 – 2016	Mgr. Degree (equivalent to MSc.) in Molecular Biology; Faculty of Science, Department of Biology, Charles University Prague Specialization: Molecular biology and genetics of Prokaryotes
2012 – 2014	Mgr. Degree in Biochemistry; Faculty of Science, Department of Chemistry, Charles University Prague Specialization: Protein biology, Enzymology, Organic chemistry
2009 – 2013	BSc. in Molecular Biology; Faculty of Science, Department of Biology, Charles University Prague
2008 – 2012	BSc. in Biochemistry; Faculty of Science, Department of Chemistry, Charles University Prague

GRANTS AND AWARDS

2014 – 2017	**Microbial metabolisms of the morphine alkaloids** Grant Agency of Charles University
2017	**1st Price in Biocev Science photo**

Participation in research teams

2015 – 2018	**Interleukins of the IL-10 family: specificity and targeted modulation of interactions with receptors, Applicant: Bohdan Schneider** Czech Science Foundation (16-20507S)

RESEARCH EXPERIENCE

Institute of Biotechnology AS CR, v.v.i.

2014 – 2018	Graduate Research Assistant; Supervisor: B. Schneider Interferon gamma and Interleukins of the IL-10 family: specificity and targeted modulation of interaction with receptors; Evolution of IFNg and IL-10 family interleukins; Structure-function studies on RAYT tyrosine transposases and REP sequences;

Institute of Microbiology AS CR, v.v.i.

2014 – 2017 Graduate Research Assistant; Supervisor: P. Kyslík
Morphine alkaloid induced changes and toxicity in bacterial cells study; Old Yellow Enzyme family structure-function studies;

2009 – 2014 Undergraduate Research Assistant; Supervisor: M. Šulc, Advisor: P. Kyslík
Characterization of biotransformation potential of *Agrobacterium bohemicum* using HPLC (HPLC*MS) and FPLC instruments;

PUBLICATIONS

1. Kyslíková, E., Babiak, P., Štěpánek, V., **Zahradník, J.**, Palyzová, A., Marešová, H., Valešová, R., Hájíček, J. Kyslík, P. (2013) Biotransformation of codeine to 14-OH-codeine derivatives by Rhizobium radiobacter R89-1. *J Mol Catal B: Enzymatic* 87: 1-5

2. Černý, J., Biedermannová, L., Mikulecký, P., **Zahradník, J.**, Charnavets, T., Šebo, P., Schneider, B. (2015) Redesigning Protein Cavities as a Strategy for Increasing Affinity in Protein-Protein Interaction: Interferon-γ Receptor 1 as a Model. *Biomed Res Int* 2015: 716945.

3. Mikulecký, P., **Zahradník, J.**, Kolenko, P., Černý, J., Charnavets, T., Kolářová, L., Nečasová, I., Pham, P.N., Schneider, B. (2016) Crystal structure of human interferon-γ receptor 2 reveals the structural basis for receptor specificity. *Acta Crystallogr D Struct Biol* 72(9):1017-25. **(Corresponding structure PDB code: 5eh1)**

4. Grulich, M., Brezovský, M., Štěpánek, V., Palyzová, A., Marešová, H., **Zahradník, J.**, Kyslíková, E., Kyslík, P. (2017) In-silico driven engineering of enantioselectivity of a penicillin G acylase towards active pharmaceutical ingredients. *J Mol Catal B: Enzymatic* 133 (1):S53-S59

5. Palyzova, A., **Zahradník, J.**, Marešová, H., Sokolovská, L., Kyslíková, E., Grulich, M., Štěpánek, V., Řezanka, T., Kyslík, P. (2017) Potential of the strain *Raoultella* sp. KDF8 for removal of analgesics. *Folia Microbiol* 63(3), 273-282

6. **Zahradník, J.**, Nunvar, J., Pařízková, H., Kolářová, L., Palyzová, A., Marešová, H., Grulich, M., Kyslík, P. (2018) *Agrobacterium bohemicum* sp.nov. isolated from poppy seed wastes in central Bohemia. *Syst Appl Microbiol* 41(3), 184-190

7. **Zahradník, J.**, Kolenko, P., Palyzová, A., Černý, J., Kolářová, L., Kyslíková, E., Marešová, H., Grulich, M., Nunvář, J., Šulc , M., Kyslík, P., Schneider, B. (2018) Bacterial Old Yellow Enzymes exhibit autogenic blocking of FMN binding site as reveals a crystal structure of XdpB one member. *PLoS ONE* 13(4): e0195299. **(Corresponding structure PDB code: 5epd)**

8. **Zahradník, J.**, Kolářová, L., Pařízková, H., Kolenko, P., Schneider, B. (2018) Interferons type II and their receptors R1 and R2 in fish species: Structure, function & evolution. *Fish Shellfish Immunol 79,* 140-152 **(Corresponding structure PDB code: 6f1e)**

Reports

1. **Zahradník, J.**, Kyslíková, E. Kyslík, P. (2016) Draft Genome Sequence of *Agrobacterium* sp. Strain R89-1, a Morphine Alkaloid-Biotransforming Bacterium. *Genome Announc* 4(2): e00196-16

2. **Zahradník, J.**, Plačková, M., Palyzová, A., Marešová, H., Kyslíková, E., Kyslík, P. (2017) Draft genome sequence of *Pantoea agglomerans* JM1, strain exhibiting valacyclovir-like hydrolase activity isolated from a soil polluted by industrial production of beta-lactam antibiotics. *Genome Announc* 5(38): e00921-17

REFERENCES

Doc. RNDr. Miroslav Šulc, Ph.D.
Head of Biochemistry Department
Charles University Prague
Hlavova 2030/8, CZ-128 40
Prague 2
mis@natur.cuni.cz

Doc. Bohdan Schneider, Ph.D.
Head of Lab. Biomol. Recogn.
Institute of Biotechnology CAS
Průmyslová 595, CZ-252 42
Vestec
Bohdan.Schneider@ibt.cas.cz

RNDr. Pavel Kyslík, Ph.D.
Head of Lab. Enzyme Technol.
Institute of Microbiology CAS
Vídeňská 1083, CZ-142 20
Prague
Kyslik@biomed.cas.cz

7. Supplements

A) Publication:

Černý, J., Biedermannová, L., Mikulecký, P., Zahradník, J., Charnavets, T., Šebo, P., Schneider, B. (2015) Redesigning Protein Cavities as a Strategy for Increasing Affinity in Protein-Protein Interaction: Interferon-γ Receptor 1 as a Model. *Biomed Res Int* 2015: 716945.

B) Publication:

Mikulecký, P., Zahradník, J., Kolenko, P., Černý, J., Charnavets, T., Kolářová, L., Nečasová, I., Pham, P.N., Schneider, B. (2016): Crystal structure of human interferon-γ receptor 2 reveals the structural basis for receptor specificity. *Acta Crystallogr D Struct Biol* 72(9):1017-25.

C) Publication:

Zahradník, J., Kolářová, L., Pařízková, H., Kolenko, P., Schneider, B. (2018) Interferons type II and their receptors R1 and R2 in fish species: Structure, function & evolution. *Fish Shellfish Immunol* 79, 140-152

Hindawi Publishing Corporation
BioMed Research International
Volume 2015, Article ID 716945, 12 pages
http://dx.doi.org/10.1155/2015/716945

Research Article

Redesigning Protein Cavities as a Strategy for Increasing Affinity in Protein-Protein Interaction: Interferon-γ Receptor 1 as a Model

Jiří Černý, Lada Biedermannová, Pavel Mikulecký, Jiří Zahradník, Tatsiana Charnavets, Peter Šebo, and Bohdan Schneider

Laboratory of Biomolecular Recognition, Institute of Biotechnology, Academy of Sciences of the Czech Republic, Vídeňská 1083, 142 20 Prague, Czech Republic

Correspondence should be addressed to Bohdan Schneider; bohdan.schneider@gmail.com

Received 2 October 2014; Revised 22 December 2014; Accepted 28 December 2014

Academic Editor: Yuedong Yang

Combining computational and experimental tools, we present a new strategy for designing high affinity variants of a binding protein. The affinity is increased by mutating residues not at the interface, but at positions lining internal cavities of one of the interacting molecules. Filling the cavities lowers flexibility of the binding protein, possibly reducing entropic penalty of binding. The approach was tested using the interferon-γ receptor 1 (IFNγR1) complex with IFNγ as a model. Mutations were selected from 52 amino acid positions lining the IFNγR1 internal cavities by using a protocol based on FoldX prediction of free energy changes. The final four mutations filling the IFNγR1 cavities and potentially improving the affinity to IFNγ were expressed, purified, and refolded, and their affinity towards IFNγ was measured by SPR. While individual cavity mutations yielded receptor constructs exhibiting only slight increase of affinity compared to WT, combinations of these mutations with previously characterized variant N96W led to a significant sevenfold increase. The affinity increase in the high affinity receptor variant N96W+V35L is linked to the restriction of its molecular fluctuations in the unbound state. The results demonstrate that mutating cavity residues is a viable strategy for designing protein variants with increased affinity.

1. Introduction

In studying specificity and affinity of protein-protein interactions, the main focus is traditionally on the structural properties of the interface, for example, complementarity of the residue composition, hydrogen-bonding networks, and the role of hydration [1]. However, there is also a significant contribution of the conformational dynamics to the binding affinity. Analysis of molecular dynamics simulations of 17 protein-protein complexes and their unbound components with quasi-harmonic analysis [2] concluded that the protein flexibility has an important influence on the thermodynamics of binding. Moreover, changes in the protein conformational dynamics may lead to substantial changes in affinity to binding partners without an apparent structural change of the complex. For example, reorganization of the hydrogen bonding networks and solvent bridges of the interacting molecules upon mutation, which was accompanied only by subtle structural changes, leads to radically different binding free energy [3, 4]. A recent work [5] shows that the apparent change in the amino acid dynamics determined by NMR spectroscopy is linearly related to the change in the overall binding entropy and also that changes in side-chain dynamics determined from NMR data can be used as a quantitative estimate of changes in conformational entropy [6, 7]. Also, an analysis of crystallographic B-factors has revealed a significant decrease of flexibility of residues exposed to solvent compared to flexibility of residues interacting with another biomolecule and further compared to their flexibility in the protein core [8]. This "freezing" of atoms upon complexation and in the protein core is only slightly larger for the side chain atoms than for the main chain atoms. Entropic cost specific for side-chain freezing has been computationally evaluated as a small, but important contribution to the thermodynamics

of binding [9, 10]. These results indicate that changes in amino acid conformational entropy upon binding contribute significantly to the free energy of protein-protein association.

However important the interaction interface is for the affinity, the interaction is influenced by the whole composition of the cognate molecules, so that modulation of affinity can be achieved by changing other residues than residues at the interface. One such possible alternative approach would be filling cavities in one of the binding partners, thus influencing the stability and dynamics of the interacting proteins [11–14]. Thermodynamic consequences of introducing cavity-filling mutations have been discussed for residues at the interaction interface [15–17] showing that filling the interfacial cavity increases affinity due to both gain in binding enthalpy and a loss in binding entropy, the latter being attributed to a loss of conformational degrees of freedom. It has been shown that interactions between the internal "core" residues is responsible for the folding and thermal stability of a protein [18]. Here, we decided to test whether the protein-protein affinity could be increased by mutations not on the interface, but in cavities inside one of the cognate protein molecules.

This study follows our previous article [21] in which we designed mutations increasing the affinity of human interferon-γ receptor 1 (IFNγR1) towards its natural cognate molecule interferon-γ (IFNγ), an important protein of innate immunity [22, 23]. Here, we retain this model system and the main contours of the protocol but replace the search for interface mutations by searching for mutations in the receptor cavities in order to further increase its interaction affinity to IFNγ and our computer analysis revealed four such cavity mutants. Combining one of these cavity mutations with the best variant designed in our previous study led to a sevenfold increase in affinity compared to the wild-type receptor. We show that the affinity increase in this mutant is related to the restricted flexibility of amino acids in the unbound state of IFNγR1.

2. Materials and Methods

2.1. Outline of the Protocol. Our computational predictions are based on the analysis of crystal structures of complexes between IFNγ and the extracellular part of IFNγR1, namely, the structures of PDB codes 1fg9 [19] and 1fyh [20] that contain four crystallographically independent IFNγ/IFNγR1 complexes. Throughout the paper, IFNγR1 residues are numbered as in UniProt entry P15260. We used the empirical force field implemented in the software FoldX [24] to search for mutations within the positions lining the internal cavities of IFNγR1 molecule that would increase its stability and/or its affinity to IFNγ. All designed mutants of IFNγR1 were subsequently expressed and purified and their affinity to a "single-chain" form of IFNγ (IFNγSC, [25]) was measured. Individual steps of the computational protocol as well as experimental procedures are described below.

2.2. In Silico Design of Variants. The program 3V [26] was used to identify internal cavities in all four available structures of IFNγR1 molecules complexed with IFNγ. In total, 52 cavity-lining residues, which were identified as encapsulating the cavities in at least one of the four structures, were extracted using the VMD program [27]. Each of 52 amino acid residues identified as lining the internal receptor cavities was mutated in all four crystal IFNγ/IFNγR1 complexes to 20 amino acid residues using the "`positionscan`" and "`analyzecomplex`" FoldX keywords. This represented $52 \times 4 \times 20$ mutations (including self-mutations leading to $\Delta\Delta G = 0$). Three types of changes of free energy ($\Delta\Delta G$) were calculated using the program FoldX:

(1) "$\Delta\Delta G$ of folding of IFNγR1 in complex" gauged the influence of mutations on the stability of the whole IFNγ/IFNγR1 complex;

(2) "$\Delta\Delta G$ of folding of free IFNγR1" estimated the effect of mutations on the stability of the isolated receptor;

(3) "$\Delta\Delta G$ of binding" of complex between IFNγR1 and IFNγ estimated the change of the interaction between the receptor molecule and the rest of the complex.

2.3. Modeling. IFNγR1 models are based on PDB structures 1fg9 [19] and 1fyh [20]. Missing residues in both structures were added using Modeller suite of programs [28]. The lowest energy loop models were used for further calculations.

2.4. Molecular Dynamics (MD) Simulations. MD simulations were run using GROMACS suite of programs to test the stability and dynamic properties, including analysis of values of root means square fluctuations (RMSF) [29] and the effect of variable geometry on prediction of changes of interaction free energy ($\Delta\Delta$Gs), of the IFNγ/IFNγR1 complexes (PDB codes 1fyh and 1fg9). More detailed protocol of MD and FoldX calculations follows.

2.5. Protocol of Molecular Dynamics (MD) Calculations. For the MD simulations the following setup was used: protonation state was determined by `pdb2gmx` program using parameters provided by the OpenMM [30] Zephyr [31] program. Implicit solvation (GBSA, $\varepsilon = 78.3$, with collision interval of 10.99 fs) was used in combination with parm96 force field [32]. OpenMM Zephyr implementation of GPU accelerated version of GROMACS [29] suite of programs was used to simulate the systems. The initial crystal structures were optimized and the simulation was propagated at 300 K with the time step of 2 fs. RMSF (root-mean square fluctuations) of atoms in the analyzed proteins were calculated from the 100 ns trajectory to estimate flexibility of residues; they were calculated by `g_rmsf` program in 5 ns windows.

2.6. Construction, Expression, and Purification of Recombinant IFNγR1 Variants. We followed the protocols from our previous study [21] for all proteins produced in this study. All selected IFNγR1 variants were prepared, expressed, and successfully purified to homogeneity by the following protocol.

Codon-optimized synthetic gene (GenScript) encoding extracellular domain of human IFNgR1 (residues 18–245) was cloned into the pET-28b(+) vector (Novagen) using

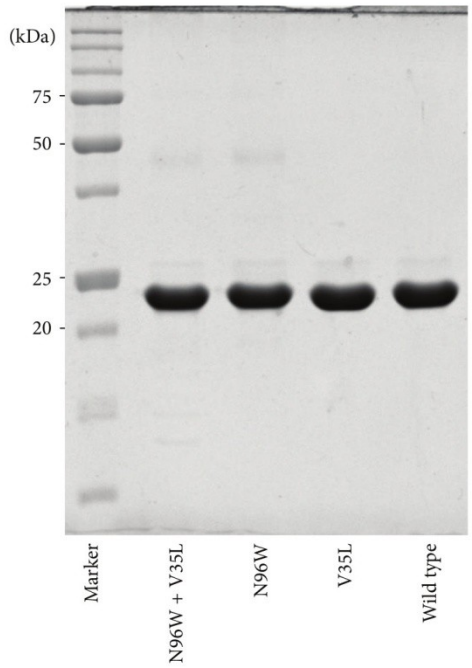

FIGURE 1: Nonreducing 12.5% SDS-PAGE gel of selected monomeric refolded recombinant His-tagged IFNγR1 variants. Proteins were extracted from inclusion bodies by 8 M urea, further purified on Ni-NTA agarose, and dialyzed, and monomeric fraction was separated on gel filtration column (see above). IFNγR1 with C-terminal His-Tag migrates at a molecular mass of 23 kDa when analyzed on nonreducing SDS-PAGE gel.

NcoI and *XhoI* restriction enzymes in frame with N-terminal start codon and C-terminal HisTag. The QuikChange II Site-Directed Mutagenesis Kit (Agilent Technologies) was used for mutating the IFNγR1 gene according to manufacturer's manual using primers listed below. Primers were designed by web-based PrimerX program (http://www.bioinformatics.org/primerx/).

The recombinant IFNγR1 variants were expressed in *Escherichia coli* BL21 (λDE3) in LB medium containing 60 μg/mL of kanamycin at 37°C for 4 hours after induction by 1 mM IPTG. Harvested cells by centrifugation (8,000 g, 10 min, 4°C) were disrupted by ultrasound in 50 mM Tris buffer pH 8 and centrifuged at 40,000 g, 30 min, 4°C, and inclusion bodies were dissolved in 50 mM Tris buffer pH 8 containing 8 M urea and 300 mM NaCl to extract protein that was further affinity-purified on Ni-NTA agarose (Qiagen) in the same buffer. Protein was eluted from resin by 250 mM Imidazole pH 8 in previous buffer and refolded by dialysis against 100 mM Tris-HCl pH 8, 150 mM NaCl, 2.5 mM EDTA, 0.5 mM Cystamine, and 2.5 mM Cysteamine overnight at 4°C. Final purification of monomeric receptor variants was performed at 4°C on a HiLoad 16/600 Superdex 200 pg (GE Healthcare) equilibrated by PBS buffer pH 7.4 (Figure 1). Monodispersity of the purified receptor protein was verified by dynamic light scattering (DLS) using Malvern Zetasizer Nano ZS90 instrument (data not shown).

2.7. Primers. Mutagenesis primers are designed for the introduction of single residue substitution into IFNγR1 WT. Mutated nucleotides are underlined. We have the following:

V35L

Forward: 5′-GTCCCGACCCCGACCAACTTGACGATT-GAAAGTTACAAC-3′

Reverse: 5′-GTTGTAACTTTCAATCGTCAAGTTGGT-CGGGGTCGGGAC-3′

A114E

Forward: 5′-GAAAGAATCAGCGTATGAAAAATCGGA-AGAATTCGCC-3′

Reverse: 5′-GGCGAATTCTTCCGATTTTTCATACGC-TGATTCTTTC-3′

D124N

Forward: 5′-CGCCGTGTGCCGTAATGGCAAAATCG-3′

Reverse: 5′-CGATTTTGCCATTACGGCACACGGCG-3′

H222Y

Forward: 5′-CTGAAGGCGTTCTGTATGTCTGGGGTG-TC-3′

Reverse: 5′-GACACCCCAGACATACAGAACGCCTTC-AG-3′

2.8. Construction, Expression, and Purification of IFNγSC. Recombinant interferon gamma in so-called single chain form (IFNγSC) described by [25] was cloned into pET-26b(+) vector (Novagen) using *NdeI* and *XhoI* restriction enzymes in frame with N-terminal start codon not to have no peptide leader nor tag.

The recombinant IFNγSC was expressed in *E. coli* BL21 (λDE3) in LB medium containing 60 μg/mL of kanamycin at 30°C for 4 hours after induction by 1 mM IPTG. Harvested cells by centrifugation (8,000 g, 10 min, 4°C) were disrupted by ultrasound in 20 mM Na-Phosphate buffer pH 7.3 and centrifuged at 40,000 g, 30 min, 4°C, and soluble fraction was further purified on SP Sepharose HP (GE Healthcare) using linear gradient of NaCl and further purified to homogeneity by gel filtration in same procedure as IFNγR1 receptor (see above).

2.9. Biophysical Characterization of the Studied Proteins. Melting temperatures of the receptor variants were measured using fluorescence-based thermal shift assay and for selected mutants by CD melting experiments. Interactions between IFNγR1 variants and IFNγSC were measured by the technique of surface plasmon resonance (SPR) as discussed in our previous study [21]. Experimental procedures are detailed below.

Table 1: Cavities in the four molecules of the IFNγR1 receptor in crystal structures 1fg9 [19] and 1fyh [20]. The receptor molecules are labeled by chain ID (chains C and D from 1fg9 and chains B and E from 1fyh). Figure 2 shows cavities 1–8 as they project into the chain C of 1fg9.

	Surface [Å^2]*	Number of residues lining the cavity†	Residues selected for mutation	Cavity observed in IFNγR1 chain of	
				1fg9	1fyh
1	134	7	V35, A114	C D	—
2	133	5	—	—	B E
3	470	14	D124	C D	—
4	262	9	H222	C D	B E
5	120	6	—	C D	E
6	165	7	—	C D	E
7	177	7	—	D	B E
8	138	5	—	C	B

*Surface calculated with a probe radius of 0.25 Å for cavities combined from all relevant receptor chains.
†Some residues are shared by neighboring cavities.

2.10. CD Measurements. CD spectra were recorded using "Chirascan-plus" (Applied Photophysics) spectrometer in steps of 1 nm over the wavelength range of 190–260 nm. Samples at a concentration of 0.2 mg/mL were placed into 0.05 cm path-length quartz cell to the thermostated holder and individual spectra were recorded at the temperature of 25°C. The CD signal was expressed as the difference between the molar absorption of the right- and left-handed circularly polarized light and the resulting spectra were buffer subtracted. To analyze the ratio of the secondary structures we used the CDNN program provided with Chirascan CD spectrometer [33]. For CD melting measurements, samples at a concentration of 1.5 mg/mL were placed into 10 mm path-length quartz cell to the thermostated holder and CD signal at 280 nm was recorded at 1°C increment at rate of 1.0°C/min over the temperature range of 25 to 65°C with an averaging time of 10 seconds. CD melting curves were normalized to relative values between 1.0 and 0.0.

2.11. Thermostability of the IFNγR1 Variants by Thermal-Based Shift Assay. Melting temperature (T_m) curves of the WT and selected variants were obtained from fluorescence-based thermal shift assay (TSA) using fluoroprobe. Experiment was performed in "CFX96 Touch Real-Time PCR Detection System" (Bio-Rad) using FRET Scan Mode. The concentration of fluorescent SYPRO Orange dye (Sigma Aldrich) was 8-fold dilution from 5000-fold stock and protein concentration was 2 μL in final volume of 25 μL. As a reference we used only buffer (PBS buffer pH 7.4) without protein. Thermal denaturation of proteins was performed in capped "Low Tube Strips, CLR" (Bio-Rad) and possible air bubbles in samples were removed by centrifugation immediately before the assay. The samples were heated from 20°C to 75°C with stepwise increment of 0.5°C per minute and a 30 s hold step for every point, followed by the fluorescence reading. Data subtraction by reference sample was normalized and used for first derivative calculation to estimate the melting temperature.

2.12. SPR Measurements. His-tagged receptor molecules were diluted to concentration of 10 μg/mL in PBST running buffer (PBS pH 7.4, 0.005% Tween 20) and immobilized on a HTG sensor chip activated with Ni^{2+} cations at a flow rate 30 μL/min for 60 s to gain similar surface protein density. Purified IFNγSC was diluted in running buffer to concentrations ranging from 0.1 to 9 nM and passed over the sensor chip for 90 seconds at a flow rate 100 μL/min (association phase). Dissociation was measured in the running buffer for 10 min at the same flow rate. Correction for nonspecific binding of IFNγSC to the chip surface was done by subtraction of the response measured on uncoated interspots and reference channel coated with His-tagged Fe-regulated protein D (FrpD) from Neisseria meningitides [34]. Data were processed in the ProteOn Manager software (version 3.1.0.6) and the doubly referenced data were fitted to the 1 : 1 "Langmuir with drift" binding model.

3. Results and Discussion

3.1. Internal Cavities Identified in IFNγR1. The cavity analysis revealed generally different number and size of cavities for each IFNγR1 crystal structure; their characteristics are listed in Table 1; their location in a representative receptor molecule (PDB entry 1fg9, chain C [19]) is highlighted in Figures 2(a) and 2(b). All amino acid residues lining cavities in all four IFNγR1 proteins complexed with IFNγ were combined, resulting in 52 residues used in subsequent *in silico* analysis.

3.2. In Silico Design of Variants. All 52 amino acids lining the cavities of the receptor molecule were subject to the mutation analysis by FoldX. The resulting $\Delta\Delta G$ values indicated potential for mutation leading to increasing the receptor affinity to IFNγ. The mutations were ordered by their $\Delta\Delta G$ values and the first 50 best mutations from each crystal structure (200 mutations in total) were further analyzed. Of these 200 mutations, twelve positions were predicted in all four or at least three crystal structures. The twelve promising positions are highlighted in orange and yellow in Figure 2(c). Following the previous study [21], where we observed significant differences between $\Delta\Delta G$ predicted directly from the crystal structures and from structures after molecular dynamics (MD) relaxation, we performed short

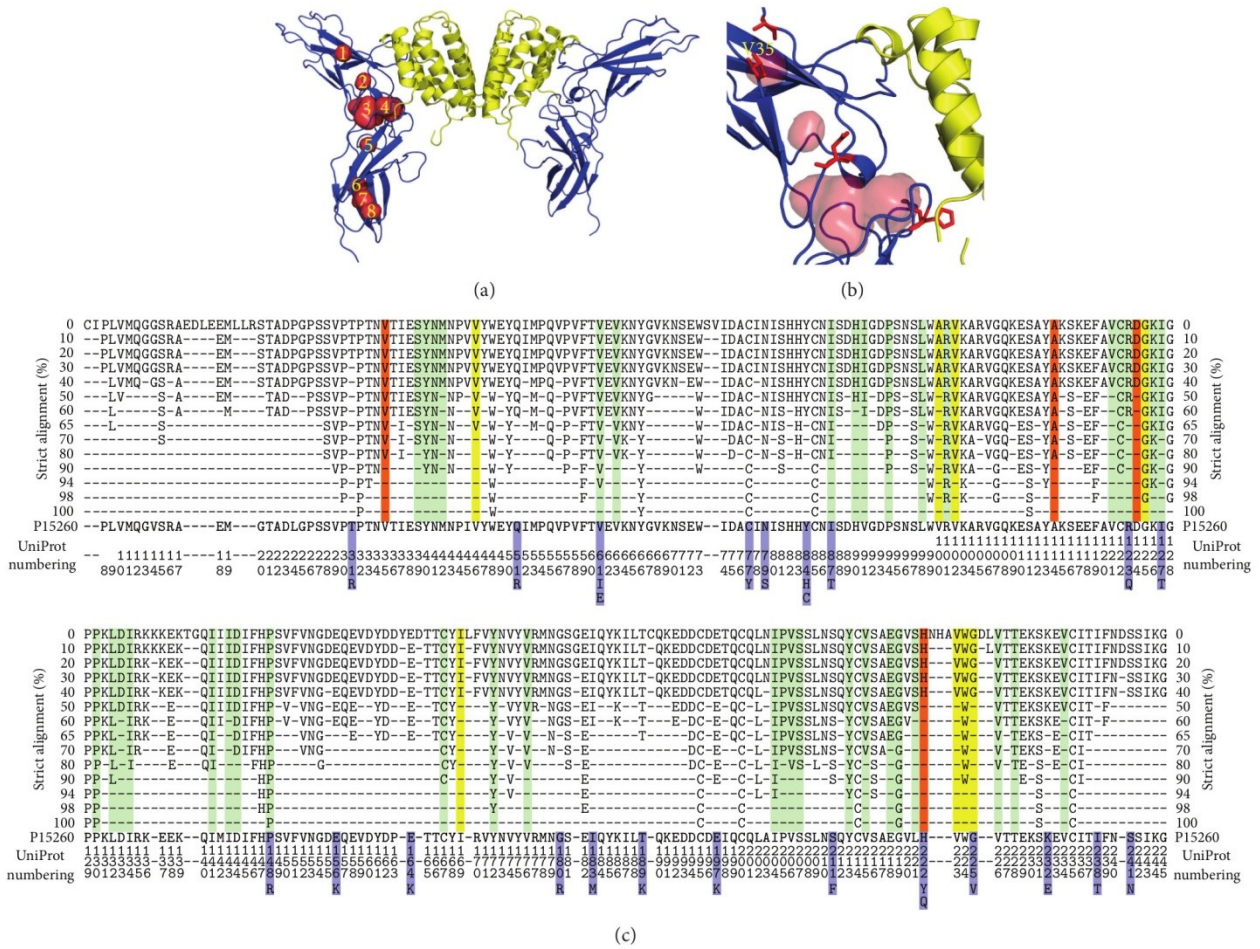

FIGURE 2: (a) The complex between IFNγ and the extracellular part of its receptor 1 (IFNγR1) from crystal structure of PDB code 1fg9 [19]. The two IFNγR1 molecules are drawn as blue cartoon and IFNγ homodimer as yellow cartoon. The eight identified cavities in the receptor molecule are shown as numbered red surfaces. (b) A close-up of the mutated cavities. The receptor cavities are drawn as red surface and residues selected for mutations as red sticks; valine 35 is labeled. (c) Residue conservancy calculated by strict alignment of 32 sequences of the extracellular part of IFNγR1 from 19 species. The residues lining the cavities and not suitable for mutation are highlighted in green, those selected by FoldX as mutable in yellow, and the residues selected for mutations after MD simulations are in red (they are also listed in Table 1). Blue highlights show IFNγR1 mutants occurring naturally in humans. Percentages of the conservation are shown on the left and right sides; analyzed sequence (residues 6–245 of the UniProt entry P15260) is shown at the bottom of the alignment.

(10 ns) MD simulations of the four crystal structures of complexes between wild type IFNγR1 and IFNγ, and repeated the FoldX mutation analysis on 500 snapshots extracted from these MD trajectories. After averaging of the predicted $\Delta\Delta G$ values for the twelve selected positions, we made the final selection of the four candidate mutations. The averaged $\Delta\Delta G$ values resulting from these calculations for structure 1fg9, receptor chain C, are summarized in Figure 3. The final selection of the four variants is listed in Table 2 together with the changes of their binding free energies averaged over 500 MD snapshots from each of the four IFNγ/IFNγR1 complexes in crystal structures 1fg9 and 1fyh.

Finally, the four consensus candidate mutations, which resulted as the best replacements of the WT sequence, were expressed, and characterized by SPR, CD, and thermal-based shift assay. The relative affinities of these four cavity-filling single mutants are shown in Figure 4(a) together with relative affinities of the double mutants combining the four cavity-filling mutations with mutation N96W.

As Table 2 and in detail Figure 3 show, the $\Delta\Delta G$ calculations revealed only modest potential gains in interaction affinity, probably because of small cavity volumes as well as the fact that they are often lined by evolutionary highly conserved residues. As opposed to the interface mutations, where the predicted $\Delta\Delta$Gs of IFNγR1 stability and binding to IFNγ served as a sufficient criterion for the selection of affinity increasing mutations, there was no clear-cut rule for selecting internal cavity mutations that would result in improved interaction energy. We thus decided to test experimental consequences of combination of three types of $\Delta\Delta G$ values

Table 2: Predicted changes of free energy changes ($\Delta\Delta G$) of the four selected IFNγR1 variants with cavity-lining mutations relative to the wild type receptor. All energy values are in kcal/mol.

Variant	$\Delta\Delta G$ of folding of IFNγR1 in complex*	$\Delta\Delta G$ of folding of free IFNγR1†	$\Delta\Delta G$ of binding of IFNγR1/IFNγ complex‡	Sequence conservation¶
V35L	−0.88	−0.85	−0.02	80%
A114E	0.28	0.46	−0.20	60%
D124N	0.65	0.88	−0.21	40%
H222Y	−0.72	−0.69	0.15	40%

*$\Delta\Delta G$ of folding of IFNγR1 bound to IFNγ measures the influence of mutations on the stability of the whole complex.
†$\Delta\Delta G$ of folding of IFNγR1 alone represents changes of the stability of the isolated receptor.
‡$\Delta\Delta G$ of binding of the whole complex between IFNγR1 and IFNγ estimates the change of the affinity between the receptor molecule and the rest of the complex.
¶Sequence conservation of amino acid residues at positions 35, 114, 124, and 222. It was based on the global alignment of 32 sequences of the extracellular part of IFNγR1 (Figure 2(c)).

[1]		GLY	ALA	VAL	LEU	ILE	SER	THR	CYS	MET	ASN	GLN	LYS	ARG	HIS	PRO	ASP	GLU	PHE	TYR	TRP
VAL	35	2.8	2.0	0.0	−0.9	−0.4	2.9	1.6	1.3	0.1	2.0	2.5	3.5	5.1	4.7	1.2	3.4	3.5	4.3	7.3	10.6
VAL	46	3.8	2.2	0.0	−0.1	−0.3	3.1	1.8	1.8	0.6	2.4	3.0	4.1	6.4	6.4	2.0	3.6	3.7	4.0	6.6	9.1
VAL	100	5.6	3.7	0.0	0.3	−0.3	4.2	2.4	2.7	0.8	3.6	3.9	5.4	7.6	6.2	5.0	5.5	5.1	4.0	6.8	9.8
VAL	102	5.2	3.3	0.0	1.2	−0.4	4.0	2.2	2.5	1.8	3.6	4.1	7.1	11.9	9.4	4.8	4.9	4.9	7.5	11.2	15.6
ALA	114	1.0	0.0	−0.2	0.1	0.1	0.3	0.2	0.1	0.3	0.6	0.2	0.2	0.7	3.3	2.3	1.1	0.3	0.7	1.0	1.9
ASP	124	3.0	2.2	2.5	1.4	2.5	2.3	2.7	2.0	1.7	0.7	1.4	1.8	2.1	2.3	5.7	0.0	1.5	1.4	1.6	2.5
GLY	125	0.0	2.0	6.0	6.4	7.7	2.9	5.6	3.0	4.7	5.7	6.8	8.1	10.1	31.3	6.2	7.1	7.1	12.0	14.1	21.8
ILE	169	5.1	3.7	1.1	0.1	0.0	4.7	3.2	2.9	0.3	3.0	3.2	4.1	5.5	3.9	1.8	4.2	3.6	1.9	4.7	7.0
HIS	222	0.7	0.1	0.8	−0.3	1.1	−0.3	0.6	0.4	−0.3	−0.6	0.5	−0.1	0.3	0.0	2.9	−0.1	0.5	−1.1	−0.7	1.1
VAL	223	2.5	2.0	0.0	0.7	0.3	3.7	1.4	2.3	0.9	3.0	3.2	3.8	6.3	14.2	7.3	4.6	4.9	7.6	11.5	15.6
TRP	224	5.5	4.7	3.5	2.8	3.1	5.5	4.9	4.5	2.4	4.8	4.2	4.2	4.0	3.3	4.6	5.9	5.2	1.1	1.5	0.0
GLY	225	0.0	1.5	3.3	2.0	3.4	2.0	3.3	1.8	1.6	2.1	2.5	2.6	2.9	4.7	4.3	2.9	3.0	2.4	2.6	2.9

[2]		GLY	ALA	VAL	LEU	ILE	SER	THR	CYS	MET	ASN	GLN	LYS	ARG	HIS	PRO	ASP	GLU	PHE	TYR	TRP
VAL	35	2.8	2.0	0.0	−0.9	−0.4	2.9	1.6	1.3	0.1	2.0	2.5	3.6	5.3	4.5	1.2	3.4	3.5	4.3	7.3	10.7
VAL	46	5.0	3.0	0.0	−0.2	−0.5	4.1	2.4	2.4	0.5	3.2	3.8	5.1	8.1	7.6	2.9	4.8	4.8	4.4	7.9	11.5
VAL	100	5.7	3.8	0.0	0.3	−0.3	4.2	2.4	2.7	0.8	3.7	4.0	5.5	7.7	5.9	5.0	5.5	5.1	4.1	6.8	9.7
VAL	102	5.2	3.3	0.0	1.2	−0.4	4.0	2.2	2.5	1.8	3.6	4.1	7.1	11.9	9.5	4.8	4.9	4.9	7.5	11.2	15.7
ALA	114	1.0	0.0	−0.2	0.2	0.2	0.3	0.2	0.1	0.4	0.7	0.3	0.3	0.7	3.4	2.3	1.2	0.5	0.8	1.1	2.0
ASP	124	2.4	1.6	2.0	0.7	1.7	1.8	2.1	1.6	0.9	0.9	1.3	1.0	1.4	1.5	4.8	0.0	1.4	1.0	1.2	1.8
GLY	125	0.0	2.0	6.0	6.4	7.8	2.9	5.6	3.0	4.8	5.8	6.8	8.2	10.2	32.2	6.2	7.1	7.2	12.1	14.2	21.9
ILE	169	5.1	3.7	1.1	0.1	0.0	4.7	3.2	2.9	0.3	3.0	3.2	4.2	5.6	3.8	1.8	4.2	3.7	1.9	4.7	7.0
HIS	222	−0.1	−0.6	0.5	−0.4	0.6	−1.0	0.2	−0.1	−0.4	−0.7	0.2	−0.5	0.0	0.0	2.3	−0.3	−0.2	−0.9	−0.7	0.6
VAL	223	0.9	0.6	0.0	0.2	−0.2	1.7	0.4	1.2	0.1	1.2	1.1	0.5	0.9	1.0	5.6	1.6	1.2	0.1	0.3	0.6
TRP	224	2.7	2.1	1.3	1.2	1.1	2.5	2.1	1.9	0.9	2.2	1.9	1.6	2.0	2.0	2.2	2.4	2.0	0.3	0.6	0.0
GLY	225	0.0	1.2	1.9	0.8	1.7	1.2	1.7	1.1	0.6	0.9	0.9	0.8	1.0	1.0	2.8	1.0	1.0	0.4	0.5	0.3

[3]		GLY	ALA	VAL	LEU	ILE	SER	THR	CYS	MET	ASN	GLN	LYS	ARG	HIS	PRO	ASP	GLU	PHE	TYR	TRP
VAL	35	0.0	0.0	0.0	0.0	0.0	0.0	0.0	0.0	0.0	0.0	0.0	−0.1	−0.2	0.0	0.0	0.0	0.0	0.0	0.0	−0.1
VAL	46	0.0	0.0	0.0	0.0	0.0	0.0	0.0	0.0	0.0	0.0	0.0	0.0	0.0	0.0	0.0	0.0	0.0	0.0	0.0	0.0
VAL	100	0.0	0.0	0.0	0.0	0.0	0.0	0.0	0.0	0.0	0.0	0.0	0.0	0.0	0.0	0.0	0.0	0.0	0.0	0.0	0.0
VAL	102	0.0	0.0	0.0	0.0	0.0	0.0	0.0	0.0	0.0	0.0	0.0	0.0	0.0	0.0	0.0	0.0	0.0	0.0	0.0	0.0
ALA	114	0.0	0.0	0.0	−0.1	−0.1	0.0	0.0	0.0	−0.1	−0.1	−0.1	−0.1	0.0	−0.1	0.0	−0.1	−0.2	−0.1	−0.1	−0.1
ASP	124	0.2	0.1	0.0	−0.1	0.1	0.1	0.0	−0.1	−0.1	−0.2	−0.2	−0.1	−0.1	0.1	0.2	0.0	−0.1	−0.1	−0.1	0.1
GLY	125	0.0	0.0	0.0	0.0	−0.1	0.0	0.0	0.0	0.0	0.0	0.0	−0.1	−0.1	−0.1	−0.1	0.0	0.0	−0.1	−0.1	−0.1
ILE	169	0.0	0.0	0.0	0.0	0.0	0.0	0.0	0.0	0.0	0.0	0.0	0.0	0.0	0.0	0.0	0.0	0.0	0.0	0.0	0.0
HIS	222	1.3	1.2	0.9	0.7	0.8	1.1	0.9	0.7	0.4	0.3	0.5	0.4	0.2	0.0	1.2	0.5	0.6	0.1	0.2	0.8
VAL	223	1.7	1.4	0.0	0.1	0.4	2.0	0.8	1.2	0.3	1.5	1.6	2.0	3.2	6.1	2.2	2.7	2.9	5.7	8.2	10.4
TRP	224	3.3	3.1	2.6	1.8	2.2	3.3	3.0	3.0	1.4	2.9	2.3	2.4	2.0	1.3	2.8	3.6	3.1	0.9	0.8	0.0
GLY	225	0.0	0.3	1.1	0.6	1.2	0.6	1.2	0.4	0.3	0.8	0.9	0.9	0.9	2.9	1.3	1.4	1.3	1.1	1.1	1.4

Figure 3: Color-coded values of free energy changes ($\Delta\Delta G$) of mutating the twelve cavity-lining residues of IFNγR1. $\Delta\Delta G$ values were calculated using the program FoldX for 500 MD snapshots and averaged. Red colored matrix fields indicate stabilization, blue ones destabilization. Shown are $\Delta\Delta G$ values calculated for PDB 1fg9 [19]; receptor chain C. analogical matrices are calculated for 1fg9 receptor chain D, and for receptor chains B and E from the structure 1fyh [20]. (1) "$\Delta\Delta G$ of folding of IFNγR1 in complex" gauged the influence of mutations on the stability of the whole IFNγ/IFNγR1 complex. (2) "$\Delta\Delta G$ of folding of free IFNγR1" estimated the effect of mutations on the stability of the isolated receptor. (3) "$\Delta\Delta G$ of binding" of complex between IFNγR1 and IFNγ made an estimate of change of the interaction between the receptor molecule and the rest of the complex.

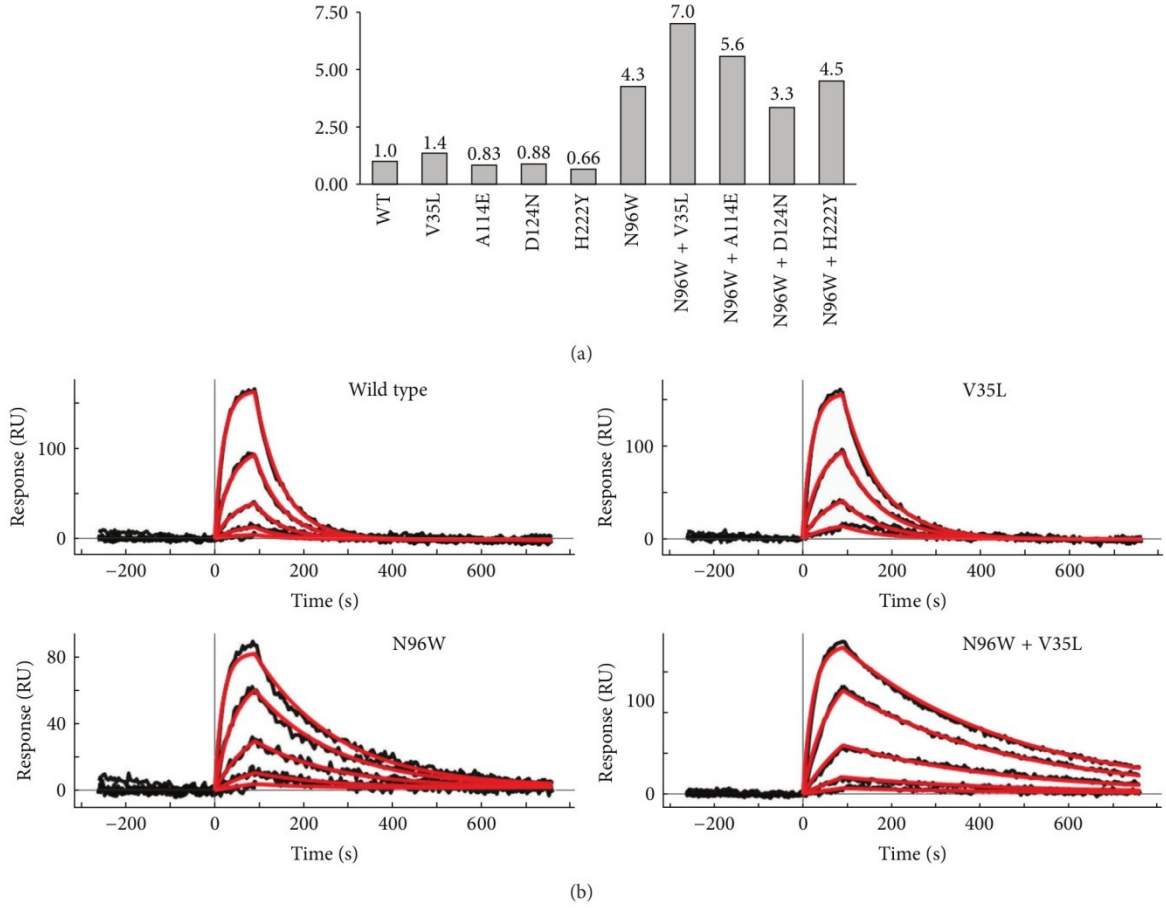

FIGURE 4: Affinities of the IFNγR1 wild type (WT) and mutants to IFNγSC obtained from SPR measurements. (a) Graph represents relative affinities of IFNγR1 variants compared to WT. All selected "cavity" single amino acid mutation variants bind to the IFNγSC with similar affinity as WT, but the V35L variant has slightly higher affinity itself and further increases the affinity of the "interface" mutant N96W if combined together. (b) SPR sensorgrams showing the interaction between IFNγSC and selected IFNγR1 variants. The V35L variant behaves similarly as WT displaying fast association and dissociation phases. Two variants (N96W and N96W + V35L) with higher affinities compared to WT bind IFNγSC with slower dissociation phase, thus increasing the affinity. Measured SPR signal is in black and calculated fitted curves are in red; concentrations of IFNγSC used for SPR measurements were as follows: 0.1, 0.3, 1.0, 3.0, and 9.0 nM.

calculated from the MD snapshots. To identify potentially favorable mutations, we combined $\Delta\Delta G$ values of folding ($\Delta\Delta G$ types (1) and (2) in the *in silico* protocol described in Materials and Methods) and of binding (type (3)). The first two mutations, V35L and H222Y, were predicted to increase $\Delta\Delta G$ of folding to a similar extent for both the complexed and free IFNγR1 ($\Delta\Delta G$ (1) and (2)), while calculated values of their $\Delta\Delta G$ of binding were virtually zero. The other two selected mutations, A114E and D124N, were predicted to slightly improve $\Delta\Delta G$ of binding while both types of their $\Delta\Delta G$ of folding were destabilizing. In the latter case, $\Delta\Delta G$ of folding of free IFNγR1 (type 2) was more unfavorable than $\Delta\Delta G$ of folding of complexed IFNγR1 (type 1). This means that the complex is predicted to be relatively more stable compared to the free IFNγR1.

3.3. Experimental Determination of the Affinities between IFNγR1 Variants and IFNγSC. Computer-designed IFNγR1 variants were expressed and purified and their affinities to IFNγSC were determined by SPR measurements; relative affinities are plotted in Figure 4(a); SPR sensograms are depicted in Figure 4(b). The calculated K_d values showed that the four selected "cavity" single amino acid mutation variants bind to the IFNγSC with similar affinity as WT; a modest increase was observed for the V35L variant. In line with our previous work, we decided to test to what extent the effect of two distant point mutations is additive. To this end, we combined the four cavity mutants designed here with the variant with the highest affinity designed previously, N96W. The results were quite encouraging: while affinity of one double mutant (N96W + H222Y) is neutral and one (N96W + D124) affinity actually decreased, two double mutants, N96W with A114E and V35L, had affinity increased compared to WT. The affinity increase of one of the double mutants, N96W + V35L, is significant, seven times higher than affinity of WT.

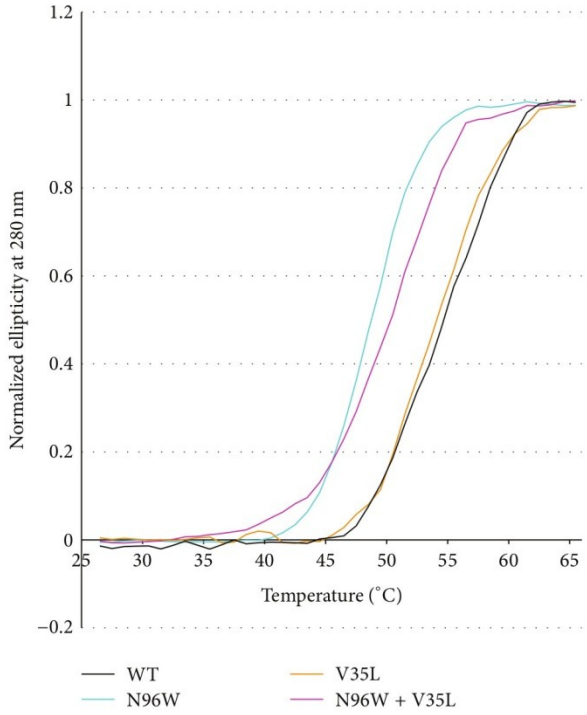

FIGURE 5: Normalized melting curves of IFNγR1 variants measured by temperature-dependent near ultraviolet circular dichroism (CD) spectra. Each data point is from the intensity measured at 280 nm. IFNγR1 WT, V35L, N96W, and N96W + V35L variants were measured in PBS buffer between 25 and 65°C at steps 1°C/minute. The melting temperature (T_m) of IFNγR1 variants was determined as 54°C for WT, 53°C for V35L, 50°C for N96W + V35L, and 48°C for N96W, respectively.

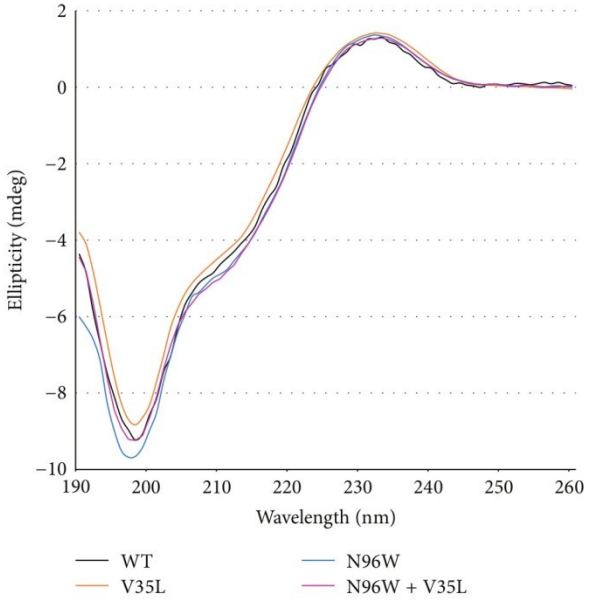

FIGURE 6: Circular dichroism (CD) spectra of IFNγR1 variants (WT, N96W, V35L, and N96W + V35L) measured in water at 25°C. CD melting curves for the same variants are shown in Figure 5.

The thermal stability (Figure 5) and secondary structure (Figure 6) of four IFNγR1 variants, V35L, N96W, N96W + V35L, and WT, were studied by CD and their melting temperatures were confirmed by thermal-based shift assay (Figure 7); the CD-measured melting temperatures are 53, 48, 50, and 54°C, respectively. Both variants with the highest affinity, N96W and N96W + V35L, have melting temperatures lower than WT, so that mutation from asparagine to tryptophan at the position 96 apparently causes a decrease of IFNγR1 thermal stability. However, the CD spectra of all four proteins are highly similar (Figure 6); their analysis provided virtually identical composition of the secondary structure elements dominated by the beta-sheet fractions indicating that no global structural rearrangements were caused by the mutations and the fold of these four variants is most likely the same. Moreover, the spectra are in agreement with the spectrum measured previously [35] for WT of IFNγR1.

3.4. Analysis of Internal Dynamics of the IFNγR1 Variants. To test how a cavity-filling mutation changes the flexibility of the receptor molecule in unbound and complexed states we analyzed root-mean square fluctuations (RMSF) of the selected variants. Comparison of RMSF sorted by their

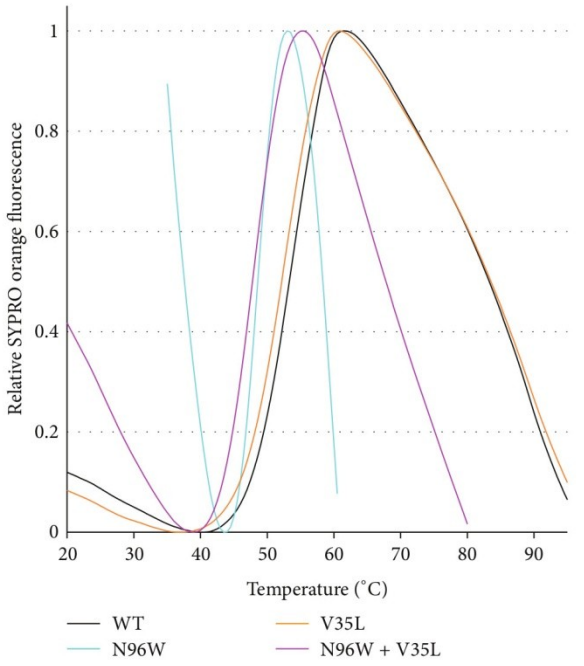

FIGURE 7: Melting temperatures of selected IFNγR1 variants determined by thermal-based shift assay. Plotted are normalized data of reference-subtracted fluorescence intensities of IFNγR1 WT, V35L, N96W, and N96W + V35L. The melting temperatures (T_m) of IFNγR1 variants were determined from the first derivatives of the curves plotted in the figure: 55°C for WT, 53°C for V35L, 49°C for N96W, and 48°C for N96W + V35L. The T_m values determined by temperature-dependent CD spectra and thermal-based shift assay are within 1°C the same.

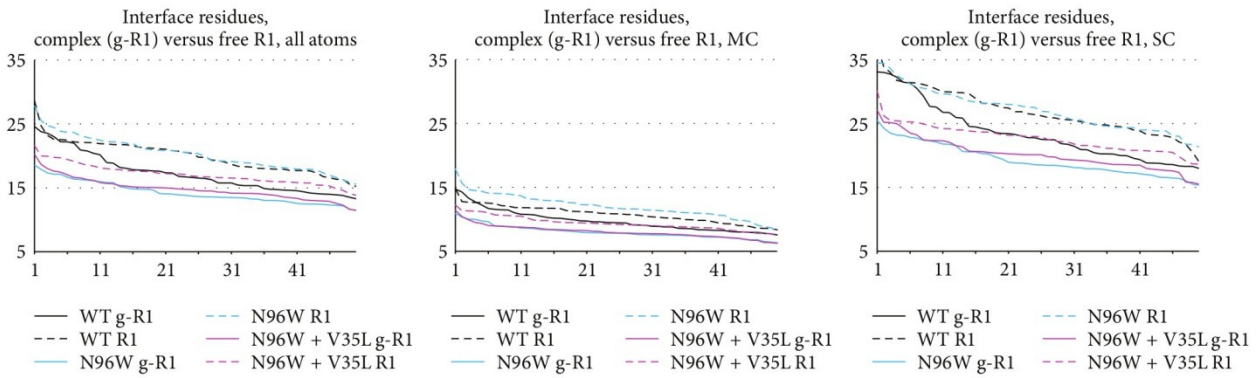

(a)

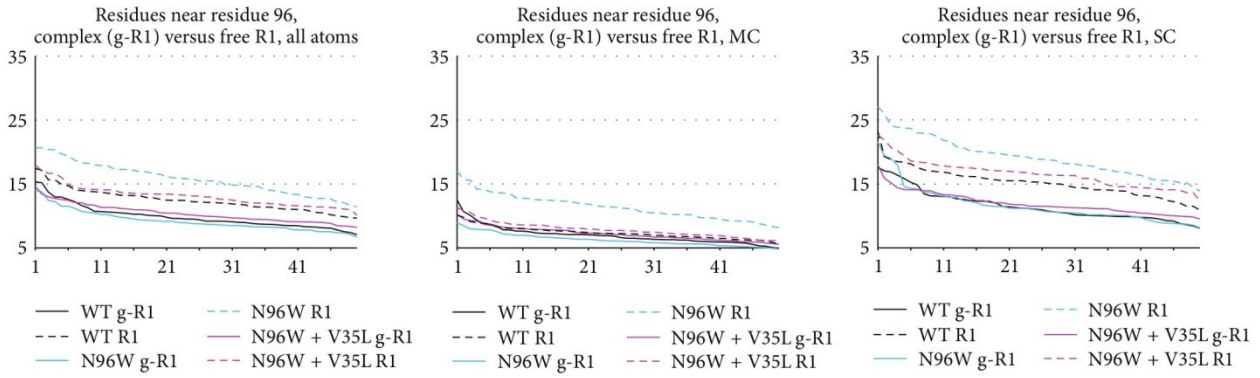

(b)

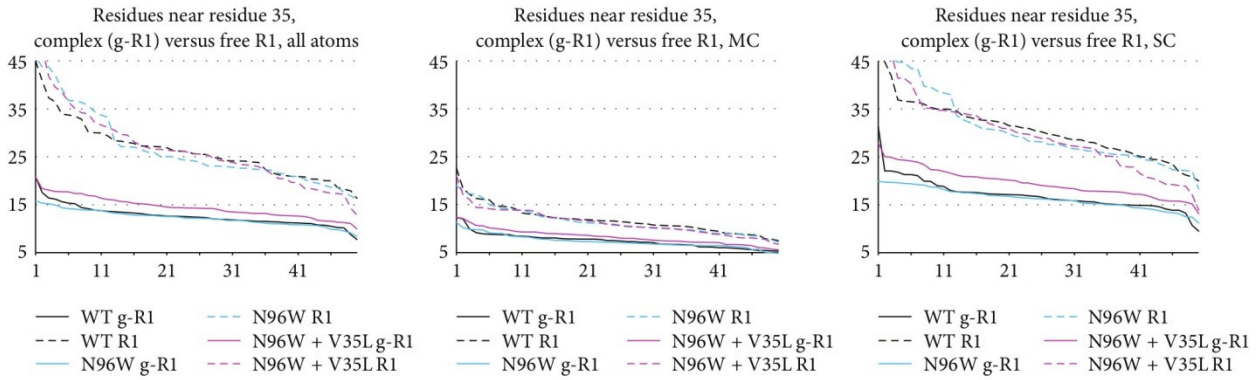

(c)

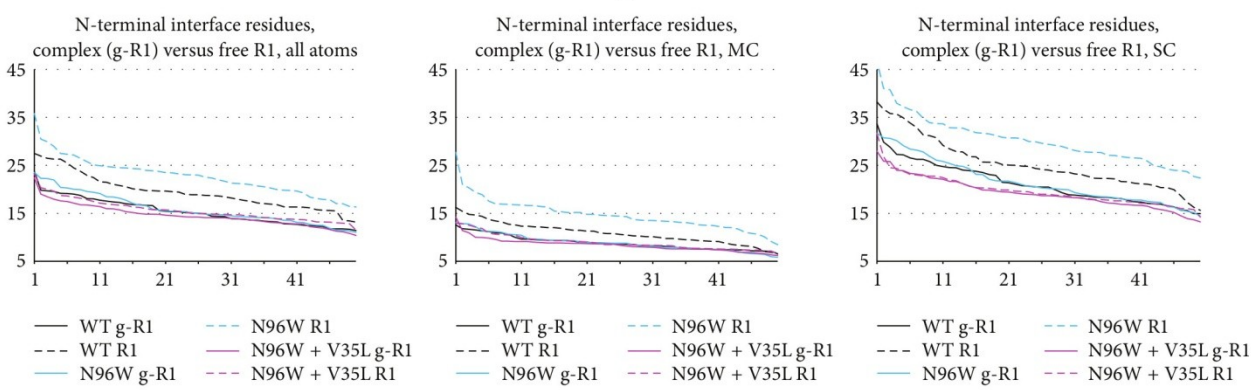

(d)

Figure 8: Continued.

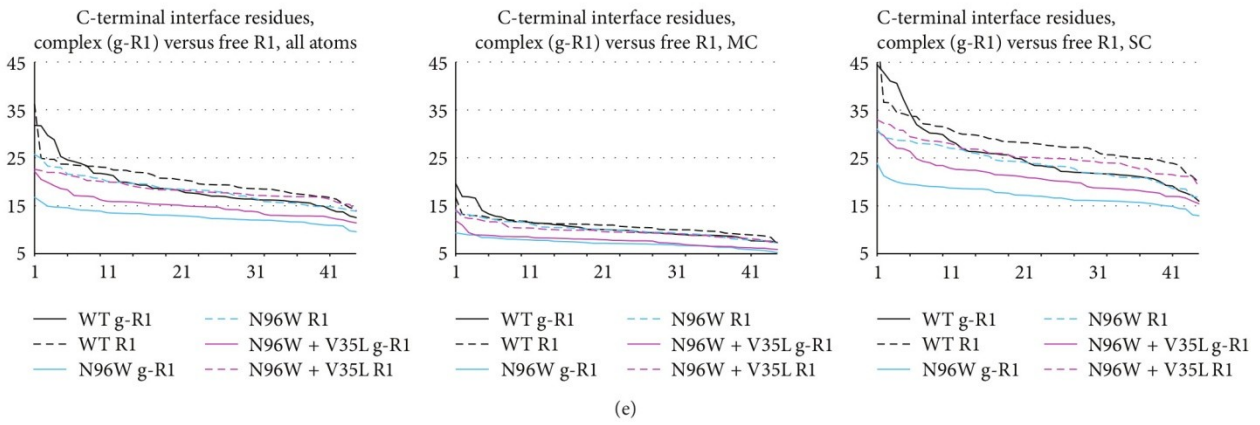

(e)

FIGURE 8: Ranked RMSF values collected at the last 50 ns of the 100 ns MD simulations of WT, N96W, and N96W + V35L variants of IFNγR1. Solid lines labeled g-R1 denote RMSF values of the IFNγ/IFNγR1 complex; dashed lines labeled R1 denote values of IFNγR1 alone. The RMSF values are on the y-axis; the rank of the values (1–50) is on the x-axis. Shown are RMSF values of all atoms, main chain atoms (MC), and side chain atoms (SC) for the following residues: (a) all 40 interface residues (i.e., residue numbers 64, 65, 66, 67, 68, 69, 70, 71, 72, 73, 93, 95, 96, 97, 99, 115, 116, 118, 123, 164, 165, 166, 168, 170, 171, 186, 189, 190, 191, 192, 193, 197, 220, 221, 222, 223, 224, 225, 226, and 227); (b) residues within 6 Å of residue 96 (i.e., residue numbers 65, 66, 67, 91, 92, 93, 94, 95, 96, 97, 98, 119, 120, 121, and 224); (c) residues within 6 Å of residue 35 (i.e., residue numbers 32, 33, 34, 35, 36, 37, 46, 47, 48, 49, 100, 101, 102, 114, 115, 116, and 117); (d) the interface residues from the N-terminal domain (i.e., residues 64 to 123); (e) the interface residues from the C-terminal domain (i.e., residues 164 to 227).

values, "ranked RMSF," for WT, N96W, and N96W + V35L, are plotted in Figure 8 (solid lines for IFNγ/IFNγR1 complexes, dashed lines for IFNγR1 alone). These plots revealed significant differences between dynamics of the variants as is detailed below.

(1) The interface residues of N96W and WT are more flexible in the free receptor than in the complex, while the flexibility of the interface residues of N96W + V35L is similar for the free and complexed receptor (Figures 8(a) and 8(d)). This indicates entropically more favorable binding of the N96W + V35L variant compared to the other two variants.

(2) Interestingly, the origin of this behavior is different in the N-terminal and C-terminal domains of the IFNγR1 molecule: in the N-terminal domain (Figure 8(d)), the flexibility of the interface residues of all variants is similar in the bound state, while being different in unbound state; they are most flexible in N96W and the least in N96W + V35L. In the C-terminal domain (Figure 8(e)), the flexibility of the three variants is similar in their free states, but it differs in the bound state between N96W, which has the lowest flexibility, and WT with the highest flexibility.

(3) The V35L mutation stiffens the receptor nonlocally and makes especially the C-terminal interface residues more flexible in the bound state compared to the N96W mutant (Figure 8(e)).

(4) To sum up, the V35L mutation brought flexibility of the free and complexed receptor closer together, indicating reduced entropy penalty of binding and resulting in the higher affinity of the N96W + V35L double mutant compared to N96W mutant.

Filling the cavity by hydrophobic groups as in the V35L mutation is stabilizing but not as much as would be implied by $\Delta\Delta G$ of the removal of the corresponding hydrophobic group to water. A compensatory effect lowering a potential increase of the protein and/or complex stability has been observed previously [13] and a comparable decrease of stabilization was also predicted here by FoldX. Filling of a cavity may stabilize the interaction by several mechanisms, for example, by reducing the entropic penalty of complexation by stiffening interacting molecules in the free state, or indirectly by destabilization of the intermediate molten globule state rather than by stabilization of the folded protein [36]. These compensatory effects further illustrate complexity of protein-protein interactions (and/or folding) and the known limits of computational approaches to increasing protein-protein affinity [37].

An important issue potentially affecting reliability of FoldX predictions is the flexibility of the receptor molecule. The first round of FoldX $\Delta\Delta G$ calculations based on the static crystal structures suggested one additional mutation, G225Y, as potentially increasing receptor affinity to IFNγ. Although further calculations using structures of snapshots from the MD simulations did not confirm this prediction, we expressed and characterized this mutation. The experimental data were in agreement with the MD-based prediction showing much lower binding affinity compared to the WT (the ratio of the respective K_d values was 0.4), and also the N96W + G225Y double mutant had a fairly low binding affinity (compared to WT, the ratio of the respective K_d values was 3.1, which is lower than for the N96W mutant). This observation can be explained by the structural properties of the receptor molecule. The loop region of IFNγR1 containing the G225 residue is flexible and any residue at the position 225 is thus only a fraction of time in the geometry, in which it may

increase the binding affinity. An important role of flexibility at the C-terminal part of the interacting IFNγ and IFNγR1 is well illustrated by a study of IFNγ modified at its C-terminal side [38].

3.5. Sequence Conservation of Mutable Residues. We checked sequence conservation for the 12 positions selected by the FoldX calculations for potential cavity-filling mutations. Global alignment of 32 sequences of the extracellular part of IFNγR1 from various organisms by Kalign as implemented in program Ugene [39] (Figure 2(c)) shows conservation between 40 and 98% for these positions; the position V35 is well conserved (80%). The independence of sequence conservation and its potential for stabilizing mutation filling-up protein cavity ("mutability") contrasts with previously observed tight correlation between conservation and mutability for receptor residues interacting with IFNγ [21]: we tested several mutations of the interface residues S97 and E118, which were conserved at the 90% level (Figure 2(c)), namely, S97X (X = L, N, W) and E118X (X = M, F, Y, W), and they did not bind IFNγSC at all (unpublished SPR data) despite the fact that binding of these mutants to IFNγ was predicted to be stronger than that of WT.

3.6. Relationship Between FoldX $\Delta\Delta G$ Values and Naturally Occurring IFNγR1 Variants. Interesting, albeit indirect, validation of the present FoldX predictions of $\Delta\Delta G$ of mutations can be found among naturally occurring IFNγR1 single-point mutations collected in the database of single nucleotide polymorphism (dbSNP) [40]. The database contains 25 nucleotide mutations at 22 unique positions of the extracellular part of the IFNγ receptor, which is studied here; these 22 positions are marked blue in Figure 2(c). Most of the $\Delta\Delta G$ predictions for these natural mutants show neutral effect on the stability of free IFNγR1 and on its complex with IFNγ. This is in agreement with the fact that only two of the natural mutants exhibit deleterious effects or are represented by a pathological phenotype.

4. Conclusions

We present a new computational strategy for designing higher affinity variants of a binding protein and show that it is possible to increase the affinity of a protein-protein interaction by mutations not at the interface, but in the interior cavities of a binding partner. The mutations were selected at positions lining internal cavities of one binding partner, and an *in silico* protocol identified mutations that would fill the protein cavities and increase the stability of the complex. We showed that the selection of such cavity mutations in interferon-γ receptor 1 (IFNγR1) could be performed based on a combination of simple empirical force-field calculations and MD simulations. The mechanism by which the cavity mutations cause affinity increase is shown to be restriction of molecular fluctuations, which can be related to reduced entropy penalty upon binding [6, 7]. IFNγR1 WT and all computationally designed receptor mutants were expressed, purified, and refolded, and the affinity towards the cognate protein, IFNγSC, was measured by SPR. While single mutants showed roughly the same affinity as WT, double mutants combining cavity mutations with the best interface mutation obtained previously [21] were successful in further increasing the binding affinity.

The results demonstrate that mutating cavity residues is a viable strategy for designing protein variants with increased binding affinity. The comparison of computational data and experiments helped to further improve our understanding of forces governing protein-protein interactions. The newly obtained high-affinity binders of IFNγ could be developed into a new diagnostic tool. The significance of the present work can be seen in the fact that small $\Delta\Delta G$ gains of cavity mutants led to significant increase of affinity when combined with more conventional mutations influencing the interface.

Conflict of Interests

The authors declare that there is no conflict of interests regarding the publication of this paper.

Acknowledgments

Support from Grant P305/10/2184 from the Czech Science Foundation is greatly acknowledged. This study was supported by BIOCEV CZ.1.05/1.1.00/02.0109 from the ERDF, Biotechnological expert CZ.1.07/2.3.00/30.0020, and by institutional Grant RVO 86 652 036.

References

[1] P. L. Kastritis and A. M. J. J. Bonvin, "Molecular origins of binding affinity: seeking the Archimedean point," *Current Opinion in Structural Biology*, vol. 23, no. 6, pp. 868–877, 2013.

[2] R. Grünberg, M. Nilges, and J. Leckner, "Flexibility and conformational entropy in protein-protein binding," *Structure*, vol. 14, no. 4, pp. 683–693, 2006.

[3] T. N. Bhat, G. A. Bentley, G. Boulot et al., "Bound water molecules and conformational stabilization help mediate an antigen-antibody association," *Proceedings of the National Academy of Sciences of the United States of America*, vol. 91, no. 3, pp. 1089–1093, 1994.

[4] Y. Urakubo, T. Ikura, and N. Ito, "Crystal structural analysis of protein-protein interactions drastically destabilized by a single mutation," *Protein Science*, vol. 17, no. 6, pp. 1055–1065, 2008.

[5] K. K. Frederick, M. S. Marlow, K. G. Valentine, and A. J. Wand, "Conformational entropy in molecular recognition by proteins," *Nature*, vol. 448, no. 7151, pp. 325–329, 2007.

[6] M. S. Marlow, J. Dogan, K. K. Frederick, K. G. Valentine, and A. J. Wand, "The role of conformational entropy in molecular recognition by calmodulin," *Nature Chemical Biology*, vol. 6, no. 5, pp. 352–358, 2010.

[7] A. J. Wand, "The dark energy of proteins comes to light: conformational entropy and its role in protein function revealed by NMR relaxation," *Current Opinion in Structural Biology*, vol. 23, no. 1, pp. 75–81, 2013.

[8] B. Schneider, J. C. Gelly, A. G. de Brevern, and J. Cerny, "Local dynamics of proteins and DNA evaluated from crystallographic B factors," *Acta Crystallographica D: Biological Crystallography*, vol. 70, part 9, pp. 2413–2419, 2014.

[9] C. Wang, O. Schueler-Furman, and D. Baker, "Improved side-chain modeling for protein-protein docking," *Protein Science*, vol. 14, no. 5, pp. 1328–1339, 2005.

[10] C. Cole and J. Warwicker, "Side-chain conformational entropy at protein-protein interfaces," *Protein Science*, vol. 11, no. 12, pp. 2860–2870, 2002.

[11] M. Bueno, N. Cremades, J. L. Neira, and J. Sancho, "Filling small, empty protein cavities: structural and energetic consequences," *Journal of Molecular Biology*, vol. 358, no. 3, pp. 701–712, 2006.

[12] T. Ohmura, T. Ueda, K. Ootsuka, M. Saito, and T. Imoto, "Stabilization of hen egg white lysozyme by a cavity-filling mutation," *Protein Science*, vol. 10, no. 2, pp. 313–320, 2001.

[13] M. Tanaka, H. Chon, C. Angkawidjaja, Y. Koga, K. Takano, and S. Kanaya, "Protein core adaptability: crystal structures of the cavity-filling variants of *Escherichia coli* rnase HI," *Protein and Peptide Letters*, vol. 17, no. 9, pp. 1163–1169, 2010.

[14] T. Koudelakova, R. Chaloupkova, J. Brezovsky et al., "Engineering enzyme stability and resistance to an organic cosolvent by modification of residues in the access tunnel," *Angewandte Chemie—International Edition*, vol. 52, no. 7, pp. 1959–1963, 2013.

[15] S. Atwell, M. Ultsch, A. M. de Vos, and J. A. Wells, "Structural plasticity in a remodeled protein-protein interface," *Science*, vol. 278, no. 5340, pp. 1125–1128, 1997.

[16] Y. Kawasaki, E. E. Chufan, V. Lafont et al., "How much binding affinity can be gained by filling a cavity?" *Chemical Biology and Drug Design*, vol. 75, no. 2, pp. 143–151, 2010.

[17] L. Morellato-Castillo, P. Acharya, O. Combes et al., "Interfacial cavity filling to optimize CD4-mimetic miniprotein interactions with HIV-1 surface glycoprotein," *Journal of Medicinal Chemistry*, vol. 56, no. 12, pp. 5033–5047, 2013.

[18] J. Černý, J. Vondrášek, and P. Hobza, "Loss of dispersion energy changes the stability and folding/unfolding equilibrium of the trp-cage protein," *The Journal of Physical Chemistry B*, vol. 113, no. 16, pp. 5657–5660, 2009.

[19] D. J. Thiel, M.-H. Le Du, R. L. Walter et al., "Observation of an unexpected third receptor-molecule in the crystal structure of human interferon-γ receptor complex," *Structure*, vol. 8, no. 9, pp. 927–936, 2000.

[20] M. Randal and A. A. Kossiakoff, "Crystallization and preliminary X-ray analysis of a 1:1 complex between a designed monomeric interferon-gamma and its soluble receptor," *Protein Science*, vol. 7, no. 4, pp. 1057–1060, 1998.

[21] P. Mikulecký, J. Černý, L. Biedermannová et al., "Increasing affinity of interferon-γ receptor 1 to interferon-γ by computer-aided design," *BioMed Research International*, vol. 2013, Article ID 752514, 12 pages, 2013.

[22] K. Schroder, P. J. Hertzog, T. Ravasi, and D. A. Hume, "Interferon-gamma: an overview of signals, mechanisms and functions," *Journal of Leukocyte Biology*, vol. 75, no. 2, pp. 163–189, 2004.

[23] E. C. Borden, G. C. Sen, G. Uze et al., "Interferons at age 50: past, current and future impact on biomedicine," *Nature Reviews Drug Discovery*, vol. 6, no. 12, pp. 975–990, 2007.

[24] J. Schymkowitz, J. Borg, F. Stricher, R. Nys, F. Rousseau, and L. Serrano, "The FoldX web server: an online force field," *Nucleic Acids Research*, vol. 33, no. 2, pp. W382–W388, 2005.

[25] A. Landar, B. Curry, M. H. Parker et al., "Design, characterization, and structure of a biologically active single-chain mutant of human IFN-γ," *Journal of Molecular Biology*, vol. 299, no. 1, pp. 169–179, 2000.

[26] N. R. Voss and M. Gerstein, "3V: cavity, channel and cleft volume calculator and extractor," *Nucleic Acids Research*, vol. 38, no. 2, pp. W555–W562, 2010.

[27] W. Humphrey, A. Dalke, and K. Schulten, "VMD: visual molecular dynamics," *Journal of Molecular Graphics*, vol. 14, no. 1, pp. 33–38, 1996.

[28] B. Webb and A. Sali, "Protein structure modeling with MODELLER," *Methods in Molecular Biology*, vol. 1137, pp. 1–15, 2014.

[29] B. Hess, C. Kutzner, D. van der Spoel, and E. Lindahl, "GROMACS 4: algorithms for highly efficient, load-balanced, and scalable molecular simulation," *Journal of Chemical Theory and Computation*, vol. 4, no. 3, pp. 435–447, 2008.

[30] P. Eastman and V. S. Pande, "OpenMM: a hardware-independent framework for molecular simulations," *Computing in Science & Engineering*, vol. 12, no. 4, pp. 34–39, 2010.

[31] M. S. Friedrichs, P. Eastman, V. Vaidyanathan et al., "Accelerating molecular dynamic simulation on graphics processing units," *Journal of Computational Chemistry*, vol. 30, no. 6, pp. 864–872, 2009.

[32] P. A. Kollman, "Advances and continuing challenges in achieving realistic and predictive simulations of the properties of organic and biological molecules," *Accounts of Chemical Research*, vol. 29, no. 10, pp. 461–469, 1996.

[33] G. Bohm, R. Muhr, and R. Jaenicke, "Quantitative analysis of protein far UV circular dichroism spectra by neural networks," *Protein Engineering*, vol. 5, no. 3, pp. 191–195, 1992.

[34] E. Sviridova, L. Bumba, P. Rezacova et al., "Crystallization and preliminary crystallographic characterization of the iron-regulated outer membrane lipoprotein FrpD from *Neisseria meningitidis*," *Acta Crystallographica Section F: Structural Biology and Crystallization Communications*, vol. 66, part 9, pp. 1119–1123, 2010.

[35] M. Fountoulakis and R. Gentz, "Effect of glycosylation on properties of soluble interferon gamma receptors produced in prokaryotic and eukaryotic expression systems," *Nature Biotechnology*, vol. 10, no. 10, pp. 1143–1147, 1992.

[36] T. Sengupta, Y. Tsutsui, and P. L. Wintrode, "Local and global effects of a cavity filling mutation in a metastable serpin," *Biochemistry*, vol. 48, no. 34, pp. 8233–8240, 2009.

[37] T. S. Chen and A. E. Keating, "Designing specific protein-protein interactions using computation, experimental library screening, or integrated methods," *Protein Science*, vol. 21, no. 7, pp. 949–963, 2012.

[38] E. Saesen, S. Sarrazin, C. Laguri et al., "Insights into the mechanism by which interferon-γ basic amino acid clusters mediate protein binding to heparan sulfate," *Journal of the American Chemical Society*, vol. 135, no. 25, pp. 9384–9390, 2013.

[39] K. Okonechnikov, O. Golosova, M. Fursov, and UGENE Team, "Unipro ugene: a unified bioinformatics toolkit," *Bioinformatics*, vol. 28, no. 8, pp. 1166–1167, 2012.

[40] S. T. Sherry, M.-H. Ward, M. Kholodov et al., "DbSNP: the NCBI database of genetic variation," *Nucleic Acids Research*, vol. 29, no. 1, pp. 308–311, 2001.

STRUCTURAL BIOLOGY

ISSN 2059-7983

Crystal structure of human interferon-γ receptor 2 reveals the structural basis for receptor specificity

Pavel Mikulecký,‡ Jirí Zahradník,‡ Petr Kolenko, Jiří Černý, Tatsiana Charnavets, Lucie Kolářová, Iva Nečasová, Phuong Ngoc Pham and Bohdan Schneider*

Institute of Biotechnology CAS, BIOCEV, Prumyslova 595, 252 50 Vestec, Czech Republic. *Correspondence e-mail: bohdan.schneider@gmail.com

Received 17 May 2016
Accepted 27 July 2016

Edited by Z. S. Derewenda, University of Virginia, USA

‡ These authors share first authorship.

Keywords: interferon-γ receptor 2; fibronectin type III domain; class 2 cytokine receptors.

PDB reference: interferon-γ receptor 2, 5eh1

Supporting information: this article has supporting information at journals.iucr.org/d

Interferon-γ receptor 2 is a cell-surface receptor that is required for interferon-γ signalling and therefore plays a critical immunoregulatory role in innate and adaptive immunity against viral and also bacterial and protozoal infections. A crystal structure of the extracellular part of human interferon-γ receptor 2 (IFNγR2) was solved by molecular replacement at 1.8 Å resolution. Similar to other class 2 receptors, IFNγR2 has two fibronectin type III domains. The characteristic structural features of IFNγR2 are concentrated in its N-terminal domain: an extensive π–cation motif of stacked residues KWRWRH, a NAG–W–NAG sandwich (where NAG stands for *N*-acetyl-D-glucosamine) and finally a helix formed by residues 78–85, which is unique among class 2 receptors. Mass spectrometry and mutational analyses showed the importance of N-linked glycosylation to the stability of the protein and confirmed the presence of two disulfide bonds. Structure-based bioinformatic analysis revealed independent evolutionary behaviour of both receptor domains and, together with multiple sequence alignment, identified putative binding sites for interferon-γ and receptor 1, the ligands of IFNγR2.

1. Introduction

Interferon-γ receptor 2 is a cell-surface receptor that represents a crucial molecule in the interferon-γ (IFNγ) signalization pathway, influencing innate and adaptive immunity against pathogens and tumours (Schoenborn & Wilson, 2007; Lin & Young, 2013). The signalling cascade is initiated by the binding of IFNγ to its high-affinity cell surface receptor 1, forming a binary complex with a structure that has already been determined [PDB entries 1fg9 (Thiel *et al.*, 2000) and 1fyh (Landar *et al.*, 2000)]. However, to activate this binary complex and activate the JAK/STAT signalization pathway (Jung *et al.*, 1987; Cook *et al.*, 1994; Hemmi *et al.*, 1994), IFNγ receptor 2 must participate in a ternary complex created by a homodimer of IFNγ, two molecules of receptor 1 and molecule(s) of receptor 2. To date, detailed structural and biophysical characterization of IFNγ receptor 2, the key molecule for proper IFNγ signalization, is lacking.

From its sequence similarity, IFNγ receptor 2 (also known as IFNγ receptor β chain or accessory factor 1, AF-1), has been classified as a member of the class 2 receptor family. This large group of cytokine receptors includes IFNγ receptor 1, receptors of interferon-α and interferon-β, receptors of interleukin-10 and interleukin-20, and receptors of other interleukins belonging to the IL-10 family (Langer *et al.*, 2004). The mature IFNγ receptor 2 protein comprises of 310 amino acids and has a predicted molecular mass of 35 kDa. It consists of a relatively short 69-amino-acid intracellular domain, a 21-amino-acid transmembrane domain and a 220-

amino-acid extracellular domain that is structured into two fibronectin type III domains. The extracellular domain contains five cysteine residues and six potential N-linked glycosylation sites. Such extensive glycosylation contributes to a significant size heterogeneity, which is observed even when the receptor molecule is isolated from the same cell type; the molecular weight of mature receptor 2 of human interferon-γ ranges from 61 to 67 kDa (Bach *et al.*, 1995).

Despite its biological significance, three-dimensional structural data on IFNγ receptor 2 are lacking. Here, we report a 1.8 Å resolution crystal structure of the extracellular portion of IFNγ receptor 2 (hereafter called IFNγR2); the structure has been deposited in the Protein Data Bank as entry 5eh1. The structure and sequence of IFNγR2 are discussed in the context of the structures and sequences of the related class 2 cytokine receptors, with emphasis on the sequentially closest receptors of interleukins from the IL-10 family. Structure-based and sequence-based alignments suggested regions securing binding specificity of these receptors for their cytokine ligands.

2. Materials and methods

2.1. Cloning, expression and purification of IFNγR2

The gene encoding the extracellular part of IFNγR2 (residues 28–247 of UniProt entry P38484) was cloned into a *Drosophila* pMT-BiP-V5-His_A vector using BglII and AgeI restriction enzymes in frame with an N-terminal BiP signal peptide and a C-terminal 6×His tag. This expression vector was co-transfected into insect Schneider S2 cells along with the pCoBlast selection plasmid using Effectene Transfection Reagent according to the manufacturer's instructions. Blasticidin-resistant S2 cells were selected by growing the cells in HyClone SFX Medium supplemented with 10% FBS and 25 µg ml^{-1} blasticidin S. Large-scale protein expression was achieved after expansion and substitution into HyClone SFX serum-free medium, and protein expression was induced by the addition of 0.75 m*M* $CuSO_4$ for 6 d (the cell concentration was approximately 35 million per millilitre) and 1.5 m*M* $CuSO_4$ for a further 2 d until the percentage of living cells did not decrease below 95%. After expression, the cells were discarded by centrifugation and the medium containing secreted glycosylated IFNγR2 protein was supplemented with the following additives at the following final concentrations: 5 m*M* $CaCl_2$, 1 m*M* $NiSO_4$, 250 m*M* NaCl and 50 m*M* Tris–HCl pH 8. The protein was purified on an IMAC HP column charged with $NiSO_4$ and equilibrated with EQ buffer (50 m*M* Tris–HCl pH 8, 500 m*M* NaCl). The column was washed with W buffer (50 m*M* Tris–HCl pH 8, 500 m*M* NaCl, 20 m*M* imidazole pH 8) and the protein was eluted with EL buffer (50 m*M* Tris–HCl pH 8, 500 m*M* NaCl, 250 m*M* imidazole pH 8). It was further purified to homogeneity by size-exclusion chromatography at room temperature on a HiLoad 16/600 Superdex 200 pg column (GE Healthcare) equilibrated with HN buffer (10 m*M* HEPES pH 7.5, 100 m*M* NaCl). Samples were analyzed by 12% SDS–PAGE.

IFNγR2 was produced in insect cells as a secreted protein bearing oligosaccharide moieties of approximately 10 kDa according to SDS–PAGE analysis. Deglycosylation by peptide: N-glycosidase F (PNGase F) or endoglycosidase H (Endo H) with a C-terminal *Strep*-tag (§S1, Supporting Information) was performed after purification of IFNγR2 on an IMAC column during dialysis against TN buffer (50 m*M* Tris buffer pH 8, 150 m*M* NaCl) or HN buffer, respectively. Endoglycosidases were removed on a *Strep*-Tactin column and the nonbound fraction containing IFNγR2 was further purified by size-exclusion chromatography in HN buffer.

The single IFNγR2 variants (N110Q, N137Q and N231Q, respectively) were introduced using the QuikChange II Site-Directed Mutagenesis Kit (Agilent Technologies). Primers are listed in Supplementary Table S1. The fully mutated IFNγR2 variant bearing N56Q, N110Q, N137Q and N231Q mutations was obtained as a GeneArt Strings DNA Fragment and was cloned with the same protocol as the wild type. The expression and purification of all IFNγR2 variants were performed in the same way as described above.

2.2. Biophysical measurements

Circular-dichroism (CD) spectra were recorded using a Chirascan-plus spectrometer (Applied Photophysics) in steps of 1 nm over the wavelength range 185–260 nm. Samples diluted with water to a concentration of 0.2 mg ml^{-1} were placed into the holder in a 0.05 cm path-length quartz cell and individual spectra were recorded at a temperature of 23°C. The CD signal was expressed as the ellipticity and the resulting spectra were buffer-subtracted. To analyze the ratio of secondary structures, we used the *CDNN* program (Böhm *et al.*, 1992) provided with the Chirascan CD spectrometer. CD melting measurements were performed using samples diluted with water to a protein concentration of 0.5 mg ml^{-1}. A 10 mm path-length quartz cell was placed into the thermostated holder and sample absorption was recorded at 280 nm in 1°C increments at a rate of 0.5°C min^{-1} over the temperature range 20–85°C with an averaging time of 12 s. Melting curves were normalized to relative values between 0.0 and 1.0 to visually magnify differences between the melting profiles, and the melting temperature (T_m) was estimated from the first derivative of the melting curves.

2.3. Glycosylation analysis and disulfide-bond determination

IFNγR2 glycosylation sites were determined by MALDI-MS analysis preceded by protein digestion as described previously (Plíhal *et al.*, 2004). Disulfide bonds in IFNγR2 were determined by SDS–PAGE and subsequent identification by mass spectrometry (MS) in analogy to the previously described procedure (Pompach *et al.*, 2009). 20 µg of sample in nonreducing conditions was loaded onto a 4–12% gradient gel (Life Technologies) in the presence of 200 µ*M* cystamine. Bands corresponding to highly glycosylated IFNγR2 were excised and subjected to in-gel deglycosylation and proteolysis. Deglycosylation using Endo H (New England Biolabs) was carried out for 4 h at 37°C and the resulting

Table 1
Data-collection statistics and structure-refinement parameters.

Values in parentheses are for the highest resolution shell.

X-ray source	MX 14.1, HZB
Wavelength (Å)	0.91841
Total oscillation angle (°)	180
Resolution range (Å)	62.88–1.80 (1.91–1.80)
Space group	$P6_122$
Unit-cell parameters (Å)	$a = b = 58.102$, $c = 377.266$
No. of measured reflections	688675 (110540)
No. of unique reflections	36723 (5733)
Average multiplicity	18.8 (19.3)
Completeness (%)	99.9 (99.8)
Average $I/\sigma(I)$	17.6 (2.5)
Overall B factor from Wilson plot (Å^2)	20
Average B factor (Å^2)	28
No. of non-H atoms	
Protein	1734
Saccharides	42
Waters	311
All	2121
R_{merge}	0.148 (1.395)
Half-data-set correlation coefficient $CC_{1/2}$	99.9 (81.2)
No. of reflections, test set	1820
Final $R_{work}/R_{free}/R_{all}$	0.190/0.222/0.191
Ramachandran plot	
Residues in favoured region	213 [96.3%]
Residues in allowed regions	219 [99.1%]
Outliers	2 [0.9%]

partly deglycosylated sample was digested with trypsin (sequencing grade, Promega) for 12 h at 37°C at a protein:enzyme ratio of 30:1(*w*/*w*). After digestion, the tryptic peptide mixture was desalted on a peptide MicroTrap column (Michrom Bioresources) and separated on a reversed-phase C18 column (Acclaim PepMap 100, 5 µm, 0.1 × 20 mm; Thermo Scientific). The mobile phases consisted of 0.1% formic acid in 2% acetonitrile (solvent *A*) and 0.1% formic acid in 98% acetonitrile (solvent *B*). Peptides were eluted under the following gradient conditions: 2–45% solvent *B* in 40 min, 45–95% solvent *B* in 5 min. The flow rate was 0.5 µl min^{-1} and the column was directly connected to the mass spectrometer. Mass spectra were acquired on a solariX XR FTMS instrument equipped with a 12 T superconducting magnet (Bruker Daltonics). For the identification of disulfide bonds, we used the *Links* algorithm, previously described as *ASAP* (*Automated Spectrum Assignment Program*; Schilling *et al.*, 2003). To generate deconvoluted spectra and export the *m*/*z* values, we used a script utilizing the *SNAP* 2.0 algorithm of the *DataAnalysis* 4.2 software suite (Bruker Daltonics).

2.4. Crystallization and diffraction data collection

Crystals of Endo H-deglycosylated IFNγR2 receptor were grown using the sitting-drop vapour-diffusion method in 96-3 three-well Intelli-Plate trays (Art Robbins Instruments). The reservoir solution consisted of 0.1 *M* MES pH 5.0, 10% PEG 6000 (final pH 6.0): condition No. 61 of The JCSG Core I Suite (Qiagen). Drops consisting of 0.2 µl protein sample (15 mg ml^{-1} protein in HN buffer) and 0.2 µl reservoir solution were prepared with a Gryphon liquid-pipette robot (Dunn Labortechnik) and were equilibrated against 100 µl reservoir solution. Crystals appeared after 30 d of incubation at 291 K. Crystals were mounted in Round LithoLoops (Molecular Dimensions) and flash-cooled in liquid nitrogen after cryoprotection in 20%(*v*/*v*) glycerol. X-ray diffraction data were collected at 100 K on beamline MX 14.1 of the BESSY II synchrotron-radiation source at the Helmholtz-Zentrum Berlin (HZB). A native data set was collected at a wavelength of 0.918 Å.

2.5. Data processing, structure determination and refinement

The diffraction and refinement statistics are summarized in Table 1. Diffraction data were processed and scaled using the *XDS* program package (Kabsch, 2010). The structure was solved with *BALBES* (Long *et al.*, 2008), but the structure model needed significant manual remodelling. Only the C-terminal domain of IFNγR2 was found and the initial *R* factors were about 0.49 and 0.52 for R_{work} and R_{free}, respectively. Residues missing from the initial model were built in with significant help from *ARP*/*wARP* (Langer *et al.*, 2008); manual corrections and building were performed using *Coot* (Emsley & Cowtan, 2004). Refinement was then carried out with *REFMAC*5 (Murshudov *et al.*, 2011) and the structure was validated by *MolProbity* (Chen *et al.*, 2010). The coordinates and structure factors have been deposited in the PDB with accession code 5eh1.

2.6. Sequence and structural bioinformatics

The UniProt database was searched with the *BLAST* tool (Camacho *et al.*, 2009) using the sequence of the extracellular part of IFNγR2 as the query sequence. The automated result was manually reviewed to select 90 sequences from different species. These sequences were used to calculate a multiple sequence alignment with *Clustal Omega* (Sievers *et al.*, 2011) as implemented in *UGENE* (Okonechnikov *et al.*, 2012). The *ConSurf* server (Glaser *et al.*, 2003) was used to estimate the evolutionary conservation of amino-acid positions in the protein structures. The calculations were based on the crystal structure of IFNγR2 (PDB entry 5eh1) and the alignment prepared by *Clustal Omega*. Structural comparison was prepared by *MatchMaker* as implemented in the *UCSF Chimera* software (Pettersen *et al.*, 2004).

Root-mean-square deviation (r.m.s.d.) values between the N- and C-terminal domains were calculated using *VMD* (Humphrey *et al.*, 1996). The backbone atoms of 34 sequentially conserved residues in each domain (listed in Supplementary Table S2) were used for the structure superposition of all possible pairs of N- and C-terminal domains of the 12 available crystal structures of class 2 cytokine receptors. The *VMD* commands `measure fit` and `move` were used for the structural overlay, followed by `measure rmsd` operating on the same selection of residues and backbone atoms for the calculation of r.m.s.d. values. The stability of the N-terminal domain of IFNγR2 was estimated by calculating the pairwise interaction energy at the DFT-D level as detailed in Supplementary Fig. S3.

3. Results and discussion

3.1. Summary

IFNγR2 was produced in insect S2 cells, purified, characterized by biophysical techniques (Fig. 1) and its crystal structure was solved at 1.8 Å resolution. Fig. 2 highlights some of the structural features of IFNγR2; Figs. 3 and 4 provide a comparison of IFNγR2 to the other cytokine receptors from the class 2 family, with the aim of correlating the sequences and structures of these proteins.

3.2. Glycosylation and overall fold stability

The IFNγR2 protein has six potential glycosylation sites (Asn56, Asn110, Asn137, Asn231, Asn85 and Asn219), of which the first four were confirmed by mass-spectrometric analysis as glycosylated in our construct; the crystal structure later revealed that position Asn85 was also glycosylated. The greatest heterogeneity was observed at position Asn137. To remove oligosaccharide moieties from these residues, we used two endoglycosidases, Endo H and PNGase F, but both enzymes left several forms of IFNγR2 with residual glycosylation as observed by a distribution of molecular mass on SDS–PAGE (Supplementary Fig. S1). Mass spectrometry identified α(1–3)-fucose at position Asn231. Because α(1–3)-fucose abolishes the activity of both endoglycosidases, its presence is a likely to be reason for the mass distribution of IFNγR2. Deglycosylation by Endo H caused an approximately 7 kDa shift in molecular weight on SDS–PAGE and, in contrast to deglycosylation by PNGase, did not induce protein oligomerization, as checked by size-exclusion chromatography. Measurements using CD spectroscopy (Fig. 1) and thermal shift assay (§S1 in Supporting Information and Supplementary Fig. S2) showed no significant difference in melting temperatures between the glycosylated and Endo H-deglycosylated forms of the IFNγR2 protein. Because the CD spectra of these two forms are also virtually identical, we believe that deglycosylation does not influence the secondary structure of IFNγR2. Although the CD spectra of IFNγR2 and IFNγR1 differ considerably (Černý *et al.*, 2015), both proteins belong to the same fold of the fibronectin type III domain family (Pfam PF00041).

Besides deglycosylation by the endoglycosidases, we designated asparagine-to-glutamine mutants to decrease the level of glycosylation. We prepared a fully mutated IFNγR2 variant bearing N56Q, N110Q, N137Q and N231Q mutations and single-point mutants N110Q, N137Q and N231Q, respectively. All of these constructs were transfected into insect S2 cells, but none of them were secreted into the cell-culture medium. This correlates with the earlier observation that IFNγR2 mutants with changed glycosylation patterns were located in the cytoplasmic fraction (Moncada-Vélez, 2013). Structurally significant is glycosylation at positions Asn110 and Asn137, where the bound *N*-acetyl-D-glucosamine (NAG) residues sandwich Trp131 (Fig. 2*b*), thus shielding its hydrophobic surfaces from solvent. As suggested by the failure to express and/or purify the N56Q, N110Q, N137Q and N231Q mutants, glycosylation is necessary for IFNγR2 production by stabilizing the fold and transport to and/or across the cellular membrane.

3.3. The IFNγR2 fold is stable without disulfide bonds

IFNγR2 contains five cysteine residues, and our mass-spectrometric analysis identified disulfide bonds linking Cys86 to Cys94 and Cys209 to Cys234. We observed the same protein mobility under nonreducing and reducing conditions during SDS–PAGE analysis. The melting temperature of both glycosylated and deglycosylated IFNγR2 measured by thermal shift assay (Supplementary Fig. S2) decreased by only $\sim$1°C in the presence of 5 m*M* TCEP (a reducing agent to break the disulfide bonds), so that the IFNγR2 fold is stable without S—S bonds. This contrasts with the behaviour of IFNγR1 (Fountoulakis *et al.*, 1990), in which the protein fold is

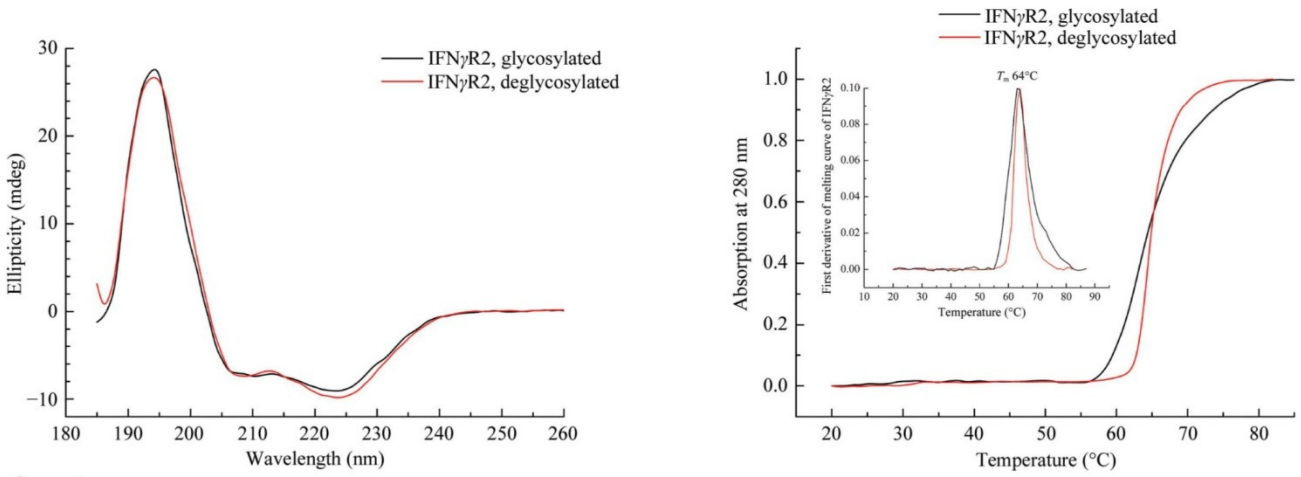

Figure 1
Left: circular-dichroism (CD) spectra of glycosylated and deglycosylated IFNγR2. The CD spectra of both proteins are highly similar, suggesting that the partial removal of the oligosaccharide moieties did not affect the overall structure of IFNγR2. Right: normalized melting curves measured from temperature-dependent CD spectra at 280 nm. The melting temperature was estimated as 64°C for both glycosylated and deglycosylated IFNγR2.

stabilized to a large extent by S—S bridges. The fifth IFNγR2 cysteine residue, Cys174, does not form an intramolecular S—S bridge but is bound to a monomeric cysteine. Binding of free cysteine to the sterically accessible Cys174 probably occurs after secreting IFNγR2 into the cell-culture medium, which contains free cysteine and stabilizes the monomeric form of IFNγR2.

3.4. The overall structure of the extracellular portion of IFNγR2

The structure of IFNγR2 was solved at 1.8 Å resolution and electron density was observed for amino-acid residues 28–240 of UniProt entry P38484, except for two two-residue loops. Data-collection and refinement parameters are shown in Table 1. The extracellular part of the IFNγR2 molecule consists of two domains (Fig. 2), the N-terminal D1 domain of UniProt residues 28–133 and the C-terminal D2 domain of residues 144–247. Both domains belong to the immunoglobulin fold with fibronectin type III topology, forming β-sandwiches (Pfam PF00041). The inter-domain torsion angle is approximately 120°, similar to those of IFNγR1 (Thiel *et al.*, 2000; Walter *et al.*, 1995) and human tissue factor (Harlos *et al.*, 1994); the D1–D2 torsion angle is defined in Supplementary Table S3. The D1 domain is composed of three β-strands stacked on a layer of four β-strands, and the D2 domain is created by four β-strands arranged against four other β-strands; both domains are connected by a short linker (residues 134–143 in IFNγR2) comprising a short helix that is also found in IFNγR1, human tissue factor and other receptors.

3.5. Structural motifs in D1 and D2

D1 contains a distinct structural motif of six stacked residues: Lys68, Trp74, Arg114, Trp126, Arg116 and His123. The average distance between the mean planes of the individual side chains of this extensive π–cation interaction is 3.65 Å.

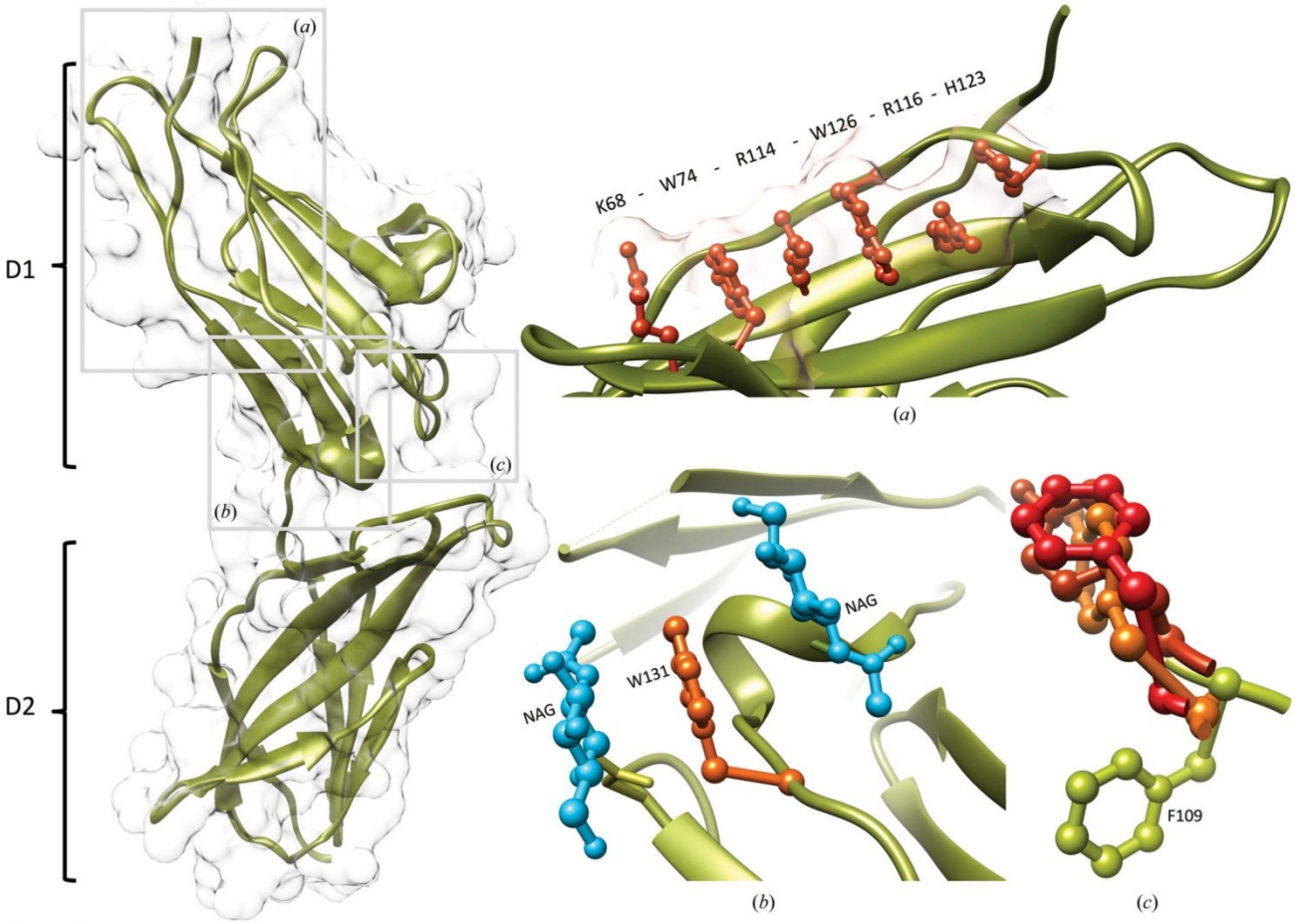

Figure 2
Left: ribbon and surface representations of the IFNγR2 structure. D1 and D2 indicate domains 1 and 2, respectively. Insets: (*a*) residues Lys68, Trp74, Arg114, Trp126, Arg116 and His123 of the D1 domain form a stacking motif on the IFNγR2 surface. (*b*) *N*-Acetyl-D-glucosamines (NAGs; blue) glycosylating Asn110 and Asn137 sandwich Trp131 (orange), reducing its hydrophobic character. (*c*) The superposition of aromatic binding epitopes shows differences between IFNγR2 (Phe109 in green) on one side and promiscuous shared cytokine receptors on the other [in red; Tyr82 of IL10R2 (PDB entry 3lqm; Yoon *et al.*, 2010), Phe169 of gp130 (PDB entry 1bqu; Bravo *et al.*, 1998) and Tyr103 of γ_c receptor (PDB entry 4gs7; Ring *et al.*, 2012)]. No corresponding aromatic residue is observed in IL20R2 (Logsdon *et al.*, 2012).

Analysis of the interaction energies in D1 revealed that the motif contributes significantly to the overall stability of the whole domain. These six surface residues are involved in interactions that are comparable in strength to the hydrophobic core of the domain and are likely to play an important role in the process of domain folding. The residues responsible for domain stability are depicted in Supplementary Fig. S3, in which the colour and thickness of the cartoon representation show the relative interaction energy per residue ranging from low (blue) to high (red) stabilizing values.

An analogous stacking motif with the consensus sequence WS*X*WS (Bazan, 1990) has been predicted by sequence alignments in D1 of the class 1 receptor family (McElroy *et al.*, 2009), but such a motif is missing in the D2 domains of both class 1 and class 2 receptors. Based on the presence of the KWRWRH motif in IFNγR2, we performed structural alignment of the class 2 receptor structures and discovered a similar but sequentially noncontinuous motif with the sequence (*X*)WRWR(*X*), where *X* is K, R or H. The important role of large aromatic tryptophan residues in stabilizing the fibronectin fold by stitching together two β-strands is accompanied in D1 by a structural role for charged residues, especially arginines. Besides the discussed (*X*)WRWR(*X*) motif, we found a tight overlap of a continuous chain of residues R-L/V-R-A (residues Arg114-Leu115-Arg116-Ala117 in IFNγR2): the average r.m.s.d. between motifs from two receptors is 0.6 Å. The other important residues that are conserved in D1 of the available class 2 receptor structures are residues corresponding to Trp49, Ser124 and the Cys86/Cys96 pair forming a disulfide bond in IFNγR2. A unique feature of IFNγR2 D1 is a short helix (residues 78–85), which is present in no other discussed receptor structure.

Sequential and structural comparison of D2 revealed a considerable sequence variability, within which we identified the conservation of two proline residues, Pro142 and Pro143, and the structurally well conserved motif 175-YNVA*X*W-180, with r.m.s.d. values about 1 Å but low sequence similarity. Another characteristic structural feature of D2 is the formation of a disulfide bridge between Cys209 and Cys234. Higher values for the *B* factors in D2 indicate its higher flexibility compared with D1. A higher flexibility of D2 compared with D1 was also indicated in our previous studies of IFNγR1 (Mikulecký *et al.*, 2013; Černý *et al.*, 2015).

3.6. Structural alignment of domains D1 and D2 in IFNγR2 and in other class 2 receptors

We performed alignment of the IFNγR2 structure with the 11 remaining available structures of the class 2 receptor family in order to gauge their similarity and reveal their unique features. The alignment was measured by overlapping 34 residues in the N-terminal D1 and the same number of residues in the C-terminal D2; the r.m.s.d. values of the overlapped residues are listed in Fig. 3 and the overlapped residues are listed in Supplementary Table S2. The D1 domains are mutually more similar than the D2 domains, as highlighted by

PDB code	1fg9	5eh1	1j7v	3lqm	4doh	4doh	3dlq	3g9v	3og6	3se4	3se4	2puq
Chain ID	*C*	*A*	*R*	*A*	*E*	*B*	*R*	*A*	*B*	*A*	*C*	*T*
Receptor	IFNγR1	IFNγR2	IL10R1	IL10R2	IL20R1	IL20R2	IL22R	IL22BP	IL28R	IFNαR1	IFNαR2	TF
IFNγR1	*0.82*	0.87	0.73	0.73	0.80	0.78	0.90	0.71	0.82	1.35	1.12	0.85
IFNγR2	1.27	*0.79*	0.93	0.97	0.79	0.79	0.96	0.80	0.85	1.45	1.25	1.04
IL10R1	1.22	1.12	*1.07*	0.74	0.97	0.88	0.94	1.43	1.13	0.81	0.67	0.66
IL10R2	1.00	1.14	1.05	*0.89*	0.95	1.05	0.65	0.87	0.68	0.80	1.11	0.93
IL20R1	0.93	1.32	0.89	1.33	*1.59*	0.93	0.97	0.63	0.75	0.59	1.36	1.15
IL20R2	1.32	1.51	1.23	0.99	1.33	*0.91*	0.93	0.66	0.82	1.48	1.25	1.21
IL22R	1.20	1.49	1.09	0.86	1.04	1.16	*4.19*	1.20	1.19	0.87	0.98	1.03
IL22BP	1.32	1.48	0.94	1.20	1.18	1.30	1.17	*0.93*	1.02	1.16	1.11	0.96
IL28R	1.21	1.16	1.34	1.29	1.30	1.32	1.18	1.45	*0.91*	1.09	0.77	0.86
IFNαR1	1.16	0.96	1.31	1.33	1.33	0.98	1.75	1.26	1.59	*1.77*	0.94	1.20
IFNαR2	1.35	1.80	1.40	1.29	1.19	1.81	1.58	1.14	1.46	1.22	*1.43*	1.02
TF	1.38	1.16	1.23	1.26	1.44	1.04	1.16	1.40	1.43	1.16	1.81	*0.86*

Figure 3
Structural differences between the N-terminal (D1) and C-terminal (D2) domains of 12 class 2 cytokine receptors gauged by the r.m.s.d. values for backbone atoms of their 34 residues. R.m.s.d. values comparing D1 and D2 domains are shown above and below the diagonal, respectively. For instance, comparison between D1 of IL20R2 and IL22BP gives an r.m.s.d. of 0.66 Å; the r.m.s.d. between their D2 domains is 1.30 Å. R.m.s.d. values that are smaller and larger than the off-diagonal average r.m.s.d. value are highlighted in blue and red hues, respectively. The diagonal (in grey) shows the lowest r.m.s.d. values for 34 residues from D1 and D2 within each receptor structure; the r.m.s.d. between D1 and D2 of IL10R2 is 0.89 Å. References to the analyzed structures are as follows: IFNγR1, Thiel *et al.* (2000); IFNγR2, this work; IL10R1, Josephson *et al.* (2001); IL10R2, Yoon *et al.* (2010); IL20R1 and IL20R2, Logsdon *et al.* (2012); IL22R, Bleicher *et al.* (2008); IL22BP, de Moura *et al.* (2009); IL28R, Miknis *et al.* (2010); IFNαR1 and IFNαR2, Thomas *et al.* (2011); TF (human tissue factor), Larsen *et al.* (2007).

blue and red hues in Fig. 3; the average r.m.s.d. between two D1 domains is 0.95 Å and that between two D2 domains is 1.3 Å. A high similarity within D1 and D2, respectively, indicates that modulation of the specificity of receptors takes place in only a few variable regions, which are discussed below.

D1 domains bear two conflicting structural features: strict fold conservation reflected by high structural similarity of the selected residues, and at the same time the presence of two structurally highly variable loops corresponding to residues 70–73 and 97–107 in IFNγR2. The third variable loop was located in the D2 domain (residues 162–171 in IFNγR2); the loops are coloured red and yellow for D1 and green for D2 in Fig. 4. Given the fairly uniform core of both domains and variability concentrated in the three localized regions, we suggest that the binding specificity of the individual receptors is controlled by these variable regions. However, there is another factor that contributes to the receptor specificity, the different mutual orientation of D1 and D2 (Supplementary Table S3), which displaces these variable regions to different positions, thus providing a unique binding interface for each receptor.

Several structural and sequential features of receptors of interferon-α and interferon-β (PDB entry 3se4; Thomas *et al.*, 2011), here labelled IFNαR1 and IFNαR2, distinguishes them from the other analyzed receptors. Specifically, IFNαR1 is composed of four instead of two domains; here, we analyzed D1 and D2. The D3–D4 pair cannot be analyzed as D4 is not resolved in the electron density. Further dissimilarities of IFNαR1 and IFNαR2 are found in the composition of their π–cation motifs: in IFNαR1 only four residues stack in D1 (Trp46, Arg76, Trp87 and Arg78) and three in D3 (Trp250, Arg279 and Trp291), while D1 of IFNαR2 does not have the motif at all and is replaced by the motif YVTV.

3.7. Similarity among receptors and consequences for evolution

As discovered previously (Yoon *et al.*, 2010), an aromatic tyrosine or phenylalanine residue situated in the cleft between D1 and D2 of gp130 (PDB entry 1bqu; Bravo *et al.*, 1998), γ_c (PDB entry 4gs7; Ring *et al.*, 2012) and IL10R2 (PDB entry 3lqm; Yoon *et al.*, 2010) serves as the key binding epitope of promiscuous class 1 and 2 receptors, implying the existence of a common ancestor. Superposition of these receptor structures shows that the orientation of Phe109 and three residues in gp130, γ_c and IL10R2 are quite different (Fig. 2*c*). No preferred rotamer of Phe109 overlaps the three former residues without significant rebuilding of the IFNγR2 backbone. The structural difference between IFNγR2 and the other receptors, especially IL10R2, is significant and suggests that there is not a common binding epitope for these receptors.

Significant sequence similarity between IFNγR2, IL10R2 and IL20R2 (20–25% sequence identity among different species; analysis not shown) points to their evolutionary relationship. If proven, it would be analogous to the evolutionary relationship between receptors 1 of the cytokines IFNγR1, IL10R1 and IL20R1 (Langer *et al.*, 2004). We may therefore hypothesize that these three cytokine systems have evolved from a common ancestral system: while interferon-γ evolved early in evolution and is known in fish species (Savan *et al.*, 2009), its receptor 2 emerged later in connection with the evolution of amphibians. The specific function of IFNγR2 therefore evolved from an older promiscuously functioning molecule. A likely candidate is IL10R2, because it is evolutionarily older and is known in primitive fishes, while IL20R2 emerges similarly to IFNγR2 in amphibians. The lack of a common binding epitope between IFNγR2 and the other class 2 receptors, notably IL10R2 (Fig. 2*c*), indirectly supports this hypothesis.

3.8. The sequence alignment of IFNγR2 from various species suggests its binding interface

In an attempt to identify the putative interface by which IFNγR2 forms a functional ternary complex with its binding partners interferon-γ and receptor 1, we aligned the IFNγR2 sequences from 90 species and used the *ConSurf* server to project the consensus onto the structure of IFNγR2 (Fig. 4*b*). The 32 conserved residues (purple in Fig. 4*b*) are mainly located in the inward arched part of the U-shaped receptor molecule. This part of the molecule contains the previously described stacking motif (Fig. 2*a*) and plays an important role in maintaining the overall structure. The 34 most variable residues are predominantly on the opposite side of the molecule (cyan in Fig. 4*b*). These regions of sequentially least conserved residues coincide with the location of the structurally variable loops derived by the superposition of receptor structures. We therefore conclude that the putative IFNγR2 interface for forming the active ternary complex with IFNγ and IFNγR1 is likely to be in the receptor 2 region with the most variable residues. This conclusion is supported by an analogous observation in the IFNγR1 system: the least sequentially conserved residues form the interface with the binding partner (Mikulecký *et al.*, 2013).

The composition of the ternary signalling complexes of dimeric cytokines discussed here, IFNγ and IL-10, is understood less than for monomeric examples such as IL-20, for which the ternary complex has a known crystal structure (Logsdon *et al.*, 2012). One of the reasons is the existence of two binding interfaces in the dimeric cytokines and the resulting different and more complex stoichiometry of the complexes; the crystal structure of an IFNγ–IFNγR1 complex with an unexpected 2:3 stoichiometry serves as an example (Thiel *et al.*, 2000). The topology and structure of the signalling ternary complex of IFNγ have been extensively studied and reviewed (Pestka *et al.*, 1997; Hoffmann *et al.*, 2015). Experiments in solution and on the cell surfaces indicated a 2:2:2 or 2:2:1 stoichiometry of the signalling IFNγ complex (Marsters *et al.*, 1995); cross-linking of different components of the IFNγ complex expressed in cloned cell lines have shown direct contact between IFNγR1 and IFNγR2 (Krause *et al.*, 2006) and also between IFNγ and IFNγR2 (Kotenko *et al.*, 1995). The newly determined structure of IFNγR2 may spur new experiments exploring the topology and three-dimensional structure of the signalizing ternary complex of IFNγ.

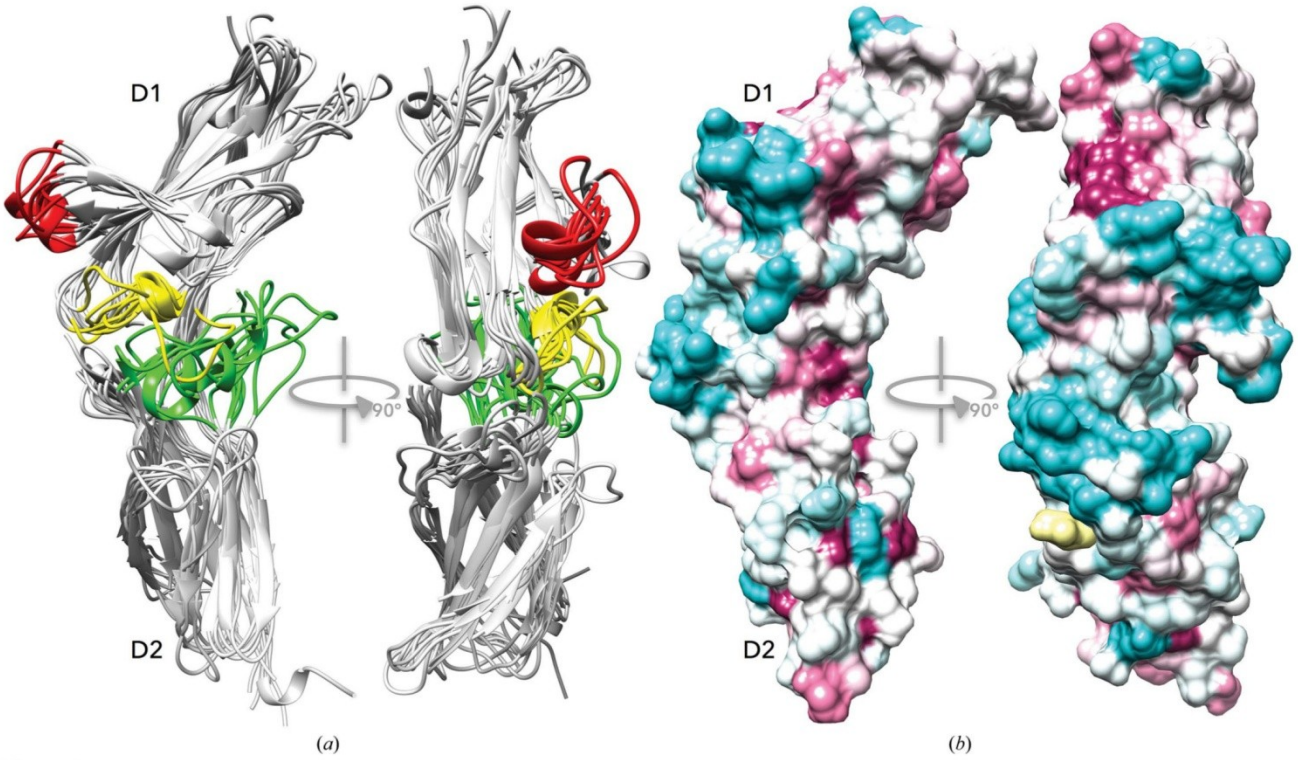

Figure 4
Structurally variable regions and a proposed interaction interface of the cytokine receptors. (*a*) Cartoon representation of the structural superposition of the D1 and D2 domains of the nine receptor structures. The backbone of the selected residues (listed in Supplementary Table S2) was superimposed independently for each domain and was then drawn on top of the IFNγR2 structure. The aligned cores of both domains overlap tightly (for r.m.s.d. values, see Fig. 3), but two regions in D1 (red and yellow) and one in D2 (green) are highly variable. (*b*) Sequences of IFNγR2 from 90 species with the sequentially most variable regions coloured cyan and conserved regions in purple drawn on the surface of the IFNγR2 structure by *ConSurf* (Glaser *et al.*, 2003). The IFNγR2 free cysteine Cys174 is highlighted in yellow. (*a*) and (*b*) show IFNγR2 in the same orientation.

4. Conclusions

A partially deglycosylated extracellular part of the interferon-γ receptor 2, IFNγR2, was crystallized and its structure was determined at 1.8 Å resolution and deposited in the PDB with accession code 5eh1. The electron-density map was interpreted for amino-acid residues 28–240, apart from two short loops. The IFNγR2 structure revealed the fold common to other cytokine receptors: two fibronectin type III domains connected by a short linker. IFNγR2 is a glycoprotein with five of the six potential N-linked glycosylation sites glycosylated, as confirmed by mass spectrometry and the crystal structure. Our analysis of glycosylation also uncovers the role of the oligosaccharide moieties at Asn110 and Asn137, which sandwich Trp131 and shield its hydrophobic aromatic ring from the solvent. Both potential disulfide bonds form but are not critical for the stability of IFNγR2, as it is also stable in a reducing environment. The fifth cysteine Cys174 is bound to the monomeric cysteine.

Structure and sequence alignments revealed some important features of the 12 class 2 receptors. Their N-terminal D1 domains are more mutually similar than their C-terminal D2 domains (Fig. 3). D1 carries a distinctive so far unrecognized structural feature: a π–cation motif of sequentially distant stacked residues (X)WRWR(X) (KWRWRH in IFNγR2; Fig. 2*a*). Analysis of the receptor structures revealed three structurally highly variable regions (Fig. 4*a*), which most likely bring about binding specificity for their interacting partners. This hypothesis is further supported by the alignment of IFNγR2 sequences from various species, which identified the highest sequence variability at positions coinciding with the structurally variable regions (Fig. 4*b*). An important structural feature distinguishing IFNγR2 from the related IL10R2, gp130 and γ_c receptors is the specific positioning of the aromatic recognition epitope in IFNγR2 (Fig. 2*c*).

We believe that the determination of the structure of the so-far missing component of the interferon-γ signalling complex will enable a deeper understanding of the functioning of this important immunity cascade.

5. Related literature

The following references are cited in the Supporting Information for this article: Cancino-Díaz *et al.* (2002), Černý *et al.* (2007), Furche *et al.* (2014), O'Boyle *et al.* (2011) and Rüger *et al.* (2015).

Acknowledgements

This study was supported by the Czech Science Foundation (GA CR) grant No. 16-20507S and by project BIOCEV

CZ.1.05/1.1.00/02.0109 from the ERDF. It was conducted at the Institute of Biotechnology CAS with help of the institutional grant RVO: 86652036. We thank HZB for the allocation of synchrotron-radiation beamtime.

References

Bach, E. A., Szabo, S. J., Dighe, A. S., Ashkenazi, A., Aguet, M., Murphy, K. M. & Schreiber, R. D. (1995). *Science*, **270**, 1215–1218.

Bazan, J. F. (1990). *Proc. Natl Acad. Sci. USA*, **87**, 6934–6938.

Bleicher, L., de Moura, P. R., Watanabe, L., Colau, D., Dumoutier, L., Renauld, J.-C. & Polikarpov, I. (2008). *FEBS Lett.* **582**, 2985–2992.

Böhm, G., Muhr, R. & Jaenicke, R. (1992). *Protein Eng. Des. Sel.* **5**, 191–195.

Bravo, J., Staunton, D., Heath, J. K. & Jones, E. Y. (1998). *EMBO J.* **17**, 1665–1674.

Camacho, C., Coulouris, G., Avagyan, V., Ma, N., Papadopoulos, J., Bealer, K. & Madden, T. L. (2009). *BMC Bioinformatics*, **10**, 421.

Cancino-Díaz, J. C., Reyes-Maldonado, E., Bañuelos-Pánuco, C. A., Jiménez-Zamudio, L., García-Latorre, E., León-Dorantes, G., Blancas-González, F., Paredes-Cabrera, G. & Cancino-Díaz, M. E. (2002). *J. Investig. Dermatol.* **119**, 1114–1120.

Černý, J., Biedermannová, L., Mikulecký, P., Zahradnik, J., Charnavets, T., Šebo, P. & Schneider, B. (2015). *Biomed Res. Int.* **2015**, 716945.

Černý, J., Jurečka, P., Hobza, P. & Valdés, H. (2007). *J. Phys. Chem. A*, **111**, 1146–1154.

Chen, V. B., Arendall, W. B., Headd, J. J., Keedy, D. A., Immormino, R. M., Kapral, G. J., Murray, L. W., Richardson, J. S. & Richardson, D. C. (2010). *Acta Cryst.* D**66**, 12–21.

Cook, J. R., Emanuel, S. L., Donnelly, R. J., Soh, J., Mariano, T. M., Schwartz, B., Rhee, S. & Pestka, S. (1994). *J. Biol. Chem.* **269**, 7013–7018.

Emsley, P. & Cowtan, K. (2004). *Acta Cryst.* D**60**, 2126–2132.

Fountoulakis, M., Juranville, J.-F., Stüber, D., Weibel, E. K. & Garotta, G. (1990). *J. Biol. Chem.* **265**, 13268–13275.

Furche, F., Ahlrichs, R., Hättig, C., Klopper, W., Sierka, M. & Weigend, F. (2014). *Wiley Interdiscipl. Rev. Comput. Mol. Sci.* **4**, 91–100.

Glaser, F., Pupko, T., Paz, I., Bell, R. E., Bechor-Shental, D., Martz, E. & Ben-Tal, N. (2003). *Bioinformatics*, **19**, 163–164.

Harlos, K., Martin, D. M., O'Brien, D. P., Jones, E. Y., Stuart, D. I., Polikarpov, I., Miller, A., Tuddenham, E. G. & Boys, C. W. (1994). *Nature (London)*, **370**, 662–666.

Hemmi, S., Böhni, R., Stark, G., Di Marco, F. & Aguet, M. (1994). *Cell*, **76**, 803–810.

Hoffmann, H. H., Schneider, W. M. & Rice, C. M. (2015). *Trends Immunol.* **36**, 124–138.

Humphrey, W., Dalke, A. & Schulten, K. (1996). *J. Mol. Graph.* **14**, 33–38.

Josephson, K., Logsdon, N. J. & Walter, M. R. (2001). *Immunity*, **15**, 35–46.

Jung, V., Rashidbaigi, A., Jones, C., Tischfield, J. A., Shows, T. B. & Pestka, S. (1987). *Proc. Natl Acad. Sci. USA*, **84**, 4151–4155.

Kabsch, W. (2010). *Acta Cryst.* D**66**, 125–132.

Kotenko, S. V., Izotova, L. S., Pollack, B. P., Mariano, T. M., Donnelly, R. J., Muthukumaran, G., Cook, J. R., Garotta, G., Silvennoinen, O., Ihle, J. N. & Pestka, S. (1995). *J. Biol. Chem.* **270**, 20915–20921.

Krause, C. D., Lavnikova, N., Xie, J., Mei, E., Mirochnitchenko, O. V., Jia, Y., Hochstrasser, R. M. & Pestka, S. (2006). *Cell Res.* **16**, 55–69.

Landar, A., Curry, B., Parker, M. H., DiGiacomo, R., Indelicato, S. R., Nagabhushan, T. L., Rizzi, G. & Walter, M. R. (2000). *J. Mol. Biol.* **299**, 169–179.

Langer, G., Cohen, S. X., Lamzin, V. S. & Perrakis, A. (2008). *Nature Protoc.* **3**, 1171–1179.

Langer, J. A., Cutrone, E. C. & Kotenko, S. (2004). *Cytokine Growth Factor Rev.* **15**, 33–48.

Larsen, K. S., Østergaard, H., Bjelke, J. R., Olsen, O. H., Rasmussen, H. B., Christensen, L., Kragelund, B. B. & Stennicke, H. R. (2007). *Biochem. J.* **405**, 429–438.

Lin, F.-C. & Young, H. A. (2013). *Adv. Biosci. Biotechnol.* **04**, 6–13.

Logsdon, N. J., Deshpande, A., Harris, B. D., Rajashankar, K. R. & Walter, M. R. (2012). *Proc. Natl Acad. Sci. USA*, **109**, 12704–12709.

Long, F., Vagin, A. A., Young, P. & Murshudov, G. N. (2008). *Acta Cryst.* D**64**, 125–132.

Marsters, S. A., Pennica, D., Bach, E., Schreiber, R. D. & Ashkenazi, A. (1995). *Proc. Natl Acad. Sci. USA*, **92**, 5401–5405.

McElroy, C. A., Dohm, J. A. & Walsh, S. T. R. (2009). *Structure*, **17**, 54–65.

Miknis, Z., Margracheva, E., Li, W., Zdanov, A., Kotenko, S. W. & Wlodawer, A. (2010). *J. Mol. Biol.* **404**, 650–664.

Mikulecký, P., Černý, J., Biedermannová, L., Petroková, H., Kuchař, M., Vondrášek, J., Malý, P., Šebo, P. & Schneider, B. (2013). *Biomed Res. Int.* **2013**, 752514.

Moncada-Vélez, M. *et al.* (2013). *Blood*, **122**, 2390–2401.

Moura, P. R. de, Watanabe, L., Bleicher, L., Colau, D., Dumoutier, L., Lemaire, M. M., Renauld, J.-C. & Polikarpov, I. (2009). *FEBS Lett.* **583**, 1072–1077.

Murshudov, G. N., Skubák, P., Lebedev, A. A., Pannu, N. S., Steiner, R. A., Nicholls, R. A., Winn, M. D., Long, F. & Vagin, A. A. (2011). *Acta Cryst.* D**67**, 355–367.

O'Boyle, N. M., Banck, M., James, C. A., Morley, C., Vandermeersch, T. & Hutchison, G. R. (2011). *J. Cheminform.* **3**, 33.

Okonechnikov, K., Golosova, O. & Fursov, M. (2012). *Bioinformatics*, **28**, 1166–1167.

Pestka, S., Kotenko, S. V., Muthukumaran, G., Izotova, L. S., Cook, J. R. & Garotta, G. (1997). *Cytokine Growth Factor Rev.* **8**, 189–206.

Pettersen, E. F., Goddard, T. D., Huang, C. C., Couch, G. S., Greenblatt, D. M., Meng, E. C. & Ferrin, T. E. (2004). *J. Comput. Chem.* **25**, 1605–1612.

Plíhal, O., Sklenář, J., Kmoníčková, J., Man, P., Pompach, P., Havlíček, V., Křen, V. & Bezouška, K. (2004). *Biochem. Soc. Trans.* **32**, 764–765.

Pompach, P., Man, P., Kavan, D., Hofbauerová, K., Kumar, V., Bezouška, K., Havlíček, V. & Novák, P. (2009). *J. Mass Spectrom.* **44**, 1571–1578.

Ring, A. M., Lin, J.-X., Feng, D., Mitra, S., Rickert, M., Bowman, G. R., Pande, V. S., Li, P., Moraga, I., Spolski, R., Özkan, E., Leonard, W. J. & Garcia, K. C. (2012). *Nature Immunol.* **13**, 1187–1195.

Rüger, R., van Lenthe, E., Lu, Y., Frenzel, J., Heine, T. & Visscher, L. (2015). *J. Chem. Theory Comput.* **11**, 157–167.

Savan, R., Ravichandran, S., Collins, J. R., Sakai, M. & Young, H. A. (2009). *Cytokine Growth Factor Rev.* **20**, 115–124.

Schilling, B., Row, R. H., Gibson, B. W., Guo, X. & Young, M. M. (2003). *J. Am. Soc. Mass Spectrom.* **14**, 834–850.

Schoenborn, J. R. & Wilson, C. B. (2007). *Adv. Immunol.* **96**, 41–101.

Sievers, F., Wilm, A., Dineen, D., Gibson, T. J., Karplus, K., Li, W., Lopez, R., McWilliam, H., Remmert, M., Söding, J., Thompson, J. D. & Higgins, D. G. (2011). *Mol. Syst. Biol.* **7**, 539.

Thiel, D. J., le Du, M.-H., Walter, R. L., D'Arcy, A., Chène, C., Fountoulakis, M., Garotta, G., Winkler, F. K. & Ealick, S. E. (2000). *Structure*, **8**, 927–936.

Thomas, C., Moraga, I., Levin, D., Krutzik, P. O., Podoplelova, Y., Trejo, A., Lee, C., Yarden, G., Vleck, S. E., Glenn, J. S., Nolan, G. P., Piehler, J., Schreiber, G. & Garcia, K. C. (2011). *Cell*, **146**, 621–632.

Walter, M. R., Windsor, W. T., Nagabhushan, T. L., Lundell, D. J., Lunn, C. A., Zauodny, P. J. & Narula, S. K. (1995). *Nature (London)*, **376**, 230–235.

Yoon, S.-I., Jones, B. C., Logsdon, N. J., Harris, B. D., Deshpande, A., Radaeva, S., Halloran, B. A., Gao, B. & Walter, M. R. (2010). *Structure*, **18**, 638–648.

Fish and Shellfish Immunology 79 (2018) 140–152

Contents lists available at ScienceDirect

Fish and Shellfish Immunology

journal homepage: www.elsevier.com/locate/fsi

Full length article

Interferons type II and their receptors R1 and R2 in fish species: Evolution, structure, and function

Jiří Zahradník*, Lucie Kolářová, Hana Pařízková, Petr Kolenko, Bohdan Schneider**

Laboratory of Biomolecular Recognition, Institute of Biotechnology of the Czech Academy of Sciences, v. v. i., BIOCEV, Průmyslová 595, CZ-252 42 Vestec, Czech Republic

ARTICLE INFO

Keywords:
Interferon gamma
Type II interferons
Jak-Stat pathway
Fibronectin type III domain
Class 2 cytokine receptors
Fish immunity
Bioinformatics
Crystal structure
SAXS

ABSTRACT

Interferon gamma (IFN-γ) is one of the key players in the immune system of vertebrates. The evolution and properties of IFN-γ and its receptors in fish species are of special interest as they point to the origin of innate immunity in vertebrates. We studied the phylogeny, biophysical and structural properties of IFN-γ and its receptors. Our phylogeny analysis suggests the existence of two groups of IFN-γ related proteins, one specific for *Acanthomorpha*, the other for *Cypriniformes, Characiformes* and *Siluriformes*. The analysis further shows an ancient duplication of the gene for IFN-γ receptor 1 (IFN- γR1) and the parallel existence of the duplicated genes in all current teleost fish species. In contrast, only one gene can be found for receptor 2, IFN- γR2. The specificity of the interaction between IFN- γ and both types of IFN- γR1 was determined by microscale thermophoresis measurements of the equilibrium dissociation constants for the proteins from three fish species. The measured preference of IFN- γ for one of the two forms of receptor 1agrees with the bioinformatic analysis of the coevolution between IFN- γ and receptor 1. To elucidate structural relationships between IFN-γ of fish and other vertebrate species, we determined the crystal structure of IFN-γ from olive flounder (*Paralichthys olivaceus*, PoliIFN-γ) at crystallographic resolution of 2.3 Å and the low-resolution structures of *Takifugu rubripes, Oreochromis niloticus,* and *Larimichthys crocea* IFN-γ by small angle X-ray diffraction. The overall PoliIFN-γ fold is the same as the fold of the other known IFN- γ structures but there are some significant structural differences, namely the additional C-terminal helix G and a different angle between helices C and D in PoliIFN-γ.

1. Introduction

Interferons are proteins described by Isaacs and Lindenmann more than 60 years ago [1]. The name interferon is derived from the ability to interfere with viral infections. Interferons evolved in early chordates and represent ancient immunity elements [2]. Interferon gamma (IFN-γ) is now considered to be one of the key molecules in the regulation of the innate and adaptive immunity [3].

1.1. Interferon-γ and its signaling

IFN-γ is the only member of type II cytokines in mammals and plays a significant role in cell defense against intracellular pathogens. The IFN-γ function is best described in humans, where it mediates Th1 immunity and activates macrophages. The signaling of IFN-γ is initiated by the binding of the IFN-γ active form, a noncovalent homodimer, to receptor R1 [4–7] and subsequently to receptor R2 [8,9]. Formation of the IFN-γ/R1/R2 ternary complex results in spatial changes to cytoplasmic domains of receptors [10]. It leads to the binding of Janus activator kinase (JAK2) to the cytoplasmic part of receptor 2 and the attachment of JAK1 to the cytoplasmic part of receptor 1 [11], and the subsequent JAKs auto phosphorylation and phosphorylation of R1 [12,13]. This phosphorylation creates a binding site for the signal transducer and activator of the transcription (STAT1). After STAT1 is phosphorylated, it dimerizes and enters the cell nucleus where it induces expression of a variety of genes [14]. This sequence of events is described as the canonical pathway of IFN-γ signaling. So-called non-canonical IFN-γ signaling involves the endocytosis of the IFN-γ/R1/R2 complex, the creation of the IFN-γ/R1/STAT1α/JAK1/JAK2 complex and its transport to the nucleus. The IFN-γ nuclear localization signal (NLS) and polycationic C-terminus are crucial for the non-canonical IFN-γ signaling [15,16]. The IFN-γ/R1/Stat1α complex is responsible for the specificity of the interaction with the DNA regulatory sequences known as GAS - gamma interferon activation sites [17].

1.2. Interferon-γ in fish species

Teleost fish are an attractive target for studying evolution due to

* Corresponding author.
** Corresponding author.
E-mail addresses: jiri.zahradnik@ibt.cas.cz (J. Zahradník), bohdan.schneider@gmail.com, bohdan@ibt.cas.cz (B. Schneider).

https://doi.org/10.1016/j.fsi.2018.05.008
Received 15 February 2018; Received in revised form 27 April 2018; Accepted 2 May 2018
Available online 06 May 2018

their vast genomic variability [18]. During their evolution fish underwent three rounds of whole genome duplications (WGD) [19,20]. Two of these duplications are common to all vertebrates, the third one is specific for teleost fish. It occurred after fish and tetrapods split about 225–333 million years ago and it shows a specific evolutionary adaptation of fish [21]. Salmonid fish underwent one more WGD 96 million years ago [22], so did common carp (*Cyprinus carpio*) 12 Mya, [23]. In contrast to mammalian genomes, teleost genomes contain additional multiple families of active transposable elements which play an important role in the accelerated evolution of fish species [18]. Signaling pathway studies in fish provide important clues for understanding the evolution of specific immune adaptations of the antiviral defense system in early tetrapods and teleosts. Understanding the fish immune system may thus help the aquaculture industry's fight against fish viruses, whose occurrence remains a significant limiting factor in aquaculture production as well as in the sustainability of biodiversity in the world's oceans [24].

Type II interferon genes evolved early in the chordates evolution and are therefore present in extant cartilaginous fish (sharks and rays), bony fish, as well as in tetrapods [25]. It is assumed that they have evolved from a class II helical cytokine ancestor. Unlike humans with only one IFN-γ, the fish type II interferon family is broader in some species, consisting of two members, IFN-γ and fish-specific IFN-γ related (IFN-γrel) proteins. Moreover, in some fish species the *IFN*-γ gene is additionally duplicated resulting in two similar *IFN*-γ copies.

The first identified fish IFN-γ molecule was from the japanese pufferfish (*Takifugu rubripes*, Fugu) genome [26]. The *IFN*-γ gene was localized in the locus, which contains cytokine genes from the interleukin 10 family – *IL-22* and *IL-26*. These interleukins are tightly linked to *IFN*-γ in other species as well, including human, mouse, and frog. This fact supports the idea of gene synteny and helps *IFN*- γ identification in various genomes [21,27]. In salmonids and common carp, two *IFN*-γ genes are present likely due to the fourth WGD. Comparative studies of duplicated copies of *IFN*-γ were performed for atlantic salmon (*Salmo salar*) [28], common carp (*Cyprinus carpio*) [29] and rainbow trout (*Oncorhynchus mykiss*) [30]. Both IFN-γ paralogs appear to be biologically relevant and have a similar regulatory mechanism in these species.

Only some of the *IFN*-γ genes have been described at protein level. The FuguIFN-γ protein (UniProtKB - Q708J2) is expressed as 189 amino acid long pre-protein with the signal peptide 22 amino acids long and one potential glycosylation site. The gene composed of 3760 nucleotides (85% AT content) has 4 exons and 3 introns, which is similar to the composition of mammalian *IFN*-γ genes [26]. Approximately the same gene and protein characteristics were identified in rainbow trout (188 aa, AT rich) [31].

The biological functions of IFN-γ as well as its signaling pathways in fish are similar to those in mammals [31]. The highest expression level of IFN-γ has been found in the spleen, gill, and kidney of black seabream (*Acanthopagrus schlegelii*) [32] or zebrafish (*Danio rerio*) [33]. The IFN-γ expression is induced by various stimuli including lipopolysaccharides and poly I:C. IFN-γ has been shown to induce an inflammatory response and to protect the host from bacterial infection by stimulating the expression of genes of pro-inflammatory cytokines [31] in large yellow croaker (*Larimichthys crocea)* [34], atlantic cod (*Gadus morhua*) [35], nile tilapia (*Oreochromis niloticus*) [36], and atlantic halibut (*Hippoglossus hippoglossus* L.) [37].

1.3. Interferon-γ related protein in fish species

The comparative genomics analysis of the zebrafish and fugu genomes revealed the presence of a second *IFN*-γ gene in the locus containing interleukin 10 family genes. This gene was named interferon gamma 2 because of a low amino acid identity (17.0%) with the original *IFN*-γ gene [27]. The name interferon gamma related (*IFN*-γ*rel*) gene was proposed later to distinguish between these two distinct genes and the highly similar *IFN*-γ copies in salmonids and cyprinids [38].

The IFN-γrel is not a clear homolog of the mammalian IFN-γ as identified by its gene synteny. Despite the sequence divergence, the genomic localization seems to be well conserved. Therefore, it is assumed that *IFN*-γ*rel* originated by the duplication of the *IFN*-γ gene [21,27]. The IFN-γrel protein has been widely accepted as a second member of type II family [38]. Some hypotheses suggest that the novel IFN-γrel protein might have diverged, acquired a new function, and therefore have different affinities to the receptors [21,27]. The *IFN*-γ*rel* gene has been identified mostly in the cyprinid family including zebrafish [27], grass carp (*Ctenopharyngodon idella*) [39], common carp [29], and gold fish (*Carassius aurutus* L.) [40], and also channel catfish (*Ictalurus punctatus*, *Siluriformes*) [41], and in fugu (*T. rubripes*, *Acanthomorpha*) [27]. C-termini of IFN-γrel sequences show significant differences, which indicates the existence of multiple IFN-γrel isoforms [31].

The zebrafish cDNA of the *IFN*-γ*rel* gene encodes a 171-aa peptide with the 25-aa long signal sequence; the mature protein is 17.3 kDa in weight with two putative glycosylation sites [27]. Expression of common carp IFN-γrel protein was reported with N terminal 6xHis tag but without analysis of the protein [42].

The differences between IFN-γ and IFN-γrel signaling are poorly understood. The fish and human IFN-γ have analogical functions [43] and also IFN-γrel in *Cypriniformes* regulates antibacterial and antiviral activity. IFN-γrel is known not to be able to induce the genes of Toll-like receptors [44], and of interferon regulatory factors 1 [30] and 11 [38]. Studies of IFN- γrel bioactivity in ginbuna crucian carp (*Carassius auratus langsdorfii*) have reported that it is active as a monomer. This would be surprising because IFN-γ is known to function as a homodimer [45].

1.4. Interferon-γ receptors in fish species

Human IFN-γ induces a cell response through a receptor complex consisting of an IFN-γ homodimer and extracellular domains of two molecules of receptor 1 (IFN-γR1) and extracellular domains of two receptors 2 (IFN-γR2). The receptor molecules contain one conserved glycosylation site, an extensive cation-π motif in the D1 domain [9], and highly conserved cysteine residues capable of forming three potential disulfide bonds in R1 [46] and two in R2. All these signatures rank IFN-γ receptors into the class II receptor family with two fibronectin type III domains labeled D1 and D2 [47]. The intracellular part of receptors exhibits conserved potential phosphorylation sites. The phosphorylation sites are targeted by Jak1, Protein kinase C [48,49] and STAT1 [50] in the IFN-γR1, and by Jak2 [51] and leucine-leucine internalization motif in the IFN-γR2 [52].

Isoforms of interferon-γ receptors 1 and 2 were described in goldfish (*Carassius auratus* L.), zebrafish [40,53], rainbow trout, and stickleback (*Gasterosteus aculeatus*) [54]. Phylogenetic analysis places the teleost IFN-γR1 receptors separately from those of higher vertebrates and further still from IFN-γR2 sequences. IFN-γR1 exhibits higher expression levels than IFN-γR2 and a significantly higher expression in macrophages than in other cell types. The expression of IFN-γR2 is more tightly regulated than the expression of IFN-γR1. *IFN-γR2* gene synteny shows a conserved locus containing four clustered genes coding for *IFN-γR2*, interleukin 10 receptor beta (*IL-10RB*), interferon-α receptor 1 (*IFN-αR1*) and interferon-α receptor 2 (*IFN-αR2*) genes, similarly to the locus synteny in the human genome [54]. Two isoforms of IFN-γR1, named IFN-γR1-1 and IFN-γR1-2, were described in zebrafish and goldfish. An expression analysis in zebrafish tissues showed a significantly higher expression of IFN-γR1-1 than IFN-γR1-2, in goldfish there was a high expression of IFN-γR1-1 in the kidney and spleen, but also a high expression of IFN-γR1-2 in the brain [55]. Microscopy binding studies indicate that IFN-γR1-1 binds to IFN-γ1 but not to IFN-γR2, and IFN-γR1-2 preferentially binds to IFN-γrel [55].

1.5. Subject of this study

Even though the fish type II interferon system is actively studied, its many important aspects are still unknown. This is especially true for the biophysical studies of complex interactions between different type II interferons and their receptors. Here we report a thorough phylogeny study of IFN-γ, its receptors, and their co-evolution in fish species based on the combination of sequence and structure-based bioinformatics. The bioinformatic results are discussed in the light of the determined crystal structure of IFN-γ from olive flounder (PDB code 6F1E), the low-resolution topologies obtained by Small Angle X-ray diffraction (SAXS), and the binding affinities between IFN-γ and receptors of three species.

2. Methods

2.1. Expression and purification of recombinant IFN-γ proteins

Genes encoding for the interferon gamma proteins are detailed in Supplementary Material Table S1a; they are *Takifugu rubripes* TrubIFN-γ, Uniprot Q708J2, AA: 23–189; *Oreochromis niloticus* OnilIFN-γ, I3KNL7, AA: 23–206; *Paralichthys olivaceus* PoliIFN-γ, B3IXK1, AA: 24–198; *Ctenopharyngodon idella* CidIFN-γ2, gb AGG22551.1, AA: 26–182; *Epinephelus coioides* EcoiIFN-γ, gb AFM31242.1, AA: 22–200; *Larimichthys crocea* LcroIFN-γ, gb AIZ77177.1, AA: 22–200; variant of PoliIFN-γΔR with the C terminal deletion AA: 24–187. The genes were modified by a restriction enzyme site removal and optimization, obtained as DNA Strings (Thermo Fisher Scientific, Table S1a), and cloned to pET26b using restriction free cloning [56] or Transfer-PCR [57] in the position of *Nde*I and *Xho*I. All primers are listed in Table S1b. All used clones were verified by sequencing and single colony isolates were isolated by QIAprep® Miniprep Kit and used to transform expression hosts *E. coli* Rosetta™(DE3). Expression plasmids with OnilIFN-γ, TrubIFN-γ and PoliIFN-γ were deposited in Addgene plasmid repository (https://www.addgene.org/) under IDs 107287, 107288 and 107289 respectively. The cultures were grown in LB medium (1.0% tryptone, 0.5% yeast extract, 1.0% sodium chloride; pH 7.0) supplemented by trace elements TE (1 mM $MgSO_4$, 0.3 mM $CaCl_2$, 170 μM EDTA,30 μM $FeCl_3$, 6 μM $ZnCl_2$, 1 μM $CuCl_2$, 0.3 μM $CoCl_2$, 1 μM H_3BO_3, 70 nM $MnCl_2$) in 5 L Erlenmeyer flasks with 1 L of LBTE medium in Max Q 4000 shaker, Barnstead, Lab-Line (250 rpm, 30 °C). Heterologous expression was induced by 1 mM IPTG at OD_{600} of 0.6, the expression temperature was lowered to 16 °C and growth continued for 16 h. Cells were harvested by centrifugation (5000 g, 10 min, 4 °C) and stored in −20 °C for further use. Two-step purifications of interferons were based on SP Sepharose and gel filtration chromatography providing usually 10 mg/L of single band purity protein. Cells were disintegrated by sonication (Sonicator 3000, Misonix, 15–20 W) in buffer, (phosphate buffer saline, PBS: 137 mM NaCl, 2.7 mM KCl, 10 mM Na_2HPO_4, 1.8 mM KH_2PO_4) treated with 5 U/ml Benzonase® Nuclease, centrifuged (40 000 g, 4 °C, 30 min), and loaded on a HiTrap SP HP 5 ml (Ge Healthcare) column. Elution was performed by gradient 0–2 M NaCl (200 mM Na_2HPO_4, 50 mM NaH_2PO_4, 2 mM EDTA, 4 mM benzamidine, pH 7.3). Fractions with IFN-γ (eluted by high salt over 1 M NaCl) were immediately pooled and loaded on a HiLoad 16/600 Superdex 75 gel chromatography column pre-equilibrated in citrate buffer (100 mM, pH 6.0). All operations were performed on a NGC Chromatography system (Bio-Rad). The purified proteins were concentrated by Vivaspin Protein Concentrator Spin Columns to 10 mg/ml and directly used for crystallization or biophysical measurements. Identities of all expressed proteins were verified by mass spectrometry.

2.2. PoliIFN-γ protein crystallization and data collection

Crystals of PoliIFN-γ (Fig. S1) were grown using the hanging-drop vapor-diffusion method in a Greiner pre-greased 24 well Combo Plate with reservoir solution (optimized screen condition Index HT A9, Hampton research) consisting of 0.1 M Bis-Tris pH 5.5, 3 M NaCl and drops consisting mixture of 1 μl protein solution (10 mg/ml protein in 100 mM citrate buffer, pH 6.0) and 1 μl precipitant solution (the same as reservoir solution). After the growth during 2–3 days at ambient temperature (about 293 K), crystals were mounted in Round LithoLoops (Molecular Dimensions), some of them soaked with selenourea according to the method described previously [58], cryo-protected in 25% glycerol, and flash-cooled in liquid nitrogen.

Table 1
Data processing statistics and structure refinement parameters. Values in parentheses refer to the highest resolution shell.

	Native dataset	Selenourea soak
PDB code	6F1E	not deposited
Data processing statistics		
Wavelength (Å)	0.91841	0.97934
Space group	$P2_12_12_1$	$P2_12_12_1$
Unit-cell parameters a, b, c (Å); α, β, γ (°)	78.1, 78.1, 441.8 90.0, 90.0, 90.0	57.7, 83.0, 95.1 90.0, 90.0, 90.0
Resolution range (Å)	47.30–2.30 (2.38–2.30)	49.31–2.29 (2.37–2.29)
No. of observations	260,836 (24,236)	674,517 (57,880)
No. of unique reflections	20,255 (2032)	21,043 (1892)
Data completeness (%)	99.6 (97.4)	99.1 (92.1)
Average redundancy	12.9 (11.9)	32.1 (30.6)
Average I/σ(I)	13.5 (0.9)	18.9 (2.3)
Solvent content (%)	64.2	
Matthews coefficient (Å3/Da)	3.4	
Rmerge	0.102 (2.711)	0.138 (1.806)
Rpim	0.042 (1.163)	0.034 (0.455)
CC1/2	0.999 (0.559)	0.999 (0.737)
Structure refinement parameters		
Rwork	0.227	
Rfree	0.297	
Rall	0.229	
Average B-factor (Å2)	78	
RMSD bond lengths from ideal (Å)	0.014	
RMSD bond angles from ideal (°)	1.599	
Number of non-hydrogen atoms	2286	
Number of water molecules	38	
Ramachandran statistics: residues in favored regions (%); number of outliers	100; 0	

The X-ray diffraction data were collected at 100 K on the beamline MX 14.1 of the BESSY II synchrotron-radiation source at the Helmholtz-Zentrum Berlin (HZB). A native data set was collected at a wavelength of 0.918 Å, anomalous dispersion data set from a crystal soaked with selenourea were collected at a wavelength of 0.979 Å. The diffraction data statistics are shown in Table 1.

The PDB database (www.rcsb.org, [59]) was searched for the other IFN-γ structures using the Sequence & Structure Alignment and comparison tools; they are all mammalian: human, 1HIG [60], 1FG9 [5], 3BES [61]), rabbit *Oryctolagus cuniculus* 2RIG [62], and bovine *Bos taurus* 1D9C [63], 1RFB [64].

2.3. PoliIFN-γ data processing, structure determination and refinement

The diffraction data were processed using the XDS program package [65] and scaled using the program Aimless [66] from the CCP4 program package [67]. The positions of selenium atoms were found using the SHELX program package [68] using the data up to the resolution of 2.7 Å. Experimental phases were used in the program ARP/wARP [69] to build the initial model that was later used for structure determination using the native data set. Model building and manual corrections were performed using COOT [70], automated refinement procedures were performed using the program REFMAC [71]. The structure quality was

analyzed using MOLPROBITY [72]. The final structure parameters are shown in Table 1. The coordinates and structure factors have been deposited in the PDB [59] with the accession code 6F1E.

2.4. Expression and purification of recombinant IFN-γ receptor proteins

The extracellular parts of IFN-γ receptors of *P. olivaceus*, *T. rubripes*, and *O. niloticus* were produced by the Drosophila S2 expression system. The complete gene sequences, which were characterized in most cases as a putative protein, were acquired from the GenBank database, manually inspected by global alignments, shortened into extracellular parts only (chapter 2.8), and optimized for the *Drosophila* codons by the Life Technologies web optimization service. DNA Strings (Table S1a) were cloned into a modified pMT-BiP-V5-His_A vector using Gibson assembly [73] in the position *Bgl*II and *Xho*I restriction sites (Tables S1a and S1b). This procedure leads to the *IFN-γR1* genes in frame with the BiP signal peptides and C-terminal 6x HisTags. *Drosophila* Schneider S2 cells were transfected by using Effectene Transfection Reagent (Quiagen) according to the manufacturer's instructions together with selection plasmid pCoBlast. Stable cell lines were established by growing the S2 cells in HyClone SFX Medium supplemented with 10% FBS and 25 μg/ml Blasticidin S. The established cell lines were transferred and maintained in FBS-free SFX medium for expression batches. The protein expression was induced by addition of 1.0 mM $CuSO_4$. The cell-free medium (1 L) was prepared by centrifugation at 8000 g, 4 °C, 20 min and subsequently precipitated by addition of $CaCl_2$ to the final concentration of 5 mM, $NiSO_4$ (1 mM), NaCl (250 mM), and Tris-HCl, pH 8 (50 mM). This solution was centrifuged (10 000 g, 4 °C, 20 min) and filtered (0.45 μm) prior to the IMAC purification by standard procedure. Eluted fractions (300 mM imidazole) were directly loaded on the HiLoad 16/600 Superdex 75 (GE Healthcare) equilibrated by 10 mM Hepes, pH 7.5; 100 mM NaCl buffer. The samples were analyzed by 12% SDS-PAGE and verified by mass spectrometry.

2.5. Protein glycosylation and disulfide bond analysis

The protein glycosylation and S-S bond formation were determined by protein trypsinization in solution or in 12% SDS-PAGE and subsequent analysis by MALDI-MS according to the previously published methods [9,74,75].

2.6. Biophysical measurements

Circular dichroism (CD) spectra were acquired on the Chirascan-plus spectrometer (Applied Photophysics) with wavelength steps of 1 nm (185–260 nm) at 20 °C, protein concentrations of 0.1 mg/ml; the buffer spectra were subtracted. Results were analyzed by the CDNN software [76]. Protein melting curves were recorded by detecting the change of the tryptophan fluorescence at 330 and 350 nm between 20 °C and 95 °C (step 1 °C/min) with protein concentrations 1–3 mg/ml using Prometheus NT.48 (NanoTemper Technologies). Affinity measurements were performed by MicroScale Thermophoresis (MST) using a Monolith NT.115 instrument by NanoTemper Technologies. The receptors for IFN-γ from different species were labeled by the Monolith His-Tag Labeling Kit RED-tris-NTA provided by NanoTemper Technologies according to manufacturer's instructions. The labeled proteins were measured in a citrate buffer pH 6.0 at concentration of 200 nM with ranging concentration of a ligand and MST power 20–80%. Data from triplicates were analyzed by the MO.Affinity Analysis software version 2.1.2030.

2.7. Small angle X-ray diffraction experiments

The SAXS data were collected at the EMBL P12 beamline (DESY, Hamburg). Data were collected at 293.15 K at wavelength 1.24 Å with samples at four different concentrations. Sample to detector (PILATUS 2M, Dectris Ltd.) distance was 3.0 m, covering a scattering vector ($q = 4\pi\sin(\theta)/\lambda$) range from 0.0027 to 0.48 $Å^{-1}$. Data were collected, pre-processed and subtracted using the automated acquisition and analysis SAXS pipeline [77].

The scattering-derived parameters were determined using *PRIMUSqt r3709* [78], the pair-distance distribution function was determined using *GNOM v4.6.* [79]. The similarities of SAXS profiles were evaluated by the SIBYLS Beamline workflow (http://sibyls.als.lbl.gov/saxs_similarity/).

2.8. Sequence based bioinformatics

The known sequences of IFN-γ and IFN-γ receptors were downloaded from the NCBI Protein, UniProt and Ensembl databases (https://www.ncbi.nlm.nih.gov/protein/, http://www.uniprot.org/, http://www.ensembl.org/). The resulting set of sequences was used for pBLAST and tBLASTn (https://blast.ncbi.nlm.nih.gov/Blast.cgi, [80]) search of homologous proteins in bony fish species (taxid 7898). Multiple rounds of BLAST were performed in an iterative fashion: we started with sequences annotated as IFN-γ (IFN-γ R1, IFN-γ R2), and in each subsequent round, newly identified sequences with E-value above threshold 0.01 were added to the dataset and used for the next round of search. The procedure stopped when no yet unobserved sequences were found. In case the BLAST hit was genomic DNA without annotation, the genes and their products were predicted using the Exonerate software (version 2.2.0) [81]. Genes for fish IFN-γR2 were also identified among fish genomic sequences available at the NCBI Sequence Viewer 3.22.0 (https://www.ncbi.nlm.nih.gov/projects/sviewer/) taking advantage of their clustering with better annotated genes of the transmembrane protein 50B (*TMEM50B*). The sequences of the prospective IFN-γ and receptor proteins were manually checked and those that were truncated, duplicate or probably incorrectly based on alignment analysis were removed; the resulting list of the genes accepted for the analysis is provided in Supplementary Table S2a, the discarded ones in Table S3. Sequences from *Lepisosteus oculatus* (*Holostei*) were added to the datasets as outgroups, because *Holostei* diverged from the teleostean fish before the occurrence of the last, teleost-specific WGD.

The extracellular domains of IFN-γR1 and IFN-γR2 were predicted by the alignment using Muscle version 3.8.31 [82] with the sequences of human receptors and further validated by transmembrane helix localization by the TMHMM Server v. 2.0 [83] and by the SignalP 4.1 Server [84] (CBS Prediction Servers).

For phylogenetic analysis, the sequences of IFN-γ and the extracellular domains of IFN-γ receptors were aligned by Muscle version 3.8.31. Four sequences of IFN-γ (AHZ62713.1, KKF32167.1, XP_008399113.1, XP_014906354.1) were aligned separately from the rest because of their low sequence homology and added to the alignment using the Muscle "-profile" option. Aligned sequences were trimmed automatically by the trimAl tool (version 1.2rev59) with "–strict" option [85]. Phylogenetic trees were constructed by Bayesian inference using MrBayes 3.2.6 [86] with the best fitting model of evolution chosen by ProtTest 3.4.2 [87], and by a maximum likelihood approach using the online version of PhyML 3.0, (http://www.atgc-montpellier.fr/phyml/, [88]) with the substitution model selected by SMS [89] according to BIC, BIONJ starting tree, the NNI type of tree improvement and branch supports computed by aLRT SH-like. The trees were visualized and edited using FigTree (http://tree.bio.ed.ac.uk/software/figtree/) and TreeGraph 2 [90]. The similarities between results obtained by the different tree inference methods were computed by Compare2Trees, version September 2011 [91].

Coevolution between IFN-γ and its receptors was tested using the Parafit function [92] from the R package ape [93] with 999 permutations and the Cailliez correction for negative eigenvalues. Associations between all pairs of protein molecules coming from the same organism were tested. Results were visualized using the R package phytools [94]. Coevolution at amino acid level for IFN-γ and IFN-γR1 was investigated

using the i-COMS web-server [95] with MI, plmDCA, and mfDCA statistics. Multiple sequence alignments used as input were generated by Muscle from previously gained sequences according to i-COMS format requirements.

2.9. Structural bioinformatics

Structural comparisons and root-mean-square deviation (RMSD) values were calculated by MatchMaker as implemented in the UCSF Chimera software [96] with the Needleman-Wunsch algorithm and BLOSUM62 matrix. We used the BLOSUM 45-60, BLOSUM 80, and PAM matrices for very dissimilar or short sequences according to the Pearson rules [97,98]. The starting model for homology modeling was prepared by USF Chimera, the models were calculated by Modeller 9.19 [99,100] and the resulting structural alignment was used for the phylogeny study complemented by protein sequences of all known IFN-γ and receptor structures. The topology of the disulfide bonds was used as constrains for the modeling. To remove the effect of different mutual orientation of D1 and D2 domains of the extracellular parts of the receptors [9], the domains were modeled and aligned separately by using the known structures of the receptors [5,9,101]. For each sequence, two models were generated. Variable parts were re-modeled by the loop-refinement tool in Chimera and the DOPE-HR protocol [102].

3. Results and discussion

3.1. Summary of results

Fish IFN-γ were produced in *E. coli*, purified (Supplementary Fig. S1), characterized (Supplementary Figs. S2a and b), the crystal structure for PoliIFN-γ was solved at 2.3 Å resolution (PDB entry 6F1E, Fig. 1); the structures of other proteins were analyzed by the SAXS technique (Fig. S3). The phylogeny of IFN-γ and the receptors was subjected to comparison with fish evolution (Fig. 2) together with a further analysis of the components of the IFN-γ ternary complex: IFN-γ (chapter 3.3, Fig. 3 and Figs. S4a and b), IFN-γR1 (chapter 3.4, Fig. 3 and Figs. S5a and b) and IFN-γR2 (chapter 3.6, Fig. 3 and Figs. S6a and b). Fig. 4 displays the arrangement of gene clusters of IFN-γ and IFN-γR2. Finally, we describe the molecular coevolution between IFN-γ and its receptors (chapter 3.5) based on phylogeny (Fig. 5) and our biophysical experiments (Fig. S7).

3.2. Structure of PoliIFN-γ and the related IFN-γ

The interferons-γ PoliIFN-γ, OnilIFN-γ, TrubIFN-γ and LcroIFN-γ were produced from *E. coli* Rosetta (DE3) without the use of affinity tags in contrast to the previous studies of fish interferon gamma with TrxA (pET-32a), or N-terminal His tag [34] [42]. The purification protocol was set up on a SP Sepharose anion column in a similar manner as for human IFN-γ (Fig. S1) [7]. This procedure was very efficient due to the extreme pI of fish interferons (10.5 for PoliIFN-γ) and led to the overall yield of approximately 20 mg per L of *E. coli* culture. No or poor expression was obtained for CidIFN-γ2 and EcoiIFN-γ interferons. The PoliIFN-γ was also produced from S2 cells with some of the three potential glycosylation sites occupied by insect type of N-glycosylation, with a mass shift of approximately 3 kDa for monomer (SDS-PAGE analysis) but with very low yields (0.1 mg/L). Folding of all interferons was checked by CD spectroscopy and by measuring their melting temperatures (Fig. S2a).

Diffraction quality crystals were obtained only for PoliIFN-γ; the final construct was shortened by 11 amino-acids at the C terminus to obtain better diffracting crystals. The other interferons were prone to form non-diffracting needle-like structures. The structure of PoliIFN-γΔR (GenBank: BAG50577.1 [103]) was solved at 2.3 Å resolution by experimental phasing on PoliIFN-γ (wild type, 2.7 Å) using the selenourea labeling [58].

The PoliIFN-γ crystal structure is a homodimer with 175 amino-acids in each chain corresponding to the molecular weight of 2 × 20.4 kDa. The electron density map can be interpreted for 144 and 126 residues in chain A and B, respectively, both chains are quite similar with the root mean square deviation (RMSD) between 115 Cα pairs 0.75 Å. The amino acid residues 91–110, insertion characteristic for IFN-γ proteins from *Acanthomorpha*, are not resolved in the electron density.

The overall fold of PoliIFN-γ is similar to the fold of other known IFN-γ structures but significant differences were observed (Fig. 1). Most importantly, the first monomer of PoliIFN-γ is not composed of six α-helices as in all other known IFN-γ structures, but of seven. The additional α-helix unobserved in mammalian IFN-γ was resolved close to the C-terminus of chain A, the corresponding residues in chain B are disordered. The presence of this α-helix, labeled G in Fig. 1, is interesting in the light of the previously published speculation [21] about the interaction between the C-terminal amino acids and the receptor 1. The helix G can therefore play a role in the IFN-γ - receptor interactions.

Another feature distinguishing the PoliIFN-γ structure from the

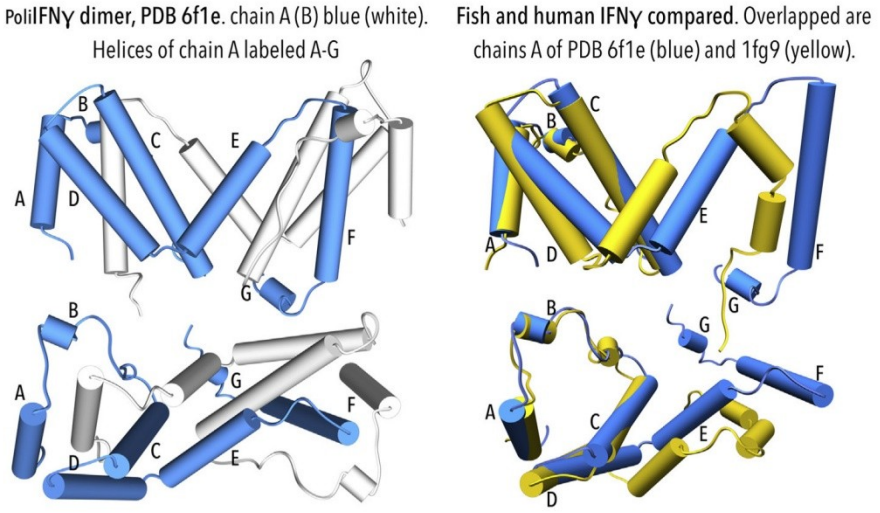

Fig. 1. Three-dimensional (3D) structure of the IFN-γ dimer from *Paralichthys olivaceus* (PoliIFN-γ, PDB 6f1e, this work, left), and the superposition of PoliIFN-γ and human IFN-γ (PDB 1FG9 [5], right). The α-helices are displayed as cylinders, top and bottom images are related by approximately 90° rotation.

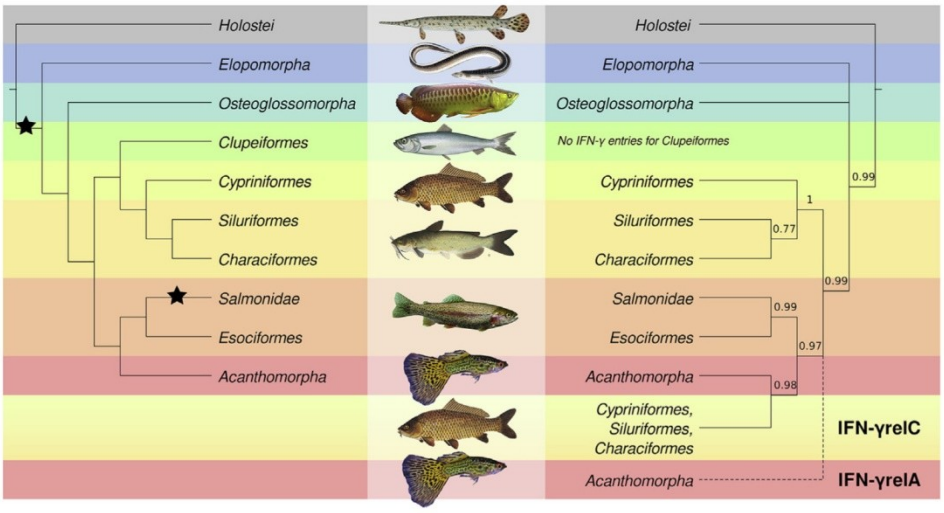

Fig. 2. Fish phylogeny (left, based on [104]) compared with the cladogram of fish IFN-γ and IFN-γ related proteins (right). Posterior probabilities of the internal branches computed by the MrBayes software are shown for the IFN-γ tree. Branches with posterior probability lower than 0.70 were collapsed. The position of the second cluster of *Acanthomorpha* sequences has low support and is thus unclear (marked by dashed line). The tree of fish phylogeny shows only orders with at least one representative of IFN-γ, IFN-γR1, or IFN-γR2 proteins in our set. There are no known IFN-γ, only IFN-γR1 entries for *Clupeiformes*. The stars mark the position of teleost-specific and salmonid-specific whole genome duplications [20] [19]. Pictures (from top to bottom): *Holostei: Lepisosteus oculatus*; *Elopomorpha: Anguilla japonica*; *Osteoglossomorpha: Scleropages formosus; Clupeiformes: Clupea harengus*; *Cypriniformes: Cyprinus carpio*; *Siluriformes: Ictalurus punctatus*; *Salmonidae: Oncorhynchus mykiss*; *Acanthomorpha: Poecilia reticulata*; *Cypriniformes: Cyprinus carpio*; *Acanthomorpha: Poecilia reticulata*; all fish pictures from Wikimedia Commons, edited.

known mammalian IFN-γ structures is the mutual orientation of helices D and E (Fig. 1). Repositioning of these helices in PoliIFN-γ, relative to the other IFN-γ structures, opens up their angle by almost 20° and results in the extension of the PoliIFN-γ structure. In consequence, neither of the PoliIFN-γ chains can be superimposed over the other known IFN-γ structures; RMSD between chains A of PoliIFN-γ and 1FG9 is 8.2 Å, and 7.5 Å for 1D9C when 121 (113) pairs of Cα atoms are considered. The close relationship between the IFN-γ molecules is observed when only the N-terminal helices A, B, C are superimposed; the RMSD values are 1.1 Å and 1.2 Å for the 40 Cα pairs for 1FG9 (Fig. 1) and 1D9C, respectively. The use of the Smith-Waterman algorithm and PAM matrices resulted in the identification of additional similarity regions among structures in loops between helix E and the first part of helix F (RMSD 0.58 Å for 19 pairs). Interestingly, the PoliIFN-γ structure is more similar to the human IFN-γ bound to receptor 1 (1FG9, [5]) than to the free form (1HIG [60]).

We measured the SAXS data of the expressed IFN-γ proteins to visualize their low-resolution structures. A comparison of the SAXS derived molecular envelope of PoliIFN-γ in solution with its crystal structure displays a general agreement. The similarity of the SAXS derived molecular envelopes of PoliIFN-γ and the other expressed fish IFN-γ proteins confirms that they all occur in solution as homodimers and it suggests their overall similarity (Fig. S3).

3.3. Evolution of IFN-γ and IFN-γrel proteins

We performed an extensive manual and computer alignment-driven search for all available IFN-γ sequences in fish species in the NCBI Protein, UniProt and Ensembl databases. The search yielded 63 sequences of IFN-γ and IFN-γ related proteins (Table S2) from 44 fish species, 28 of which were previously not correctly annotated as IFN-γ or IFN-γrel. One protein sequence was predicted by us from the genomic nucleotide sequence (Table S2b). The changes of annotations for all IFN-γ, IFN-γR1 and IFN-γR2 were recorded in Zebrafish Information Network (ZFIN, zfin.org) and were also submitted to the NCBI database. Based on our data, 18 new RefSeq database entries of IFN-γ and IFN-γrel, 55 new RefSeqs of IFN-γR1 and 30 new RefSeqs of IFN-γR2 were created. They are marked by bold font in Supplementary Table S2a. The new nomenclature introduced by ZFIN is *ifng1* for IFN-γ gene and *ifng1r* for IFN-γrel gene.

To uncover the evolutionary relationships between the retrieved IFN-γ sequences we conducted a phylogenetic analysis by the Bayesian

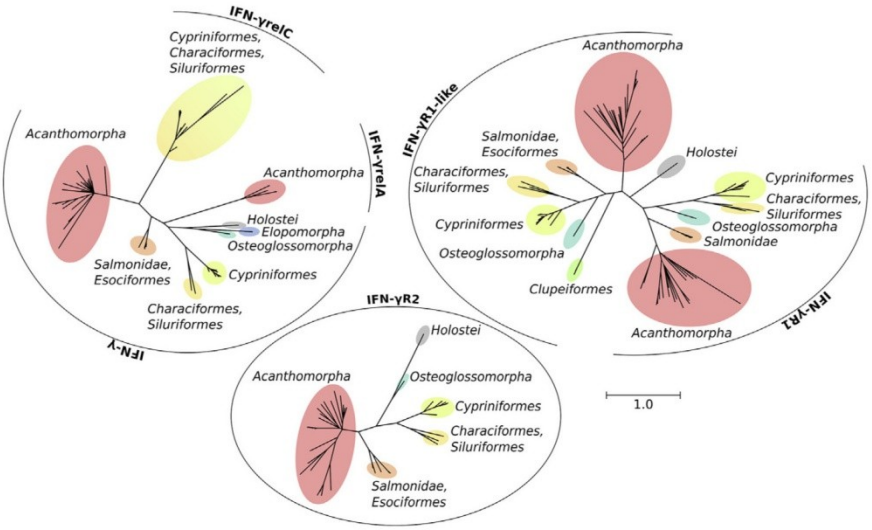

Fig. 3. Phylogeny of fish IFN-γ (top left), IFN-γ receptor 1 (top right) and IFN-γ receptor 2 (bottom). Branches with posterior probability lower than 0.5 were collapsed. The trees were computed by the Bayesian inference. Color scheme is analogous to Fig. 2. Details at the species level are given in Supplementary Figs. S4a and b; S5a, b and S6a, b. (For interpretation of the references to color in this figure legend, the reader is referred to the Web version of this article.)

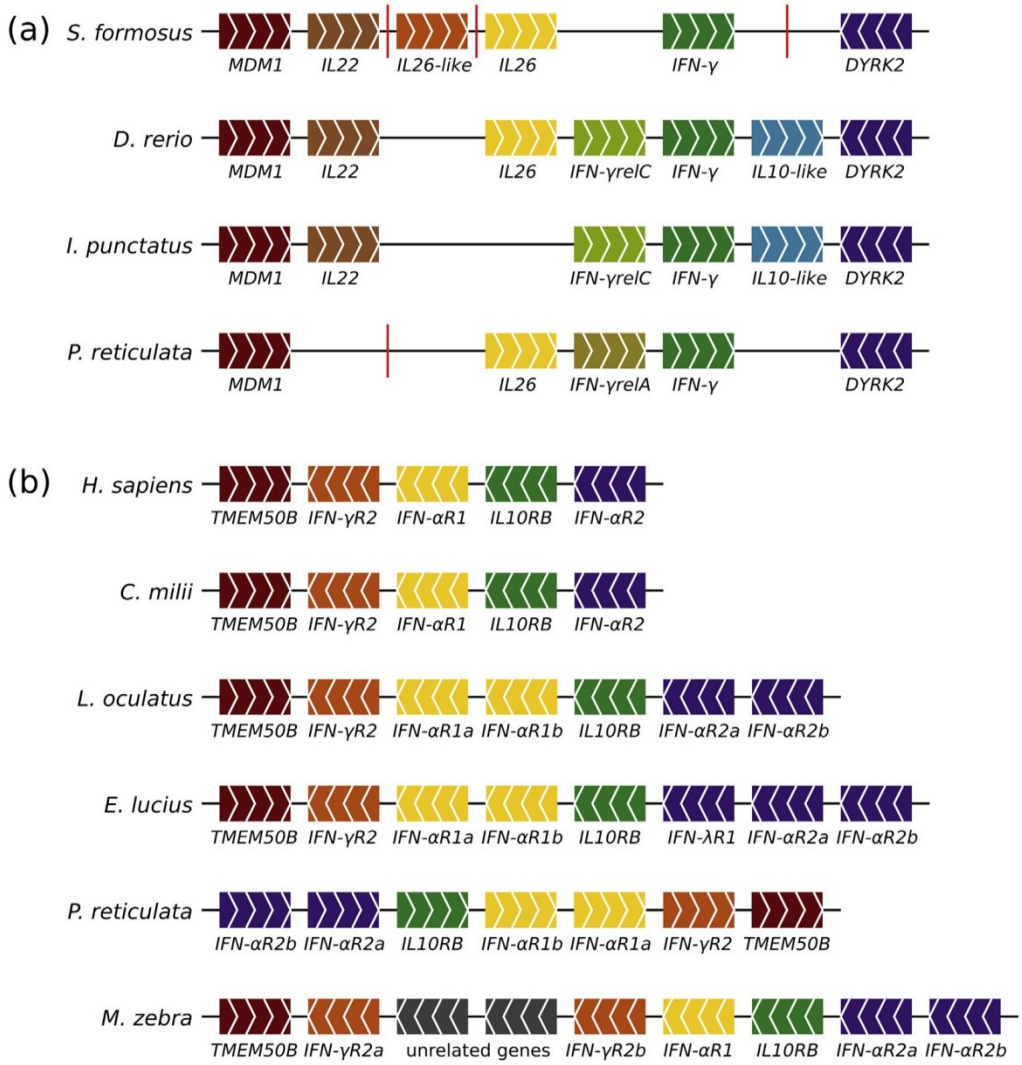

Fig. 4. *IFN-γ* and *IFN-γ receptor 2* gene clusters in different species, annotation according to the NCBI Sequence Viewer and mutual sequence homology. (a) *IFN-γ* genes in: *S. formosus*, *Osteoglossomorpha*; *D. rerio*, *Cypriniformes*; *I. punctatus*, *Siluriformes*; *P. reticulata*, *Acanthomorpha*. The cluster of *S. formosus* was constructed from two different scaffolds. (b) *IFN-γR2* genes physically co-localized in *H. sapiens* and selected fish species: *Homo sapiens*; *Callorhinchus milii*, *Chondrichthyes*; *L. oculatus*, *Holostei*; *Esox lucius*, *Esociformes*; *P. reticulata*, *Acanthomorpha, Cyprinodontiformes*; *Maylandia zebra*, *Acanthomorpha, Cichlidae*. The *E. lucius IFN-λR1* gene likely belongs to the *IFN-αR2* family despite that it is annotated as interferon-λ receptor 1. The two grey colored genes in *M. zebra* genome are likely not analogous to any other gene in the cluster and the function of their products is unknown [107]. The white arrows mark the orientation of genes, the red vertical lines indicate that the genome sequence is incomplete in this position. The lengths of genes and intergenic regions are not to scale. Only protein-coding genes are shown. The exact genomic locations and the gene identifications are listed in Tables S4a and c. (For interpretation of the references to color in this figure legend, the reader is referred to the Web version of this article.)

inference (Figs. 2 and 3 and Fig. S4a) and maximum likelihood methods (Fig. S4b) according to the previously published computations [105,106]. The topologies of the trees calculated by these two methods reflect fish phylogeny quite well and are quite similar. Differences were located only at the level of species and genera; the similarities were 84% for IFN-γ, 94% for IFN-γR1 (chapter 3.4), and 86% for IFN-γR2 (chapter 3.6). The phylogeny is summarized in Fig. 2, more details can be found in Figs. S4a, b, S5a, b (IFN-γR1), and S6a, b (IFN-γR2).

Fig. 3 summarizes our phylogenetic calculations of IFN-γ and its two receptors. The analysis shows clear separation of IFN-γ and IFN-γrel into two clearly separated paralogs of human IFN-γ ("canonical IFN-γ"). IFN-γrel then forms two distinct clusters - one comprises proteins of *Cypriniformes*, *Siluriformes,* and *Characiformes* orders (further referred to as IFN-γrelC), the other was detected in *Acanthomorpha* (IFN-γrelA).

To test the possibility that IFN-γrel proteins form two independent groups, we looked at the *IFN-γ* gene locus structure (Fig. 4a). In genomes of *D. rerio* (*Cypriniformes*), *I. punctatus* (*Siluriformes*), *Astyanax mexicanus* (*Characiformes*) and *P. reticulata* (*Acanthomorpha*) the *IFN-γ* and *IFN-γrel* genes are adjacent and in the same orientation (Fig. 4a – II-IV, data for *A. mexicanus* not shown), while there is no annotated gene in this location in the genome of *S. formosus* (*Osteoglossomorpha*) (Fig. 4a – I). This could be the result of three different scenarios: 1. The *IFN-γ* gene was duplicated once prior to the teleostean split and the second copy has been lost in *S. formosus*. 2. The *IFN-γ* gene was duplicated once after *Osteoglossomorpha* have diverged from the rest of teleosts. 3. The IFN-γrel of *Cypriniformes* and IFN-γrel of *Acanthomorpha* originated in two independent duplications of the *IFN-γ* gene. Further investigation is needed to decide, which of these hypotheses is true. The hypothesis of single IFN-γ gene duplication that occurred prior to the teleostean diversification [27] cannot be dismissed, because we could identify only 4 IFN-γrelA sequences that had a low sequence homology compared to the rest of the set and the position of their subtree (Fig. 3)

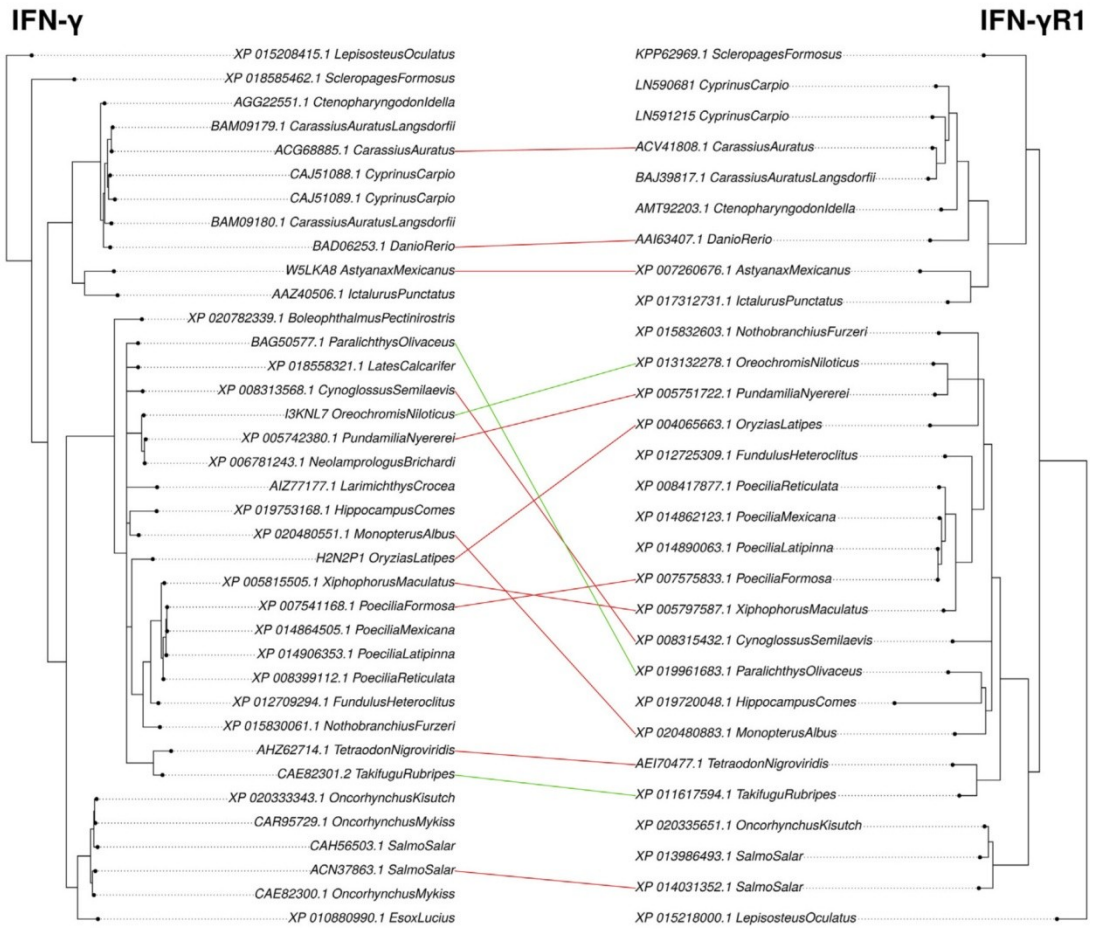

Fig. 5. The analysis of phylogenetic coevolution of IFN-γ (left) and IFN-γR1 (right). Trees computed by the Bayesian inference were used, branches corresponding to IFN-γrelA and IFN-γrelC were removed from the IFN-γ tree. All links between the receptor and ligand from the same species were tested. Significant evolutionary links are shown as red lines. A link was considered significant if the p-value of both test statistics implemented in the Parafit function was lower than 0.1. Experimentally tested pairs of IFN-γ and IFN-γR1 are shown as green lines; all three are not significant. (For interpretation of the references to color in this figure legend, the reader is referred to the Web version of this article.)

had a low statistical weight. Also, the question remains whether all *Acanthomorpha* have the IFN-γrelA protein, or if it occurs only in some species from this largest group of present fish species.

Salmonidae fish also possess two different IFN-γ proteins. However, these proteins are highly similar (over 90% of amino acid identity for *O. mykiss* and *S. salar*) and thus form only one cluster in the phylogenetic tree (Figs. S4a and S4b). These proteins likely originated in the last whole genome duplication, which *Salmonidae* underwent approximately 96 Mya [22]. Similarly, two different sequences of IFN-γ and two sequences of IFN-γrel in tetraploid *C. carpio* [23] result from the recent whole genome duplication (approx. 12 Mya) and a more recent wave of segment duplications (2.3–6.8 Mya).

3.4. Phylogeny of fish IFN-γ receptor 1

The database and BLAST search yielded 96 sequences of IFN-γ receptor 1 (Table S2a), 60 of them were previously not annotated as such. The sequences come from 44 different fish species, 32 of which were also represented by at least one representative in the IFN-γ dataset. Most of the species are represented by two distinct IFN-γR1 protein sequences, the observation has already been published for *C. auratus* and *D. rerio* [55]. The available data indicate that the IFN-γR1 protein is represented by two distinct genes in all fish orders except the evolutionary oldest one, *Holostei*. These two IFN-γR1 proteins are not close isoforms; their overall amino acid identity is below 30% (Table 2). Moreover, additional close IFN-γR1 isoforms have been identified in the genome of *C. carpio* [108], *O. kisutch*, *Sinocyclocheilus grahami*, *S. anshuiensis*, *S. rhinocerous*, and *Clupea harengus*, in the first five cases probably as a result of duplication of the whole genome.

We performed a phylogenetic study for all found sequences of the extracellular domain of IFN-γR1. Intracellular domains have been excluded from the comparison because of their low sequence homology. The IFN-γR1 sequences are split into two independent clusters (Fig. 3, Figs. S5a and S5b), as expected from their low sequence homology. Further on, these two groups are named IFN-γR1 and IFN-γR1-like as in the ZFIN database. The genes of IFN-γR1 and IFN-γR1-like groups are located on different chromosomes in genomes of fish species spanning across the whole teleostean phylogenetic tree (Table S4b). Thus, it is likely that the origin of the second IFN-γR1 copy lies in the teleost-specific whole genome duplication.

3.5. Coevolution between IFN-γ and IFN-γ receptors

Having two homologs of IFN-γ (canonical IFN-γ and IFN-γrel) and two homologs of IFN-γR1, a question arises what ligand-receptor pairs signal. The previous *in vitro* [55] and *in vivo* [53] results have suggested that canonical IFN-γ binds preferably to IFN-γR1-like (designated also as Crfb13), but not to IFN-γR1 (Crfb17), while both IFN-γR1 and IFN-γR1-like are important for IFN-γrelC signaling. We decided to test this hypothesis both programmatically by searching for the coevolution of

Table 2
Amino acid identity of the two distinct IFN-γR1 receptors of selected fish species.

Species	Order	IFN-γR1 NCBI protein ID	IFN-γR1-like NCBI protein ID	Amino acid identity %
Scleropages formosus	*Osteoglossomorpha*	KPP62969.1	XP_018604991.1	28
Danio rerio	*Cypriniformes*	AAI63407.1	NP_001165063.1	23
Ictalurus punctatus	*Siluriformes*	XP_017312731.1	XP_017319969.1	21
Oncorhynchus kisutch[a]	*Salmonidae*	XP_020335651.1	XP_020315962.1, XP_020315966.1	28/28
Poecilia reticulata	*Acanthomorpha*	XP_008417877.1	XP_008427408.1	27
Tetraodon nigroviridis	*Acanthomorpha*	AEI70477.1	AEI70478.1	25

[a] The dataset contains three IFN-γR1 sequences for *Oncorhynchus kisutch*. Two of them are highly similar, the amino acid identity indicates the similarity of the two close homologous sequences with the third one.

Table 3
The interaction affinities of the IFN-γ proteins and the extracellular parts of their receptors 1. The affinities were measured as equilibrium dissociation constants Kd by microscale thermophoresis. All interactions between IFN-γ and receptors 1 from different species have Kd values larger than 20 μM. The previous SPR experiment with the human proteins determined the Kd value as 31 ± 1 nM [7].

Interaction partners	Kd for IFN-γR1 [nM]	Kd for IFN-γR1-like [nM]
PoliIFN-γ	123 ± 15	321 ± 23
TrubIFN-γ	106 ± 8	384 ± 42
OnilIFN-γ	136 ± 8	317 ± 34
humanIFN-γ	41 ± 1	–

the receptor-ligand pairs, and experimentally by biophysical measurements of the equilibrium dissociation constants (Kd; Table 3 and Fig. S7).

We computationally tested the coevolution between: (i) IFN-γ and IFN-γR1; (ii) IFN-γ and IFN-γR1-like; (iii) IFN-γrelC and IFN-γR1, and (iv) IFN-γrelC and IFN-γR1-like. We also performed tests of coevolution between *Cypriniformes* IFN-γ and both IFN-γR1 and IFN-γR1-like to compare it with the results for IFN-γrelC. Similar tests for IFN-γrelA were not performed due to a low number of sequences (4) available for this group. IFN-γ showed no significant coevolution with either IFN-γR1 or IFN-γR1-like, however, the test statistics are much higher (and thus the proteins are more likely to have coevolved) for the relationship with IFN-γR1 (p-value = 0.078 for IFN-γR1; p-value = 0.421 for IFN-γR1-like). In addition, no coevolving pairs were discovered for IFN-γ and IFN-γR1-like proteins, while there were 11 significantly coevolving pairs observed for IFN-γ and IFN-γR1 proteins (Fig. 5). IFN-γrelC shows significant coevolution with IFN-γR1-like (p-value = 0.028), but not with IFN-γR1 (p-value = 0.198), while *Cypriniformes* IFN-γ showed no significant coevolution with either IFN-γR1 or IFN-γR1-like. Our results are thus not in an agreement with the previous results [53,55], as they support the hypothesis that IFN-γ binds to IFN-γR1, while the evolution of IFN-γrelC is driven mainly by its relation with IFN-γR1-like.

The binding affinities between IFN-γ and receptor 1 were measured by microscale thermophoresis (MST). In agreement with our coevolution computations, the MST determined that Kd values show stronger binding between IFN-γ and receptors R1 with an average affinity around 100 nM (Table 3). The Kd of receptors R1-like proteins have significantly weaker binding affinities and Kd values above 300 nM (Table 3). However, the observed differences in Kd values are within one order of magnitude and can be overcome by avidity or concentration effects on the cell surfaces. Receptor concentration on the cell surface is not known and can differ significantly according to the cell type or cell's previous activation. Situation is even more complex if we take into account the function of the receptors. Receptors 1 (R1 and R1-like) serve as high affinity binders but the signalization is finally triggered by low affinity receptors 2. Therefore, the biological function may be determined not only by the affinities of receptor 1.

3.6. Phylogeny of fish IFN-γ receptor 2

At the time of this study, only three fish IFN-γR2 proteins were annotated in the public databases (*L. oculatus*, *Holostei*; *O. mykiss*, *Salmonidae*; *S. salar*, *Salmonidae*) and their sequential similarities were not sufficient to search for more IFN-γR2 genes by BLAST. We therefore decided to search for potential *IFN-γR2* genes using their genomic location. In the human genome, the *IFN-γR2* gene is clustered with genes coding for *IFN-λR2*, *IL10RB*, *IFN-λR1* and the transmembrane protein 50B (*TMEM50B*) (Fig. 4b). The locus structure remains the same for cartilaginous fish *C. milii* (*Chondrichthyes*) and is very similar also in *L. oculatus* (*Holostei*). Thus, we have benefited from the gene synteny and searched for the *IFN-γR2* gene in fish genomes using a better annotated gene *TMEM50B*. This procedure and the subsequent rounds of BLAST searches yielded 43 different IFN-γR2 sequences coming from 38 fish species.

The structure of the *IFN-γR2* locus is quite diverse among different fish species (Fig. 4b). The phylogenetic trees of the extracellular domains of fish IFN-γR2 computed by the Bayesian inference and maximum likelihood approach (Fig. 3, Figs. S6a and b) are almost identical (86% similarity, chapter 3.3) and both trees match almost exactly the evolution of fish. There are only two differences: (i) the presence of two distinct groups of *Salmonidae* IFN-γR2, whose origin most probably lies in the Salmonid-specific whole-genome duplication, and (ii) the presence of two distinct IFN-γR2 molecules for *Cichlidae* species (Table S3). The *Cichlidae* IFN-γR2 proteins for *O. niloticus*, *Haplochromis burtoni*, and *M. zebra* are colocalized, possess over 90% amino acid identity, and form one cluster in the phylogenetic tree. Therefore, the two genes for IFN-γR2 are likely the consequence of a recent gene duplication event.

The global test of coevolution of IFN-γR2 with IFN-γ was not statistically significant (p-value 0.13), but this result is not surprising due to the low expected binding affinity between IFN-γR2 and IFN-γ [109]. On the other hand, IFN-γR2 seems to be coevolving with both IFN-γR1 and IFN-γR1-like (p-values 0.02 and 0.05). Our previously discussed data suggest that IFN-γ signals by interacting with IFN-γR1 and IFN-γrel signals by interacting with IFN-γR1-like. The significant coevolution of IFN-γR2 with both IFN-γR1 and IFN-γR1-like then implies that IFN-γR2 is involved in signaling of both IFN-γ and IFN-γrel. The promiscuity of the second receptor is a common feature for receptors of the closely related interleukin 10 family [109,110]. However, we cannot rule out the existence of the second IFN-γR2 molecule if its gene was located in a different locus; in any case, this putative gene sequence would be dissimilar from sequences of the known IFN-γR2. An indirect support for the existence of a second IFN-γR2 are the previously published experimental results [53], according to which IFN-γR2 (termed there Crfb6) is important for IFN-γrelC signaling, but not for IFN-γ signaling.

Our attempts to compute the receptor-ligand co-evolution at amino acids level by i-COMS web-server [95] and correlate its results with structural models failed. The majority of coevolving pairs were core-associated rather than intermolecular, which has been reported previously [111]. The coevolution between fish IFN-γ and its receptors is driven by frequent remodeling of the structure in the loop regions,

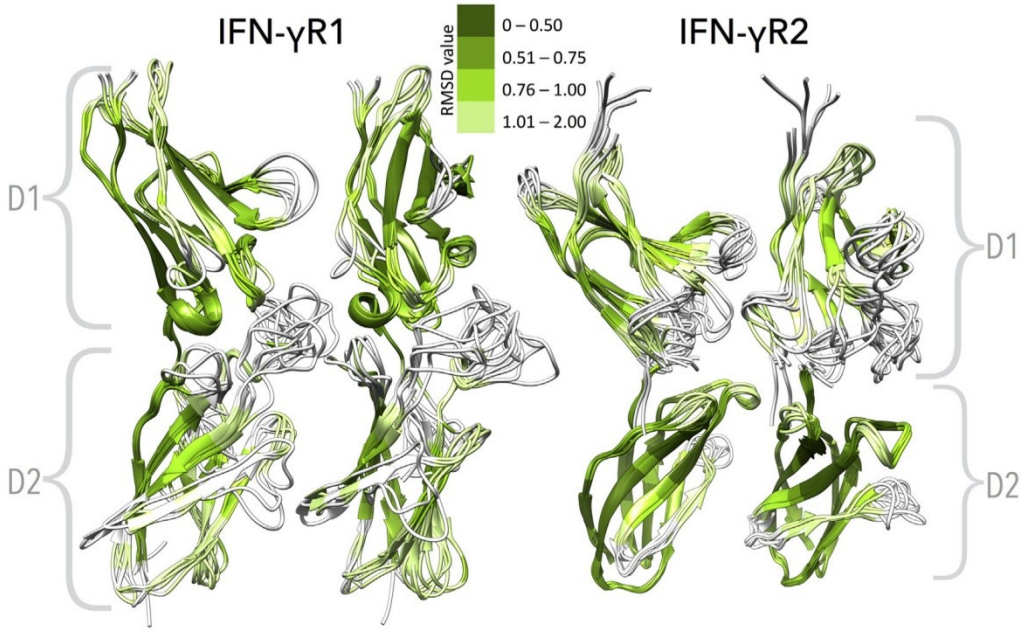

Fig. 6. Computer models of structures of the PoliIFN-γR1, TrubIFN-γR1, OnilIFN-γR1 (a) and PoliIFN-γR2, TrubIFN-γR2, OnilIFN-γR2 (b). The PoliIFN-γR1 model was based on structure of the human receptor 1 (1FG9 [5]), PoliIFN-γR2 model on structure of the human receptor 2 (5eh1 [9]). The RMSD color scheme shows the closeness of the modeled receptors to their respective template crystal structures. The models were built by minimization using the default setting in Chimera [96]. (For interpretation of the references to color in this figure legend, the reader is referred to the Web version of this article.)

which is caused by insertions or deletions in the gene (Fig. S8).

3.7. Computer modeling of the structures of IFN-γ receptors 1 and 2 and their binding interfaces with IFN-γ

The molecules of IFN-γ receptors 1 and 2 are composed of two immunoglobulin-like β-sheet domains called D1 and D2, both with fibronectin type-III topology (Pfam PF00041) [5,9]. The topologies of both domains are well conserved among class 2 cytokine receptors [112] [113]. The D1 domains are composed of three β-strands stacked on a layer of four β-strands that form sandwich-like structure and are also characteristic by an extensive cation π-stacking motif and one structurally conserved S-S bond [9]. The D2 domains form a similar β-sandwich structure with four β-strands stacked on the remaining four β-strands. This core of the class 2 cytokine receptors is fairly uniform and our sequence alignments support their existence also in fish receptors.

Homologous models of the structures of IFN-γ receptors 1 and 2 (Fig. 6) were built for the expressed proteins from species *P. olivaceus*, *T. rubripes*, and *O. niloticus*. The models of IFN-γR1 were computed based on the human (pdb 1FG9 [5]) and chicken (pdb 4EQ2, 4EQ3 [101]) structures of receptor 1 by using UCSF Chimera [96] and Modeller 9.19 [99,100]. The S-S bond formation patterns were used as constraints for the modeling (Fig. S2b). The models showed two expected Fibronectin type III domains with a majority of significant structural changes located in the loop L6 of the D2 domain (in 1FG9 residues 138–148). At the same time, the RMSD of the core parts of the compared proteins were below 1 Å. The structurally most variable part in our models of IFN-γR1 corresponds to the loop L6, which forms the recognition interface with the IFN-γ loop AB and helices B and F'. This is consistent with the assumption that the IFN-γ/IFN-γR1 recognition is controlled by the three loops located between the receptor 1 domains D1 and D2 [114] and by their mutual orientation [9]. We therefore assumed that the corresponding parts of the fish proteins contribute in a similar mutual position to the IFN-γ/R1 recognition.

Models of the second receptor IFN-γR2 were generated by the same methodology, using the crystal structures of human IFN-γR2 (pdb 5eh1 [9]) considering also IL10RB (pdb 3lqm [109]). In contrast to the IFN-γR1 models, most structural changes in the models of IFN-γR2 were identified in two D1 domain loops (residues 48–56, 70–81 in 5EH1).

4. Conclusions

Our bioinformatic analysis of IFN-γ and the extracellular parts of its two receptors disclosed unexpected diversity of sequences and revealed new attributes of evolution of this essential immunity signaling pathway in fish species. Our sequence database mining resulted in newly identified or annotated genes coding for the proteins participating in the IFN-γ signaling system: 28 IFN-γ and IFN-γrel, 60 IFN-γR1, and 40 IFN-γR2. The phylogeny of IFN-γ protein genes confirmed the existence of a group of proteins closely related to but distinct from IFN-γ named IFN-γrel. We discovered that there are likely two independent groups of IFN-γrel proteins: IFN-γ relC occurring in *Cypriniformes, Characiformes* and *Siluriformes* and IFN-γrelA occurring in *Acanthomorpha*.

Similarly to the existence of two groups of IFN-γ, the phylogeny and sequence alignments of IFN-γ receptors 1 manifest the existence of two independently evolving groups of genes labeled IFN-γR1 and IFN-γR1-like. The specificity of the binding between IFN-γ and the two types of IFN-γR1 was tested computationally by the tightness of their coevolution, and by the biophysical measurements of affinities between pairs of these proteins from three fish species (Table 3). Our coevolution studies as well as the measurement of affinities show that IFN-γ has a higher affinity for IFN-γR1 than for IFN-γR1-like so that the latter molecule is likely diverging from the original function. In contrast to IFN-γ and IFN-γR1, there is no sign of existence of two separate IFN-γR2 genes. However, this possibility cannot be ruled out in case the gene for the putative second R2 group is dissimilar and located in a different locus.

In summary, we have shown that three functionally tightly linked molecules, IFN-γ, IFN-γR1, and IFN-γR2, have probably underwent distinct evolutionary events: (i) IFN-γ being duplicated independently in at least two groups of fish; (ii) IFN-γR1 being duplicated once and preserved in both copies in all the descendants; (iii) IFN-γR2 probably

not being duplicated at all. The differences between the IFN-γ signaling in fish and mammals are illustrated by the graphical abstract.

An independent insight into IFN-γ evolution has been achieved by solving the crystal structure of IFN-γ from *Paralichthis olivaceus*. The structure of the PDB accession code 6F1E was solved by selenourea experimental phasing and revealed a fold observed in IFN-γ molecules from mammalian species: a homodimer composed of two four helix bundles. The structure however shows significant differences. Most notably, one PoliIFN-γ monomer exhibited an additional helix G at the C terminus and the dimer is more extended compared to the mammalian counterparts because the angle between helices C and D opens it up (Fig. 1). The information based on the crystal structure of PoliIFN-γ was complemented by measuring the solution SAXS data of IFN-γ proteins from three fish species and confirmed the dimeric form and shapes compatible with the shape of the known IFN-γ crystal structures.

We believe that our phylogeny work and the solved crystal structure of PoliIFN-γ helps the understanding of the complex phenomenon of IFN-γ evolution in fish species and of early stages of immunity development in vertebrates.

Acknowledgments

This study was supported by the Czech Science Foundation grant 16-20507S and by the projects New research methods to BIOCEV (CZ.1.05/2.1.00/19.0390), and CIISB (LM2015043, and CZ.02.1.01/0.0/0.0/16_013/0001776) from the ERDF. It was conducted at the Institute of Biotechnology CAS with the help of the institutional grant RVO 86652036. We thank HZB and EMBL for the allocations of a synchrotron-radiation beamtime.

Appendix A. Supplementary data

Supplementary data related to this article can be found at http://dx.doi.org/10.1016/j.fsi.2018.05.008.

References

[1] A. Isaacs, J. Lindenmann, Virus interference. I. the interferon, Proc. Roy. Soc. Lond. B Biol. Sci. 147 (927) (1957) 258–267.
[2] S. Pestka, The interferons: 50 years after their discovery, there is much more to learn, J. Biol. Chem. 282 (28) (2007) 20047–20051.
[3] J.R. Schoenborn, C.B. Wilson, Regulation of interferon-gamma during innate and adaptive immune responses, Adv. Immunol. 96 (2007) 41–101.
[4] M. Fountoulakis, J.F. Juranville, A. Maris, L. Ozmen, G. Garotta, One interferon gamma receptor binds one interferon gamma dimer, J. Biol. Chem. 265 (32) (1990) 19758–19767.
[5] D.J. Thiel, M.H. le Du, R.L. Walter, A. D'Arcy, C. Chene, M. Fountoulakis, G. Garotta, F.K. Winkler, S.E. Ealick, Observation of an unexpected third receptor molecule in the crystal structure of human interferon-gamma receptor complex, Structure (London, England : 1993) 8 (9) (2000) 927–936.
[6] L.C. Platanias, Mechanisms of type-I- and type-II-interferon-mediated signalling, Nat. Rev. Immunol. 5 (5) (2005) 375–386.
[7] P. Mikulecký, J. Černý, L. Biedermannová, H. Petroková, M. Kuchař, J. Vondrášek, P. Malý, P. Šebo, B. Schneider, Increasing affinity of interferon-γ receptor 1 to interferon-γ by computer-aided design, BioMed Res. Int. 2013 (2013) 752514.
[8] J. Soh, R.J. Donnelly, T.M. Mariano, J.R. Cook, B. Schwartz, S. Pestka, Identification of a yeast artificial chromosome clone encoding an accessory factor for the human interferon gamma receptor: evidence for multiple accessory factors, Proc. Natl. Acad. Sci. U. S. A 90 (18) (1993) 8737–8741.
[9] P. Mikulecky, J. Zahradnik, P. Kolenko, J. Cerny, T. Charnavets, L. Kolarova, I. Necasova, P.N. Pham, B. Schneider, Crystal structure of human interferon-gamma receptor 2 reveals the structural basis for receptor specificity, Acta. Cryst. D, Struct. Biol. 72 (Pt 9) (2016) 1017–1025.
[10] X. Pang, H.-X. Zhou, A common model for cytokine receptor activation: combined scissor-like rotation and self-rotation of receptor dimer induced by class I cytokine, PLoS Comput. Biol. 8 (3) (2012) e1002427.
[11] R. Ferrao, Heidi J.A. Wallweber, H. Ho, C. Tam, Y. Franke, J. Quinn, Patrick J. Lupardus, The structural basis for class II cytokine receptor recognition by JAK1, Structure (London, England : 1993) 24 (6) (2016) 897–905.
[12] M. Sakatsume, K. Igarashi, K.D. Winestock, G. Garotta, A.C. Larner, D.S. Finbloom, The Jak kinases differentially associate with the alpha and beta (accessory factor) chains of the interferon gamma receptor to form a functional receptor unit capable of activating STAT transcription factors, J. Biol. Chem. 270 (29) (1995) 17528–17534.
[13] S.V. Kotenko, L.S. Izotova, B.P. Pollack, T.M. Mariano, R.J. Donnelly, G. Muthukumaran, J.R. Cook, G. Garotta, O. Silvennoinen, J.N. Ihle, et al., Interaction between the components of the interferon gamma receptor complex, J. Biol. Chem. 270 (36) (1995) 20915–20921.
[14] H.M. Johnson, E.N. Noon-Song, R. Dabelic, C.M. Ahmed, IFN signaling: how a non-canonical model led to the development of IFN mimetics, Front. Immunol. 4 (2013) 202.
[15] P.S. Subramaniam, M.M. Green, J. Larkin 3rd, B.A. Torres, H.M. Johnson, Nuclear translocation of IFN-gamma is an intrinsic requirement for its biologic activity and can be driven by a heterologous nuclear localization sequence, J. Interferon Cytokine Res. 21 (11) (2001) 951–959.
[16] W.P. Michalski, B.J. Shiell, T.E. O'Neil, G. Beddome, J.W. Lowenthal, Recombinant chicken IFN-gamma expressed in *Escherichia coli*: analysis of C-terminal truncation and effect on biologic activity, J. Interferon Cytokine Res. 19 (4) (1999) 383–392.
[17] T. Decker, P. Kovarik, A. Meinke, GAS elements: a few nucleotides with a major impact on cytokine-induced gene expression, J. Interferon Cytokine Res. 17 (3) (1997) 121–134.
[18] J.N. Volff, Genome evolution and biodiversity in teleost fish, Heredity 94 (3) (2004) 280–294.
[19] J.S. Taylor, I. Braasch, T. Frickey, A. Meyer, Y. Van de Peer, Genome duplication, a trait shared by 22,000 species of ray-finned fish, Genome Res. 13 (3) (2003) 382–390.
[20] A. Meyer, Y. Van de Peer, From 2R to 3R: evidence for a fish-specific genome duplication (FSGD), BioEssays 27 (9) (2005) 937–945.
[21] R. Savan, S. Ravichandran, J.R. Collins, M. Sakai, H.A. Young, Structural conservation of interferon gamma among vertebrates, Cytokine Growth Factor Rev. 20 (2) (2009) 115–124.
[22] C. Berthelot, F. Brunet, D. Chalopin, A. Juanchich, M. Bernard, B. Noel, P. Bento, C. Da Silva, K. Labadie, A. Alberti, J.M. Aury, A. Louis, P. Dehais, P. Bardou, J. Montfort, C. Klopp, C. Cabau, C. Gaspin, G.H. Thorgaard, M. Boussaha, E. Quillet, R. Guyomard, D. Galiana, J. Bobe, J.N. Volff, C. Genet, P. Wincker, O. Jaillon, H. Roest Crollius, Y. Guiguen, The rainbow trout genome provides novel insights into evolution after whole-genome duplication in vertebrates, Nat. Commun. 5 (2014) 3657.
[23] L. David, S. Blum, M.W. Feldman, U. Lavi, J. Hillel, Recent duplication of the common carp (*Cyprinus carpio* L.) genome as revealed by analyses of microsatellite loci, Mol. Biol. Evol. 20 (9) (2003) 1425–1434.
[24] M. Crane, A. Hyatt, Viruses of fish: an overview of significant pathogens, Viruses 3 (11) (2011) 2025–2046.
[25] B. Venkatesh, A.P. Lee, V. Ravi, A.K. Maurya, M.M. Lian, J.B. Swann, Y. Ohta, M.F. Flajnik, Y. Sutoh, M. Kasahara, S. Hoon, V. Gangu, S.W. Roy, M. Irimia, V. Korzh, I. Kondrychyn, Z.W. Lim, B.-H. Tay, S. Tohari, K.W. Kong, S. Ho, B. Lorente-Galdos, J. Quilez, T. Marques-Bonet, B.J. Raney, P.W. Ingham, A. Tay, L.W. Hillier, P. Minx, T. Boehm, R.K. Wilson, S. Brenner, W.C. Warren, Elephant shark genome provides unique insights into gnathostome evolution, Nature 505 (7482) (2014) 174–179.
[26] J. Zou, Y. Yoshiura, J.M. Dijkstra, M. Sakai, M. Ototake, C. Secombes, Identification of an interferon gamma homologue in Fugu, *Takifugu rubripes*, Fish Shellfish Immunol. 17 (4) (2004) 403–409.
[27] D. Igawa, M. Sakai, R. Savan, An unexpected discovery of two interferon gamma-like genes along with interleukin (IL)-22 and -26 from teleost: IL-22 and -26 genes have been described for the first time outside mammals, Mol. Immunol. 43 (7) (2006) 999–1009.
[28] B. Robertsen, V. Bergan, T. Rokenes, R. Larsen, A. Albuquerque, Atlantic salmon interferon genes: cloning, sequence analysis, expression, and biological activity, J. Interferon Cytokine Res. 23 (10) (2003) 601–612.
[29] E.H. Stolte, H.F. Savelkoul, G. Wiegertjes, G. Flik, B.M. Lidy, Verburg-van Kemenade, Differential expression of two interferon-gamma genes in common carp (*Cyprinus carpio* L.), Dev. Comp. Immunol. 32 (12) (2008) 1467–1481.
[30] M.K. Purcell, K.J. Laing, J.C. Woodson, G.H. Thorgaard, J.D. Hansen, Characterization of the interferon genes in homozygous rainbow trout reveals two novel genes, alternate splicing and differential regulation of duplicated genes, Fish Shellfish Immunol. 26 (2) (2009) 293–304.
[31] J. Zou, A. Carrington, B. Collet, J.M. Dijkstra, Y. Yoshiura, N. Bols, C. Secombes, Identification and bioactivities of IFN-gamma in rainbow trout *Oncorhynchus mykiss*: the first Th1-type cytokine characterized functionally in fish, J. Imunol. (Baltimore, Md.: 1950) 175 (4) (2005) 2484–2494.
[32] Y. Xiang, W. Liu, P. Jia, Y. Li, Y. Jin, L. Chen, J. Zhang, K. Jia, M. Yi, Molecular characterization and expression analysis of interferon-gamma in black seabream *Acanthopagrus schlegelii*, Fish Shellfish Immunol. 70 (2017) 140–148.
[33] S. Yoon, A. Alnabulsi, T.Y. Wang, P.T. Lee, T.Y. Chen, S. Bird, J. Zou, C.J. Secombes, Analysis of interferon gamma protein expression in zebrafish (*Danio rerio*), Fish Shellfish Immunol. 57 (2016) 79–86.
[34] S. Yang, Q. Li, Y. Mu, J. Ao, X. Chen, Functional activities of interferon gamma in large yellow croaker *Larimichthys crocea*, Fish Shellfish Immunol. 70 (2017) 545–552.
[35] C. Furnes, M. Seppola, B. Robertsen, Molecular characterisation and expression analysis of interferon gamma in Atlantic cod (*Gadus morhua*), Fish Shellfish Immunol. 26 (2) (2009) 285–292.
[36] J. Velazquez, J. Acosta, N. Herrera, A. Morales, O. Gonzalez, F. Herrera, M.P. Estrada, Y. Carpio, Novel IFNgamma homologue identified in Nile tilapia (*Oreochromis niloticus*) links with immune response in gills under different stimuli, Fish Shellfish Immunol. 71 (2017) 275–285.
[37] A.-C. Øvergård, I. Nepstad, A.H. Nerland, S. Patel, Characterisation and expression analysis of the Atlantic halibut (*Hippoglossus hippoglossus* L.) cytokines: IL-1β, IL-6, IL-11, IL-12β and IFNγ, Mol. Biol. Rep. 39 (3) (2012) 2201–2213.

[38] B.Y. Ruan, S.N. Chen, J. Hou, B. Huang, Z.A. Laghari, L. Li, P. Nie, Two type II IFN members, IFN-gamma and IFN-gamma related (rel), regulate differentially IRF1 and IRF11 in zebrafish, Fish Shellfish Immunol. 65 (2017) 103–110.

[39] W.Q. Chen, Q.Q. Xu, M.X. Chang, J. Zou, C.J. Secombes, K.M. Peng, P. Nie, Molecular characterization and expression analysis of the IFN-gamma related gene (IFN-gammarel) in grass carp *Ctenopharyngodon idella*, Vet. Immunol. Immunopathol. 134 (3–4) (2010) 199–207.

[40] L. Grayfer, M. Belosevic, Molecular characterization, expression and functional analysis of goldfish (*Carassius aurutus* L.) interferon gamma, Dev. Comp. Immunol. 33 (2) (2009) 235–246.

[41] I. Milev-Milovanovic, S. Long, M. Wilson, E. Bengten, N.W. Miller, V.G. Chinchar, Identification and expression analysis of interferon gamma genes in channel catfish, Immunogenetics 58 (1) (2006) 70–80.

[42] J.A. Arts, E.J. Tijhaar, M. Chadzinska, H.F. Savelkoul, B.M. Verburg-van Kemenade, Functional analysis of carp interferon-gamma: evolutionary conservation of classical phagocyte activation, Fish Shellfish Immunol. 29 (5) (2010) 793–802.

[43] J. Zou, C.J. Secombes, The function of fish cytokines, Biology 5 (2) (2016).

[44] D. Lu, T. Wang, X. Zhang, T. Leng, Y. Zhang, H. Lin, A comparative study of two interferon gamma in the regulation of tetraodon TLR recognition system, Fish Shellfish Immunol. 34 (6) (2013) 1662–1663.

[45] Y. Shibasaki, T. Yabu, K. Araki, N. Mano, H. Shiba, T. Moritomo, T. Nakanishi, Peculiar monomeric interferon gammas, IFNγrel 1 and IFNγrel 2, in ginbuna crucian carp, FEBS J. 281 (4) (2014) 1046–1056.

[46] D. Stuber, A. Friedlein, M. Fountoulakis, H.W. Lahm, G. Garotta, Alignment of disulfide bonds of the extracellular domain of the interferon gamma receptor and investigation of their role in biological activity, Biochemistry 32 (9) (1993) 2423–2430.

[47] J.C. Renauld, Class II cytokine receptors and their ligands: key antiviral and inflammatory modulators, Nat. Rev. Immunol. 3 (8) (2003) 667–676.

[48] A. Celada, R.D. Schreiber, Role of protein kinase C and intracellular calcium mobilization in the induction of macrophage tumoricidal activity by interferon-gamma, J. Immunol. 137 (7) (1986) 2373.

[49] D. Watling, D. Guschin, M. Muller, O. Silvennoinen, B.A. Witthuhn, F.W. Quelle, N.C. Rogers, C. Schindler, G.R. Stark, J.N. Ihle, I.M. Kerr, Complementation by the protein tyrosine kinase JAK2 of a mutant cell line defective in the interferon-γ signal transduction pathway, Nature 366 (6451) (1993) 166–170.

[50] C.V. Ramana, M.P. Gil, R.D. Schreiber, G.R. Stark, Stat1-dependent and -independent pathways in IFN-γ-dependent signaling, Trends Immunol. 23 (2) (2002) 96–101.

[51] K. Igarashi, G. Garotta, L. Ozmen, A. Ziemiecki, A.F. Wilks, A.G. Harpur, A.C. Larner, D.S. Finbloom, Interferon-gamma induces tyrosine phosphorylation of interferon-gamma receptor and regulated association of protein tyrosine kinases, Jak1 and Jak2, with its receptor, J. Biol. Chem. 269 (20) (1994) 14333–14336.

[52] S.D. Rosenzweig, O.M. Schwartz, M.R. Brown, T.L. Leto, S.M. Holland, Characterization of a dipeptide motif regulating IFN-gamma receptor 2 plasma membrane accumulation and IFN-gamma responsiveness, J. Immunol. (Baltimore, Md.: 1950) 173 (6) (2004) 3991–3999.

[53] D. Aggad, C. Stein, D. Sieger, M. Mazel, P. Boudinot, P. Herbomel, J.-P. Levraud, G. Lutfalla, M. Leptin, Vivo analysis of Ifn-γ1 and Ifn-γ2 signaling in zebrafish, J. Immunol. 185 (11) (2010) 6774–6782.

[54] Q. Gao, P. Nie, K.D. Thompson, A. Adams, T. Wang, C.J. Secombes, J. Zou, The search for the IFN-gamma receptor in fish: functional and expression analysis of putative binding and signalling chains in rainbow trout *Oncorhynchus mykiss*, Dev. Comp. Immunol. 33 (8) (2009) 920–931.

[55] L. Grayfer, M. Belosevic, M. Belosevic, Molecular characterization of novel interferon gamma receptor 1 isoforms in zebrafish (*Danio rerio*) and goldfish (*Carassius auratus* L.), Mol. Immunol. 46 (15) (2009) 3050–3059.

[56] T. Unger, Y. Jacobovitch, A. Dantes, R. Bernheim, Y. Peleg, Applications of the Restriction Free (RF) cloning procedure for molecular manipulations and protein expression, J. Struct. Biol. 172 (1) (2010) 34–44.

[57] A. Erijman, A. Dantes, R. Bernheim, J.M. Shifman, Y. Peleg, Transfer-PCR (TPCR): a highway for DNA cloning and protein engineering, J. Struct. Biol. 175 (2) (2011) 171–177.

[58] Z. Luo, Selenourea: a convenient phasing vehicle for macromolecular X-ray crystal structures, Sci. Rep. 6 (2016) 37123.

[59] H.M. Berman, T. Battistuz, T.N. Bhat, W.F. Bluhm, P.E. Bourne, K. Burkhardt, Z. Feng, G.L. Gilliland, L. Iype, S. Jain, P. Fagan, J. Marvin, D. Padilla, V. Ravichandran, B. Schneider, N. Thanki, H. Weissig, J.D. Westbrook, C. Zardecki, The protein data bank, Acta. Cryst. D 58 (Pt 6 No 1) (2002) 899–907.

[60] S.E. Ealick, W.J. Cook, S. Vijay-Kumar, M. Carson, T.L. Nagabhushan, P.P. Trotta, C.E. Bugg, Three-dimensional structure of recombinant human interferon-gamma, Science 252 (5006) (1991) 698–702.

[61] A.A. Nuara, L.J. Walter, N.J. Logsdon, S.I. Yoon, B.C. Jones, J.M. Schriewer, R.M. Buller, M.R. Walter, Structure and mechanism of IFN-gamma antagonism by an orthopoxvirus IFN-gamma-binding protein, Proc. Natl. Acad. Sci. U. S. A 105 (6) (2008) 1861–1866.

[62] C.T. Samudzi, L.E. Burton, J.R. Rubin, Crystal structure of recombinant rabbit interferon-gamma at 2.7-A resolution, J. Biol. Chem. 266 (32) (1991) 21791–21797.

[63] M. Randal, A.A. Kossiakoff, The 2.0 A structure of bovine interferon-gamma; assessment of the structural differences between species, Acta. Cryst. D 56 (Pt 1) (2000) 14–24.

[64] C.T. Samudzi, J.R. Rubin, Structure of recombinant bovine interferon-gamma at 3.0 A resolution, Acta. Cryst. D 49 (Pt 6) (1993) 513–521.

[65] W. Kabsch, XDS, Acta. Crystallogr. D Biol. Crystallogr. 66 (Pt 2) (2010) 125–132.

[66] P.R. Evans, G.N. Murshudov, How good are my data and what is the resolution? Acta. Cryst. D 69 (Pt 7) (2013) 1204–1214.

[67] M.D. Winn, C.C. Ballard, K.D. Cowtan, E.J. Dodson, P. Emsley, P.R. Evans, R.M. Keegan, E.B. Krissinel, A.G. Leslie, A. McCoy, S.J. McNicholas, G.N. Murshudov, N.S. Pannu, E.A. Potterton, H.R. Powell, R.J. Read, A. Vagin, K.S. Wilson, Overview of the CCP4 suite and current developments, Acta. Cryst. D 67 (Pt 4) (2011) 235–242.

[68] G.M. Sheldrick, Experimental phasing with SHELXC/D/E: combining chain tracing with density modification, Acta. Crystallogr. D Biol. Crystallogr. 66 (Pt 4) (2010) 479–485.

[69] G.G. Langer, S. Hazledine, T. Wiegels, C. Carolan, V.S. Lamzin, Visual automated macromolecular model building, Acta. Cryst. D 69 (Pt 4) (2013) 635–641.

[70] P. Emsley, B. Lohkamp, W.G. Scott, K. Cowtan, Features and development of coot, Acta. Cryst. D 66 (Pt 4) (2010) 486–501.

[71] G.N. Murshudov, P. Skubak, A.A. Lebedev, N.S. Pannu, R.A. Steiner, R.A. Nicholls, M.D. Winn, F. Long, A.A. Vagin, REFMAC5 for the refinement of macromolecular crystal structures, Acta. Cryst. D 67 (Pt 4) (2011) 355–367.

[72] V.B. Chen, W.B. Arendall 3rd, J.J. Headd, D.A. Keedy, R.M. Immormino, G.J. Kapral, L.W. Murray, J.S. Richardson, D.C. Richardson, MolProbity: all-atom structure validation for macromolecular crystallography, Acta. Cryst. D 66 (Pt 1) (2010) 12–21.

[73] D.G. Gibson, L. Young, R.-Y. Chuang, J.C. Venter, C.A. Hutchison, H.O. Smith, Enzymatic assembly of DNA molecules up to several hundred kilobases, Nat. Meth. 6 (5) (2009) 343–345.

[74] O. Plihal, J. Sklenar, J. Kmonickova, P. Man, P. Pompach, V. Havlicek, V. Kren, K. Bezouska, N-glycosylated catalytic unit meets O-glycosylated propeptide: complex protein architecture in a fungal hexosaminidase, Biochem. Soc. Trans. 32 (Pt 5) (2004) 764–765.

[75] P. Pompach, P. Man, D. Kavan, K. Hofbauerová, V. Kumar, K. Bezouška, V. Havlíček, P. Novák, Modified electrophoretic and digestion conditions allow a simplified mass spectrometric evaluation of disulfide bonds, J. Mass Spect. 44 (11) (2009) 1571–1578.

[76] G. Bohm, R. Muhr, R. Jaenicke, Quantitative analysis of protein far UV circular dichroism spectra by neural networks, Prot. Eng. 5 (3) (1992) 191–195.

[77] D. Franke, A.G. Kikhney, D.I. Svergun, Automated acquisition and analysis of small angle X-ray scattering data, Nucl. Instrum. Met. Phys. Res. A 689 (2012) 52–59.

[78] P.V. Konarev, V.V. Volkov, A.V. Sokolova, M.H.J. Koch, D.I. Svergun, PRIMUS: a Windows PC-based system for small-angle scattering data analysis, J. Appl. Crystallogr. 36 (2003) 1277–1282.

[79] D. Svergun, Determination of the regularization parameter in indirect-transform methods using perceptual criteria, J. Appl. Crystallogr. 25 (4) (1992) 495–503.

[80] S.F. Altschul, W. Gish, W. Miller, E.W. Myers, D.J. Lipman, Basic local alignment search tool, J. Mol. Biol. 215 (3) (1990) 403–410.

[81] G.S.C. Slater, E. Birney, Automated generation of heuristics for biological sequence comparison, BMC Bioinf. 6 (1) (2005) 31.

[82] R.C. Edgar, MUSCLE: multiple sequence alignment with high accuracy and high throughput, Nucleic Acids Res. 32 (5) (2004) 1792–1797.

[83] A. Krogh, B. Larsson, G. von Heijne, E.L. Sonnhammer, Predicting transmembrane protein topology with a hidden Markov model: application to complete genomes, J. Mol. Biol. 305 (3) (2001) 567–580.

[84] O. Emanuelsson, S. Brunak, G. von Heijne, H. Nielsen, Locating proteins in the cell using TargetP, signalP and related tools, Nat. Protocols 2 (4) (2007) 953–971.

[85] S. Capella-Gutierrez, J.M. Silla-Martinez, T. Gabaldon, trimAl: a tool for automated alignment trimming in large-scale phylogenetic analyses, Bioinformatics (Oxford, England) 25 (15) (2009) 1972–1973.

[86] J.P. Huelsenbeck, F. Ronquist, MRBAYES: Bayesian inference of phylogenetic trees, Bioinformatics (Oxford, England) 17 (8) (2001) 754–755.

[87] F. Abascal, R. Zardoya, D. Posada, ProtTest: selection of best-fit models of protein evolution, Bioinformatics (Oxford, England) 21 (9) (2005) 2104–2105.

[88] S. Guindon, J.F. Dufayard, V. Lefort, M. Anisimova, W. Hordijk, O. Gascuel, New algorithms and methods to estimate maximum-likelihood phylogenies: assessing the performance of PhyML 3.0, Syst. Biol. 59 (3) (2010) 307–321.

[89] V. Lefort, J.E. Longueville, O. Gascuel, SMS: smart model selection in PhyML, Mol. Biol. Evol. 34 (9) (2017) 2422–2424.

[90] B.C. Stover, K.F. Muller, TreeGraph 2: combining and visualizing evidence from different phylogenetic analyses, BMC Bioinf. 11 (2010) 7.

[91] T.M. Nye, P. Lio, W.R. Gilks, A novel algorithm and web-based tool for comparing two alternative phylogenetic trees, Bioinformatics (Oxford, England) 22 (1) (2006) 117–119.

[92] P. Legendre, Y. Desdevises, E. Bazin, R.D.M. Page, A statistical test for host–parasite coevolution, Syst. Biol. 51 (2) (2002) 217–234.

[93] E. Paradis, J. Claude, K. Strimmer, APE: analyses of phylogenetics and evolution in R language, Bioinformatics (Oxford, England) 20 (2) (2004) 289–290.

[94] L.J. Revell, Phytools: an R package for phylogenetic comparative biology (and other things), Methods Ecol. Evol. 3 (2) (2012) 217–223.

[95] J. Iserte, F.L. Simonetti, D.J. Zea, E. Teppa, C. Marino-Buslje, I-COMS: inter-protein-correlated mutations server, Nucleic Acids Res. 43 (W1) (2015) W320–W325.

[96] E.F. Pettersen, T.D. Goddard, C.C. Huang, G.S. Couch, D.M. Greenblatt, E.C. Meng, T.E. Ferrin, UCSF chimera–a visualization system for exploratory research and analysis, J. Comput. Chem. 25 (13) (2004) 1605–1612.

[97] W.R. Pearson, An Introduction to Sequence Similarity ("Homology") Searching, Current Protocols in Bioinformatics, John Wiley & Sons, Inc., 2002.

[98] W.R. Pearson, Selecting the Right Similarity-scoring Matrix, Current Protocols in Bioinformatics, John Wiley & Sons, Inc., 2002.

[99] M.A. Marti-Renom, A.C. Stuart, A. Fiser, R. Sanchez, F. Melo, A. Sali, Comparative protein structure modeling of genes and genomes, Annu. Rev. Biophys. 29 (2000) 291–325.
[100] A. Fiser, R.K. Do, A. Sali, Modeling of loops in protein structures, Protein Sci.: a Publ. Prot. Soc. 9 (9) (2000) 1753–1773.
[101] Z. Ping, J. Qi, Y. Sun, G. Lu, Y. Shi, X. Wang, G.F. Gao, M. Wang, Crystal structure of the interferon gamma receptor alpha chain from chicken reveals an undetected extra helix compared with the human counterparts, J. Interferon Cytokine Res. 34 (1) (2014) 41–51.
[102] A. Sali, T.L. Blundell, Comparative protein modelling by satisfaction of spatial restraints, J. Mol. Biol. 234 (3) (1993) 779–815.
[103] T. Matsuyama, A. Fujiwara, T. Sakai, C. Nakayasu, Molecular cloning and expression analysis of interferon gamma gene in Japanese flounder *Paralichthys olivaceus*, Fish Sci. 75 (1) (2009) 253–255.
[104] T.J. Near, R.I. Eytan, A. Dornburg, K.L. Kuhn, J.A. Moore, M.P. Davis, P.C. Wainwright, M. Friedman, W.L. Smith, Resolution of ray-finned fish phylogeny and timing of diversification, Proc. Natl. Acad. Sci. U.S.A. 109 (34) (2012) 13698–13703.
[105] T.H. Ogden, M.S. Rosenberg, Multiple sequence alignment accuracy and phylogenetic inference, Syst. Biol. 55 (2) (2006) 314–328.
[106] B.G. Hall, Comparison of the accuracies of several phylogenetic methods using protein and DNA sequences, Mol. Biol. Evol. 22 (3) (2005) 792–802.
[107] Y.H. Loh, L.S. Katz, M.C. Mims, T.D. Kocher, S.V. Yi, J.T. Streelman, Comparative analysis reveals signatures of differentiation amid genomic polymorphism in Lake Malawi cichlids, Genome Biol. 9 (7) (2008) R113.
[108] P. Xu, X. Zhang, X. Wang, J. Li, G. Liu, Y. Kuang, J. Xu, X. Zheng, L. Ren, G. Wang, Y. Zhang, L. Huo, Z. Zhao, D. Cao, C. Lu, C. Li, Y. Zhou, Z. Liu, Z. Fan, G. Shan, X. Li, S. Wu, L. Song, G. Hou, Y. Jiang, Z. Jeney, D. Yu, L. Wang, C. Shao, L. Song, J. Sun, P. Ji, J. Wang, Q. Li, L. Xu, F. Sun, J. Feng, C. Wang, S. Wang, B. Wang, Y. Li, Y. Zhu, W. Xue, L. Zhao, J. Wang, Y. Gu, W. Lv, K. Wu, J. Xiao, J. Wu, Z. Zhang, J. Yu, X. Sun, Genome sequence and genetic diversity of the common carp, *Cyprinus carpio*, Nat. Genet. 46 (11) (2014) 1212–1219.
[109] S.-I. Yoon, B.C. Jones, N.J. Logsdon, B.D. Harris, A. Deshpande, S. Radaeva, B.A. Halloran, B. Gao, M.R. Walter, Structure and mechanism of receptor sharing by the IL-10R2 common chain, Structure (London, England: 1993) 18 (5) (2010) 638–648.
[110] N.J. Logsdon, A. Deshpande, B.D. Harris, K.R. Rajashankar, M.R. Walter, Structural basis for receptor sharing and activation by interleukin-20 receptor-2 (IL-20R2) binding cytokines, Proc. Natl. Acad. Sci. U. S. A 109 (31) (2012) 12704–12709.
[111] D. Talavera, S.C. Lovell, S. Whelan, Covariation is a poor measure of molecular coevolution, Mol. Biol. Evol. 32 (9) (2015) 2456–2468.
[112] R. Sabat, IL-10 family of cytokines, Cytokine Growth Factor Rev. 21 (5) (2010) 315–324.
[113] J.A. Langer, E.C. Cutrone, S. Kotenko, The class II cytokine receptor (CRF2) family: overview and patterns of receptor–ligand interactions, Cytokine Growth Factor Rev. 15 (1) (2004) 33–48.
[114] S. Pletnev, E. Magracheva, A. Wlodawer, A. Zdanov, A model of the ternary complex of interleukin-10 with its soluble receptors, BMC Struct. Biol. 5 (1) (2005) 10.